Ecophysiological Investigation of the Cyanobacterium *Synechococcus* for Potential Biomedical Application

Master's Thesis

in partial fulfillment of the academic degree

Master of Science (M.Sc.)

in Marine Microbiology

University of Bremen

Faculty Biology/ Chemistry (FB2)

University of Bremen, Glycobiochemistry

Alfred Wegener Institute,

Polar Biological Oceanography/Ecological Chemistry

submitted by Laura Johanna Gebhard

Matriculation number: 4118888

1. Reviewer: Prof. Dr. Allan Cembella

2. Reviewer: Prof. Dr. Sørge Kelm

Bremen, March 2019

Acknowledgements

This Master thesis would not have been possible without the help of many people and I would like to take this opportunity to thank them:

Prof. Dr. Allan Cembella for agreeing to be my 1st reviewer as well as for the great support.

Prof. Dr. Sørge Kelm for agreeing to be my 2nd reviewer and for hosting me at his labs at the University of Bremen.

Prof. Dr. Anya Waite for offering this Master thesis and as well as for the support throughout the six months.

Dr. Mario Waespy for the supervision in the Lab as well as always having an open ear.

Prof. Dr. Dieter Wolf-Gladrow for hosting me at the Polar Biological Oceanography section at the AWI.

Susanne Spahic for the invaluable help during the first months of organisation and the support after that.

Dr. Alexandra Kraberg for the advice and help in organising in the first months.

Erika Allhusen for the help with the pulse-amplitude modulation fluorometer.

Claudia Daniel for lending me the oxygen measurement devices.

Dr. Eva-Maria Nöthig, Andreas Rogge, Cora Hörstmann, Dr. Allison Fong and the whole Polar Biological Oceanography section at the Alfred-Wegener Institute for the warm welcome and support.

Dr. Christine Klaas, Dr. Florian Koch, Sebastian Böckmann and Dr. Sebastian Rokitta from the Marine BioGeoScience section at the AWI for the help with the flow cytometer.

Tanja Glawatty and Sabine Limberg for help with administrative issues at the AWI and the Uni Bremen respectively.

The whole Glycobiochemistry group at the University of Bremen for the warm welcome and support.

Camilla Konermann from the IMSAS at the University of Bremen for the oxygen measurements as well as Prof. Dr.-Ing. Michael J. Vellekoop for hosting me at the IMSAS labs.

Prof. Dr. Rita Groß-Hardt from the Molecular Genetics Group at the University of Bremen, for hosting the cyanobacteria in her laboratories during my experiments at the University of Bremen.

Prof. Dr. Kai Bischof, Dr. Karin Springer and Johanna Marambio from the Marine Botany Group at the University of Bremen for materials and support with the pulse amplitude modulation fluorometry.

The MPI Bremen and the Max-Planck Society for the funding during my Master's programme.

Dr. Christiane Glöckner, Dr. Solveig Bühring and Anita Tingberg for organizational help during this Master's programme.

And finally, my family and friends for the support during these past six months.

Statement - Eigenständigkeitserklärung

I hereby confirm that I have written this thesis unaided and that I have used no other resources than those mentioned.

Hiermit versichere ich, dass ich diese Arbeit selbständig verfasst und keine anderen als die angegebenen Quellen und Hilfsmittel verwendet habe.

_____ _____

(Place and Date / Ort und Datum) (Signature / Unterschrift)

Table of Contents

List of Abbreviations

air sat.	air saturation
ANOVA	analysis of variance
APC	allophycocyanin
ddH_2O	double-distilled water
ESAW	enriched artificial sea water medium
LC-MS	liquid chromatography – mass spectrometry
NAM	normalised arithmetic mean
NGM	normalised geometric mean
NM	normalised median
PAM	pulse-amplitude modulation
PBS	phycobilisome
PC	phycocyanin
PCB	phycocyanobilin
PCC	Pasteur Culture Collection
pCO_2	partial pressure of carbon dioxide
PE	phycoerythrin

PEB	phycoerythrobilin
PI	propidium iodide
PSI	photosystem I
PSII	photosystem II
PtTFPP	platinum(II)-5, 10, 15,20-tetrakis-(2,3,4,5,6-pentafluorphenyl)-porphyrin
PUB	phycourobilin
RCC	Roscoff Culture Collection

List of Figures

List of Tables

1. Abstract

Cyanobacteria are important primary producers in marine and other aqueous ecosystems. Members of the genus *Synechococcus* are globally distributed and exhibit high potential for acclimatisation and adaptation to diverse environmental conditions. The inter-disciplinary research project Endosymbiont (University of Bremen) proposes to utilize *Synechococcus* for the establishment of novel biomedical therapies based upon survival and growth under human physiological conditions. The main objective of the project is to successfully introduce living cyanobacterial cells into human keratinocytes (epidermal skin cells) in a quasi-stable functional coexistence. Such photosynthetic, endosymbiotic cells would then be able to produce oxygen and consequently promote wound healing in tissues with impaired perfusion.

In this work, one marine and one freshwater strain of *Synechococcus* were characterised with respect to their short-term growth and tolerance to different culturing conditions, such as temperature, pH and salinity ranges mimicking certain aspects of the cytosol of human keratinocytes. The marine strain *Synechococcus* sp. RCC2384 (Red Sea) was not able to grow at salinities lower than 100% of the artificial seawater medium. The freshwater strain *Synechococcus* sp. PCC7942 showed sufficient tolerance to selected osmotic conditions, with growth rates between 2.4 ± 0.64 day^{-1} (0% salinity), 1.7 ± 0.23 (10%), 2.6 ± 0.51 (20%) and 0.84 ± 0.3 day^{-1} (30%) during initial exponential growth at 30 °C. The pH that the medium was initially adjusted to had no effect on the actual pH measured in the cultures presumably due to the reduced carbonate buffer system in medium of lower salinity. However, the pH at time t_0 had significant effects on the subsequent growth rates ($t_0 – t_1$), and the pigment signal strength at t_1. This indicated a pH sensitivity regarding growth and physiological health that could not be fully evaluated for targeted pH values in this work. Nevertheless, a more acidic pH at t_0 led to higher growth rates and lower pigment fluorescence when normalised to cell concentrations. The osmotic condition likely had an indirect effect on both parameters by widening the possible pH range. Due to the adaptability shown here for *Synechococcus* sp. PCC7942 for osmotic concentration and pH range from below pH 7.0 up to pH 10.0, the strain emerges as the ideal candidate for potential future medical application.

Cyanobakterien sind wichtige Primärproduzenten in marinen und anderen aquatischen Ökosystemen. Spezies der Gattung *Synechococcus* sind global verbreitet und zeigen ein hohes Potential für Anpassung an diverse Umweltbedingungen. Das inter-disziplinäre Forschungsprojekt Endosymbiont (Universität Bremen) bezweckt *Synechococcus* für eine neuartige medizinische Therapiemethode zu verwenden, basierend auf Wachstum und Sauerstoffproduktion der Cyanobakterien unter human-physiologischen Bedingungen. Ziel des Projektes ist es, lebende *Synechococcus* Zellen in menschliche Keratinozyten (Hautzellen der Epidermis) aufzunehmen und eine quasi-stabile, funktionelle Koexistenz zu etablieren. Solch photosynthetische und endosymbiotische Zellen wären dann in der Lage Sauerstoff durch Photosynthese zu produzieren und dadurch die Wundheilung in Geweben mit beeinträchtigter Perfusion zu fördern.

In dieser Arbeit wurden ein mariner und ein Süßwasser Stamm von *Synechococcus* hinsichtlich ihrer kurzzeitigen Adaptationsfähigkeit an verschiedene Kulturbedingungen untersucht, so wie Temperatur, pH und Salinität, die einige Aspekte des Zytosols von menschlichen Keratinozyten nachahmen. Der Rote Meer Stamm *Synechococcus* sp. RCC2384 war nicht fähig in Medium von einem Salzgehalt weniger als 100% des artifiziellen Meerwasser Mediums zu wachsen. Dagegen zeigte der Süßwasser Stamm *Synechococcus* sp. PCC7942 hinreichende Toleranz zu ausgewählten Osmotischen Konzentrationen mit Wachstumsraten zwischen 2.4 ± 0.64 Tag^{-1} (0% Salzgehalt), 1.7 ± 0.23 (10%), 2.6 ± 0.51 (20%) und 0.84 ± 0.3 Tag^{-1} (30%) während der anfänglichen Phase exponentiellen Wachstums bei 30 °C. Der pH zu dem das Medium eingestellt wurde hatte keinen Einfluss auf den tatsächlich gemessenen pH, vermutlich durch das reduzierte Carbonat Puffer System in Medium mit geringem Salzgehalt. Der pH am Zeitpunkt t_0 hatte dennoch einen signifikanten Effekt auf die darauffolgenden Wachstumsraten ($t_0 – t_1$), und die Signalstärke der Pigmente an t_1. Dies zeigte eine pH Sensitivität von Wachstum und physiologischer Gesundheit die in dieser Studie nicht vollständig für gezielte pH Bedingungen untersucht werden konnte. Ein saurer pH an t_0 führte zu höheren Wachstumsraten und niedrigerer Pigment Fluoreszenz, wenn auf die Zellzahlen normalisiert wurde. Der Salzgehalt des Mediums hatte vermutlich einen indirekten Einfluss auf diese Parameter da er die mögliche pH Bandbreite bestimmte. Aufgrund der hier demonstrierten Adaptation von *Synechococcus* sp. PCC7942 an eine weite Bandbreite an osmotische Bedingungen und eine pH Toleranz von unter pH 7.0 bis zu pH 10.0, erscheint der Stamm als ein idealer Kandidat für weitere Forschung hinsichtlich möglicher medizinischer Anwendung.

2. Introduction

2.1. Cyanobacteria in Aqueous Ecosystems

Cyanobacteria are key primary producers in aquatic ecosystems. While the diversity of cyanobacteria is high in freshwater environments, marine systems are dominated by only two genera: *Procholorococcus* and *Synechococcus* (Jakubowska & Szeląg-Wasielewska, 2015). These two alone are estimated to contribute 25% of the ocean net primary production (Flombaum *et al.*, 2013). As one of the more ancient forms of life, cyanobacteria are linked to many critical events in earth history, such as the Great Oxygenation Event and the evolution of endosymbiosis and eukaryotic organisms (Ribeiro *et al.*, 2018). Nevertheless, the term cyanobacteria is a rather loose descriptor for a range of bacteria that are characterised by their ability for oxygenic photosynthesis and for having chlorophyll a as well as phycobiliproteins as their primary pigments (Castenholz *et al.*, 2001). The clash of microbiological and botanical taxonomy and classification has led to varying estimates of cyanobacterial diversity. However, the advancement of genomics has enabled a more thorough characterisation of cyanobacteria (Ribeiro *et al.*, 2018).

Cyanobacteria are ubiquitous in nature; however, they do have patterns of occurrence. In contrast to *Prochlorococcus*, *Synechococcus* has a wide geographic distribution and can be found in pelagic environments as well as coastal and subpolar regions. This adaptability is thought to be the consequence of the larger genome of *Synechococcus* relative to *Prochlorococcus* (Berube *et al.*, 2018). *Synechococcus* cells are described as unicellular, rod to coccoid in shape, < 3 μm in diameter and able to divide by binary fission from one plane (Robertson *et al.*, 2001). Although considered a genus, evidence suggests that the taxon is polyphyletic and may include numerous sub groups or even genera; for instance, Robertson *et al.* (2001) described 6 or 8 distinct groups with different phylogenetic markers.

2.1.1. The Photosynthetic Apparatus of Cyanobacteria

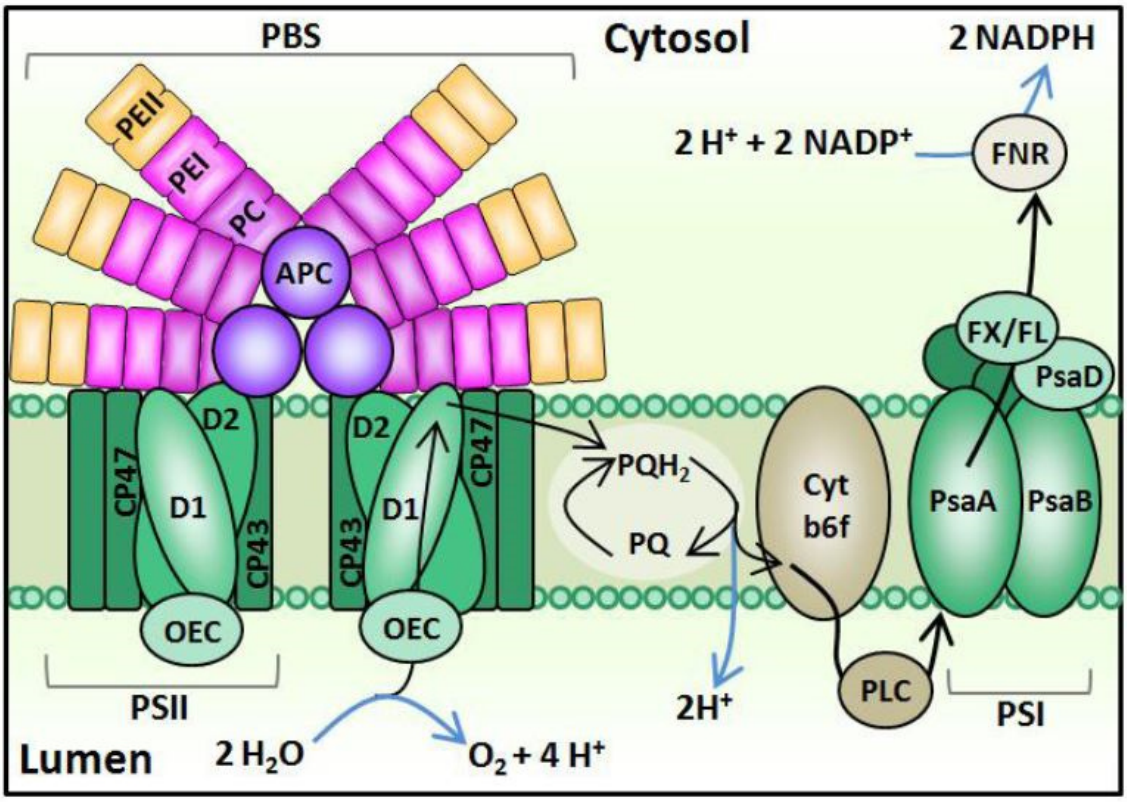

Figure 1 Schematic figure of the photosynthetic apparatus and the electron flow in cyanobacteria (taken from Mackey *et al.* (2013b)). Chemical reactions are shown in blue and the pathway of electrons is shown in black. The phycobilisome (PBS) is associated with Photosystem II (PSII). Light energy is captured by chlorophyll-a in the PSII as well as phycoerythrin (PE), phycocyanin (PC) and allophycocyanin (APC) in the PBS. From the PSII electrons are transferred to the plastoquinone (PQ)/plastoquinol (PQH_2) pool, to cytochrome b6f (Cyt b6f), to plastocyanin (PLC), to the PSI, to ferredoxin and flavodoxin (FX, FL) in that order. Finally, the ferredoxin/flavodoxin NADP reductase (FNR) creates reducing equivalents, that are further processed in the Calvin-Benson Cycle.

In general, the growth of microorganisms is controlled by the three major environmental factors light, temperature and nutrients (Malinsky-Rushansky *et al.*, 2002). For photoautotrophic organisms, the energy for growth is supplied by light. In contrast to algae and higher plants, the light-harvesting antennae of cyanobacteria are located on the cytoplasmic surface of the thylakoid membrane (Mackey *et al.*, 2013a) (Figure 1). The additional light harvesting antenna, the phycobilisome (PBS), is comprised of macromolecular complexes that form rods around a core of allophycocyanin (APC) (Six *et al.*, 2007). In the conserved core, APC binds to the chromophore phycocyanobilin (PCB; A_{max} = 620 nm; Figure 2). The rods contain phycobiliproteins that bind chromophores (phycobilins) via thioether bonds to cysteinyl residues.

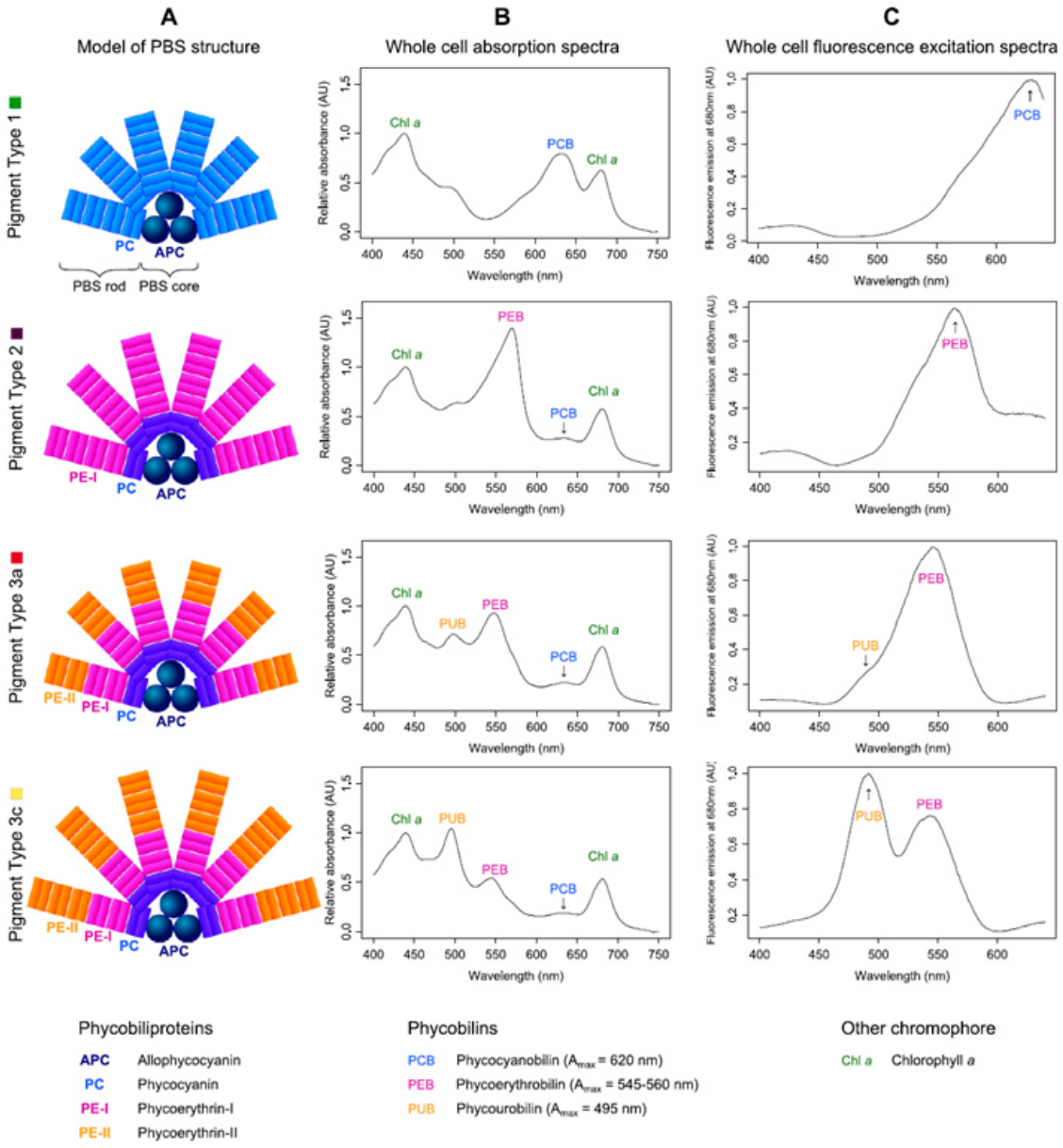

Figure 2 Schematic figures of the pigment complexes and absorption spectra of the major phycobilisome types of *Synechococcus*: composition (A), whole-cell absorption spectra (B) and whole-cell fluorescence spectra after excitation with 680 nm (C) (taken from Grébert *et al.* (2018a).

The proteins themselves are water-soluble and consist of two subunits organized in either trimeric or hexameric discs (Six *et al.*, 2007). The composition of the rods is variable and three pigment types are usually distinguished. In the first type, the rods are composed only of phycocyanin (PC) and the chromophore PCB (A_{max} = 620 nm) (Grébert *et al.*, 2018b). In type 2, the rods are composed of both PC and phycoerythrin I (PE-I), the chromophore phycoerythrobilin (PEB; A_{max} = 545 - 560 nm) binds to the latter protein. Most marine strains are grouped into the third type, where the rods are composed of PC, PE-I and -II with the chromophores PCB, PEB and phycourobilin (PUB; A_{max} = 495 nm), the

latter of which binds to PE-II. Subtypes of pigment type 3 are classified by the ratio of PUB:PEB into green-light specialists (3a), intermediate (3b), blue-light specialists (3c) as well as those with adaptable phycobilisomes (3d) (Grébert *et al.*, 2018b) (Figure 2). As a consequence of the unique characteristics of the cyanobacterial photosystem, adjustments are necessary when traditional parameters of photosynthetic health such as the efficiency of photosystem II (F_V/F_M or Φ_{PSII}) are measured, which were first developed for higher plants.

2.2. Impact of Climate Change on Cyanobacteria

The adaptive capabilities of *Synechococcus* will be necessary in order to cope with the changes brought on by climate change. Predictions foresee dramatic impacts on marine ecosystems based on the interactions between global warming, ocean acidification and the spreading of oxygen minimum zones. For instance, sea surface temperatures are expected to have risen 1 - 7 °C by the year 2100 (Houghton *et al.*, 2001). Moreover, the rising atmospheric partial pressure of carbon dioxide (pCO_2) is expected to lead to a decrease in pH in surface waters from pH 8.1 to 7.8 by the year 2100 (Houghton *et al.*, 2001). A stable, slightly alkaline pH is of high importance for many marine organisms, as an increase in pCO_2 causes an imbalance in the carbonate system (1):

$$(1)\ CO_{2\,(aq)} + H_2O \rightleftharpoons H_2CO_3 \rightleftharpoons HCO_3^- + H^+ \rightleftharpoons CO_3^{2-} + 2H^+$$

Dissolved carbon dioxide, reacts with water molecules and forms carbonic acid (H_2CO_3) which dissociates into protons and bicarbonate (HCO_3^-). Additional protons are buffered by carbonate (CO_3^{2-}) to form bicarbonate (Chou *et al.*, 2013). Ocean acidification leads to an increase in dissolved carbon dioxide, consequently increasing the concentration of bicarbonate and hydrogen ions and leading to a decrease of carbonate and pH (Chou *et al.*, 2013). Furthermore, the increased amount of dissolved inorganic carbon (DIC) will have impacts on the carbon cycle. High CO_2 concentrations have been shown to cause a shift in the carbon to nitrogen ratios towards higher carbon percentage in the biomass of planktonic species (Doney *et al.*, 2009). Therefore, the export of biological carbon into the deep sea would become more efficient whereas the food quality for higher trophic levels would decrease (Doney *et al.*, 2009).

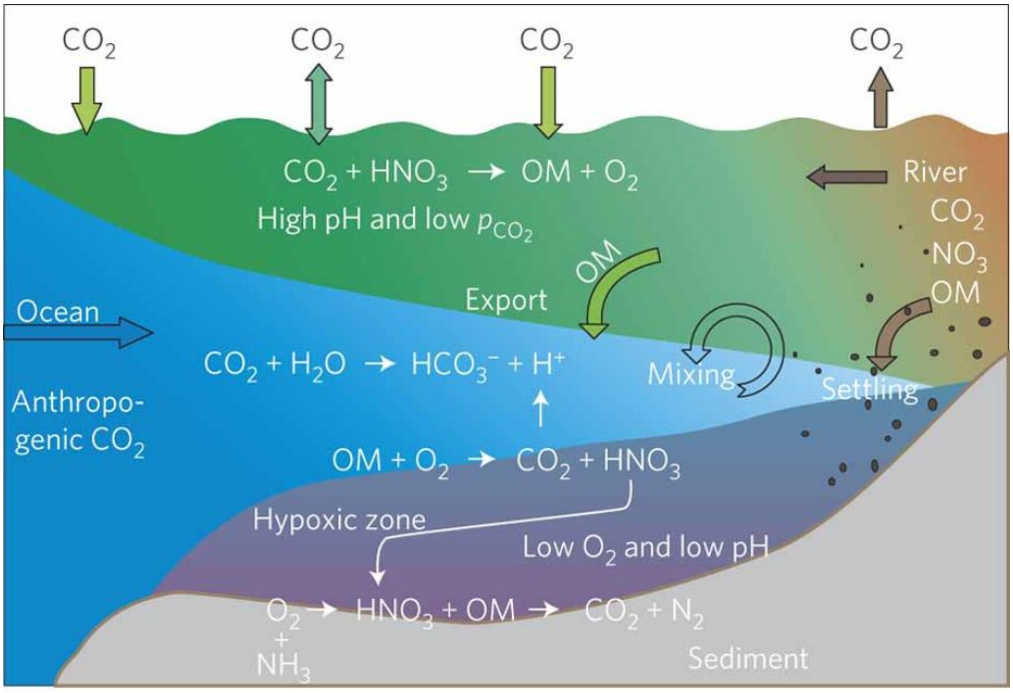

Figure 3 A conceptual model for a large river plume eutrophication, subsurface water hypoxia and acidification based on studies in the Gulf of Mexico and the East China Sea (taken from Cai *et al.* (2011a)).

Coastal waters naturally undergo fluctuations in pH; however, the interaction between eutrophication, ocean acidification and the loss of buffer capability may exaggerate the decrease in pH. Cai *et al.* (2011b) measured annual patterns of hypoxia and lowered pH, starting in spring with increasing stratification in estuaries in the East China Sea and the Gulf of Mexico (Figure 3). The decrease in pH and the decline in O_2 were positively correlated, due to the physical separation between primary production and respiration. Excess dissolved inorganic carbon and nutrient input from the river in the euphotic zone, increased organic matter export into the deeper layer. Moreover, the interplay between the imbalance of the carbonate equilibrium and the organic matter respiration accelerated the decrease in pH (Cai *et al.*, 2011b) Another hydrographic study conducted off the west coast of the USA (Feely *et al.*, 2008), showed the large-scale upwelling of carbonate undersaturated water masses with low pH. Without anthropogenic carbon input, carbonate saturation increased in the model.

2.3. Biotechnological Application of Cyanobacteria

2.3.1. State of the Art

In light of predictions of future food shortages with an ever-growing world population, cyanobacteria have caught a lot of attention as potential sources of nutrition. In contrast to traditional food sources, microalgae and cyanobacteria need very little nutrients and very little space while showing high productivity (Singh *et al.*, 2017). Several genera such as *Spirulina* sp., *Nostoc* sp. and *Aphanothece* sp. are already being used as sources of carbohydrates, lipids, proteins, pigments, vitamin, phenolics, minerals and other compounds (Kumar *et al.*, 2016)

Furthermore, cyanobacterial toxins could have potential applications as herbicides, antimicrobials and pesticides (Singh *et al.*, 2017). Other future uses for secondary metabolites could include preventing biofouling (Brown *et al.*, 2004; Dahms *et al.*, 2006), in wastewater treatment (Khan *et al.*, 2019; Werkneh & Rene, 2019) and as biofertilizers (Khan *et al.*, 2019; Rai *et al.*, 2019). Moreover, cyanobacteria could help support future energy demands by producing biohydrogen (Bandyopadhyay *et al.*, 2010; Show *et al.*, 2019), bioethanol (Gao *et al.*, 2012), biodiesel (Karatay & Dönmez, 2011; Wahlen *et al.*, 2011) and biogas (Chynoweth, 2005; Converti *et al.*, 2009) on a large scale with limited resources (Parmar *et al.*, 2011). Key components of biofuels such as hydrocarbons and fatty alcohols are already being produced by photosynthesis and production could be enhanced by genetic modification (Tan *et al.*, 2011).

2.3.2. Medical Application

In addition to applications in energy and nutrient production, cyanobacteria could also be employed in human medicine. Diverse species and strains of cyanobacteria have been shown to exhibit anti-bacterial (Fatima *et al.*, 2017; Martins *et al.*, 2008; Pushparaj *et al.*, 1998), anti-fungal (Pushparaj *et al.*, 1998; Soltani *et al.*, 2005), anti-viral (Koharudin & Gronenborn, 2011; Yasuhara-Bell *et al.*, 2010), anti-cancerous (Caro-Diaz *et al.*, 2019; El Semary & Fouda, 2015; Gerwick *et al.*, 1994) and immunosuppressive activity (Gunasekera *et al.*, 2016; Koehn *et al.*, 1992; Singh *et al.*, 2017). For instance, the phycobiliprotein c-phycocyanin has been shown to have anti-oxidant, anti-inflammatory as well as neuroprotective effects (Romay *et al.*, 2003). Specific classes of molecules of interest include cyanobacterial phenols, fatty acids, terpenoids, carotenoids, lutein, zea-

and cryptoxanthin, scytonemin, halogenated compounds, phytohormones and toxins (Singh *et al.*, 2017).

Recently, Cohen *et al.* (2017) reported the successful application of *Synechococcus* for mammalian health benefit in a more direct approach. Instead of relying on compounds produced by the cyanobacteria*, Synechococcus elongatus* PCC7942 was co-cultured with primary rat cardiomyocytes (heart muscle cells) at optimal conditions for the mammalian cells during which photosynthesis was recorded (Cohen *et al.*, 2017). Furthermore, the effect of cyanobacterial injections in cases of acute myocardial ischemia (restriction of blood supply) was tested on a rat model. The presence of *S. elongatus* significantly increased the oxygen tension in the heart tissues (Cohen *et al.*, 2017). Moreover, the surface temperature of *Synechococcus* treated tissue increased over time, indicating metabolic activity, and cardiac function improved compared to the controls. Cohen *et al.* (2017) also simulated reperfusion after induced myocardial ischemia with and without direct injection of *S. elongatus* into the hearts of rats. The injection significantly reduced molecular markers of myocardial injury and cardiac function was improved. Furthermore, *Synechococcus* did not induce a host immune response and the majority of cyanobacterial cells had disappeared from the tissue 24 hours after injection (Cohen *et al.*, 2017).

However, the treatment of heart tissue with cyanobacteria has the obvious drawback that the treated tissues would need to be exposed to light in order to facilitate photosynthesis. This carries with it the obvious risk of infections in the open wound. Cohen *et al.* (2017) proposed testing an alternate strain of cyanobacteria that synthesize chlorophyll f, a newly discovered pigment that absorbs light in the infrared spectrum (Chen *et al.*, 2010) to facilitate the transfer of light energy through closed chest cavities (Cohen *et al.*, 2017). Nevertheless, the necessary exposure to light will always be an issue for the treatment of internal organs. Therefore, taking these concepts and technologies and applying them to skin, the natural barrier between the human body and the environment, is the logical next step.

2.3.3. The Human Epidermis & Wound Healing

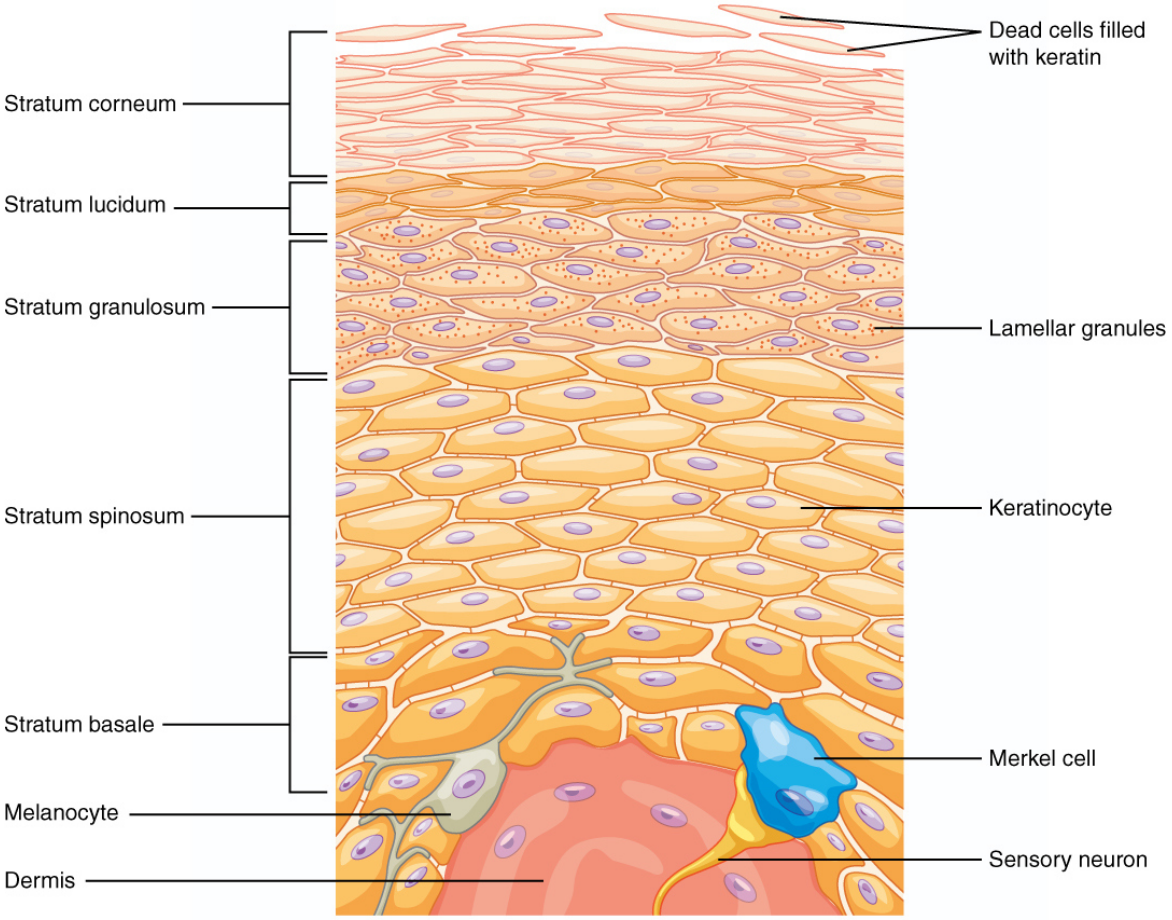

Figure 4 Schematic diagram of the structural components of the mammalian epidermis (taken from OpenStax College (2018)).

Mammalian skin can be divided into three distinct layers, the epidermis, dermis and the hypodermis. The hypodermis or subcutis is the basal layer of the skin, containing mostly fat cells that form a cushion against physical force (Shimizu, 2017). Moreover, the dermis contains structural components, largely collagen and elastic fibres, which provide strength and flexibility to the tissue. The matrix of the dermis retains water and forms the support structure for cells and the other elements of the dermis including hair follicles, blood vessels and nerve endings (Weller *et al.*, 2008). The outermost layer of mammalian skin is the epidermis, consisting mainly of keratinocytes in different stages of maturation (Figure 4). New cells are formed at the basal layer derived from epidermal stem cells and migrate towards the *stratum spinosum* where keratinocytes stop mitosis and start differentiation and the synthesis of keratin (Weller *et al.*, 2008). When the keratinocytes reach the uppermost layer of the epidermis, the *stratum corneum*, the keratin network collapses, thus flattening the cells (Shimizu, 2017). Eventually the keratinocytes die, due to being

cut off from nutrient supply and form layers of dead keratinocytes (corneocytes) into a relatively impermeable barrier (Weller *et al.*, 2008). Melanocytes in the *stratum basale* form appendages that supply surrounding keratinocytes with melanin in the form of vesicles. Melanin is a hydrophobic, dark brown pigment that is synthesized to protect skin cells from UV-radiation (Sobotta & Welsch, 2006).

The main purpose of skin is the protection from the environment, be it desiccation, toxins or pathogens. When the skin is damaged, this barrier between the organism and the environment needs to be restored quickly. This process occurs in three phases; the initial inflammatory phase is followed by the proliferative and maturational phase (Sinno & Prakash, 2013). In the inflammation response further blood loss is reduced and a blood clot is formed in the wound bed providing an extracellular matrix for the release of cytokines and growth factors (Landen *et al.*, 2016). In the proliferation phase, the epidermis is reformed by cells migrating up from the *stratum basale* or from stem cells around sweat glands and hair follicles in the surrounding tissue (Lau *et al.*, 2009). Simultaneously, new blood vessels are formed (angiogenesis) from cells in undamaged tissue areas (Landen *et al.*, 2016). In the final remodelling or maturational phase, a scar is formed, that is to say, new skin that has no hair follicles or glands as well as a different collagen pattern than intact skin (Sorg *et al.*, 2017).

Disruption of the wound healing process can have severe consequences. Chronic and hard or slow-healing wounds are associated both with long-term physical and psychological effects (Kinmond *et al.*, 2003; Posnett & Franks, 2007; 2008) as well as high costs for health services (Geraghty & LaPorta, 2019; Nunan *et al.*, 2014). Most chronic wounds are the result of restricted blood supply in the affected tissue (Nunan *et al.*, 2014). Their annual cost of treatment is estimated to account for 2 - 5% of the annual healthcare budget in industrial countries (Phillips *et al.*, 2016; Posnett & Franks, 2007; Sen *et al.*, 2009).

The pH of the skin is naturally acidic with a pH of 4 – 6. However, leakage from cells and microvessels leads to a rise of the pH in the wound bed to approximately pH 7.4 with increasing values towards the deepest point of the wound (Kruse *et al.*, 2017). In contrast to actively healing wounds, chronic wounds are characterised by an alkaline pH in the wound bed, which offers less protection against microorganisms than an acidic one (Percival *et al.*, 2014; Schneider *et al.*, 2007). The secretion of ions and organic compounds from cells in order to maintain extracellular pH is controlled by calcium, which

forms a gradient of increasing concentration from the *stratum basale* up to the *stratum granulosum* (Rinnerthaler & Richter, 2018). As a person ages, this calcium gradient decreases leading to a rise in the external pH in the epidermal layer. Along with changes to the structure of the cornified envelope (Rinnerthaler *et al.*, 2013) this weakens the protective ability of the epidermis and may further impede wound healing in old age (Rinnerthaler & Richter, 2018).

Currently, open wounds are treated by covering the affected area with skin grafts taken from other areas of the patient's body. However, this method often leads to adverse effects in the area of the donor site (Priya *et al.*, 2008; Sorg *et al.*, 2017). New approaches aim to substitute skin with biogenic or artificial materials (Zhong *et al.*, 2010), apply artificial growth factors (Tenenhaus & Rennekampff, 2016), or to genetically modify the wound bed (Priya *et al.*, 2008; Sorg *et al.*, 2017). Nevertheless, these new concepts are yet to be applied in standard treatments (Tenenhaus & Rennekampff, 2016).

A novel experimental therapy approach aims to introduce cyanobacteria into human keratinocytes to produce photosynthetic keratinocytes in a stable endosymbiotic system (Mirastschijski *et al.*, 2018). These endosymbiotic keratinocytes could then provide their own oxygen supply which would ideally trigger proliferation. A strategy for the potential direct uptake of cyanobacteria into keratinocytes has already been established within the Endosymbiont project. However, a suitable photoautotrophic cyanobacterium for the generation of an endosymbiotic keratinocyte still needs to be selected and characterised.

2.3.4. Ecophysiological Requirements of an Endosymbiont

In order to generate functional endosymbiotic keratinocytes, cyanobacterial cells would need to be able to withstand the highly specialized conditions in the human cytosol. The internal pH (pH_i) of human epidermal keratinocytes is expected to be around pH 7.4 (Kleszczyński *et al.*, 2013). Average values for the cytoplasm, nucleus and endoplasmic reticulum of eukaryotic cells have been reported to be around pH 7.2 – 7.4 (Theillet *et al.*, 2014). The cytosol of eukaryotic cells also includes a variety of molecules and ions dissolved in water, including inorganic ions, metabolites, proteins and structural components which all contribute to the osmotic pressure inside of the cell. The osmotic concentration per volume, or osmolarity, of human blood and human blood serum is around 287 - 289 mOsM (Hendry, 1961; Rocks *et al.*, 1986). In this project the expected

extracellular osmotic pressure was taken as a proxy for intracellular osmotic pressure, as co-cultures of cyanobacteria and human keratinocytes would need to be attempted before an insertion could be possible. The osmolarity of seawater is generally around 1000 mOsM, depending on the local composition and ratio of the salts, therefore, marine strains of *Synechococcus* would have to be able to adapt to much lower osmotic pressures than those present in their natural environment.

Furthermore, the potential endosymbionts would need to be functional at ambient temperatures around 30 °C. As homeothermic animals, humans maintain a constant core temperature of ca 37 °C, however, heat is also lost over the skin to the environment. The skin surface temperature is highly variable and mainly depends on the location on the body, e.g. the temperature is lower at the extremities than on the torso. Moreover, underlying muscles contribute more heat than bones or tendons, another important factor is the number of blood vessels in the area, as arteries contribute more than veins (Bierman, 1936). Skin surface temperatures have been reported as e.g. between 31 – 33.5 °C (Yosipovitch *et al.*, 1998) and < 24 °C to < 36 °C (Rubinstein & Sessler, 1990). It has been reported that burn wounds emit heat and are ca. 0.1 – 0.2 °C warmer than the surrounding intact skin tissue (Boylan *et al.*, 1992).

Therefore, a suitable candidate strain for the generation of endosymbiotic keratinocytes would need to be able to cope with highly specific conditions including temperatures of ca. 30 °C, pH 7.0 – 7.4 and osmolarity of around 290 mOsM. The genus *Synechococcus* was selected based on its wide geographic distribution (Berube *et al.*, 2018) and therefore potential for adaptability to these specific conditions which would not be common in nature except potentially in estuarine systems if several factors acted collectively.

2.3.5. Candidate Strains of *Synechococcus*

Three candidate strains of *Synechococcus* were selected based on the available literature and will hereafter be referred to by their strain number. *Synechococcus* sp. RCC2384 was first sampled at the Gulf of Aqaba on the coast of the Red Sea in Israel in 1999 and is also known as clonal strain RS9912 (Vaulot *et al.*, 2004). To date few published papers are available characterizing the strain, although the pigment type has been classified as 3a marking the strain as a green-light specialist with phycoerythrin as the main accessory pigment (Vaulot *et al.*, 2004).

Synechococcus sp. PCC7002 was first isolated on Magueyes Island, Puerto Rico in 1961 (Rippka, 2019), the strain is not considered marine due to its origin from a fish pen. Furthermore, PCC7002 has been described as having a phycobilisome of pigment type 1 (red-light maximum), containing only phycocyanin which is typical for coastal strains (Grébert *et al.*, 2018b; Mackey *et al.*, 2017). PCC7002 has displayed a remarkable adaptability to a variety of environmental conditions, from N-limited conditions (Marañón *et al.*, 2018), to a variety of salinity conditions (Castenholz *et al.*, 2001) to temperatures from 20 °C up to 38 °C (Ludwig & Bryant, 2012; Xu *et al.*, 2013; Zhu *et al.*, 2010). The strain is also considered to be pH-tolerant to an extent, being able to grow in pH at least as low as pH 7.82 (Mou *et al.*, 2017). In general, the strain is a model organism for S*ynechococcus* due to its high growth rates and tolerance of high irradiance levels (Bernstein *et al.*, 2014). Thus, many genomic sequences and transcriptome databases are available for the strain (Ludwig & Bryant, 2012; Vijayakumar & Angione, 2017; Yang *et al.*, 2015).

Synechococcus sp. PCC7942 is likewise grouped to pigment type 1 (Collier & Grossman, 1992). However, PCC942 is considered a freshwater strain and was isolated from a lake in California, USA in 1973 (Rippka, 2019). Members of the *Synechococcus* cluster 1.1 are generally referred to *Synechococcus elongatus* (Rippka & Cohen-Bazire, 1983). Under its former name *Anacystis nidulans* R2, the strain was the first cyanobacterium in which transformation with exogenous DNA could reliably be shown (Shestakov & Khyen, 1970). More recently, the metabolism of the strain was successfully manipulated towards increased O_2 production (Shih *et al.*, 2014) and increased production and secretion of glucose and fructose (Niederholtmeyer *et al.*, 2010). Moreover, PCC7942 has been employed as a model organism for research into the prokaryotic circadian clock (Golden *et al.*, 1998). PCC7942 has also been shown to grow at temperatures around 30 °C under standard conditions (Billini *et al.*, 2008; Blondin *et al.*, 1993; Kuan *et al.*, 2015; Ladas & Papageorgiou, 2000b) and within a range of 20 - 51 °C in temperature shock treatments (Billis *et al.*, 2014; Blondin *et al.*, 1993; Porankiewicz *et al.*, 1998). Furthermore, adaptability of PCC7942 to pH and salinity has been shown from pH 7.0 - 9.0 and up to 0.4 M NaCl (Billini *et al.*, 2008; Billis *et al.*, 2014; Ladas & Papageorgiou, 2000b).

In addition to the broad tolerance to a variety of environmental factors and the potential for genetic modification, recent positive findings in the co-cultivation of PCC7942 with rat cardiomyocytes and as a treatment for acute myocardial ischemia and reperfusion injury (Cohen *et al.*, 2017) strongly indicate that this strain of *Synechococcus* has the

potential to survive and produce oxygen in consortium with and to the benefit of mammalian cells.

2.4. Aim of the Work

Cyanobacteria in general, and *Synechococcus* in particular, are important primary producers in marine and other aqueous ecosystems. Their potential for adaptation to extreme conditions is well known, however, in light of the changing environmental conditions brought on by climate change there is a need to determine the limits of tolerance for these ubiquitous and abundant organisms. This will be particularly important in estuarine systems, where the interplay between anthropogenic eutrophication, increasing water column stratification and zones of varying pH and salinity create several microenvironments within one habitat (Cai *et al.*, 2011b).

In this work, the short-term adaptability of two strains of the genus *Synechococcus* to abiotic factors such as salinity/osmolarity, light level, temperature and pH will be characterised. Growth curves will be performed with strains under selected conditions, and cyanobacterial cells will be counted by flow cytometry. Growth data will be supported by pH measurements, pulse-amplitude modulation fluorometry as well as oxygen measurements of selected samples in a novel microfluidic oxygen measurement chamber in order to assess the photosynthetic efficiency of the cultures.

The time scales of adaptation, growth and oxygen production will be compared to common estuarine residence times to identify possible windows of time where adaptation and acclimatisation are possible.

Furthermore, strains will be evaluated based on their potential applicability as endosymbionts in medical therapy. Particularly, if the cyanobacterial cells are able to grow and produce oxygen in conditions mimicking certain aspects of the cytosol of human keratinocytes.

3. Materials & Methods

3.1. Culturing & Growth Kinetics

3.1.1. Origin & Maintenance of Cyanobacterial Strains

The Red Sea strain RCC2384 was purchased from the Roscoff Cuture Collection (Roscoff, France (Vaulot *et al.*, 2004). The strains PCC7002 and PCC7942 were acquired from the Pasteur Culture collection of Cyanobacteria (Paris, France) (Rippka, 2019). As part of this project the maintenance of cyanobacteria was established at the AG Glycobiochemistry at the University of Bremen. Moreover, the maintenance of the two PCC strains was established at the Alfred-Wegener Institute in Bremerhaven.

All strains were cultured in an enriched artificial seawater medium (ESAW) after a recipe from the Provasoli-Guillard National Center for Marine Algae and Microbiota (East Boothbay, ME, USA) (Berges *et al.*, 2001; Harrison *et al.*, 1980). Firstly, anhydrous salts (Table 5 in the Appendix) were dissolved in double-distilled water (ddH_2O) of less than half of the final volume and amended with the major nutrients NO_3, H_2PO_4 and SiO_3 (1, 1 and 2 mL L^{-1}), iron-EDTA (1 mL L^{-1}), trace metals (1 mL L^{-1}) and vitamin solutions (1 mL L^{-1}) (Tables 7 - 10 in the Appendix). Hydrated salts were also dissolved in ddH_2O (Table 6 in the Appendix). Subsequently, the two solutions were combined and the volume was filled up to the final volume with ddH_2O.

The concentration of salts in the original recipe of the ESAW medium (~ 0.995 OsM) was set as 100% osmolarity or osmotic concentration of ESAW. The amount of salts was adjusted accordingly when medium of lower osmolarity was prepared. The concentration of liquid ingredients was not changed between conditions. The pH of the medium was determined and if necessary, adjusted with 37% HCl (Sigma-Aldrich, St. Louis, MO, USA), 30% NaOH (Merck, Darmstadt, Germany), 1 M HCl and 1 M NaOH. Subsequently, the medium was sterile filtered through a 0.2 µm pore filter unit (Merck Millipore, MA, USA) into autoclaved glass bottles (0.5 or 1 L). Marine strains were maintained in 100% ESAW, whereas stock cultures of the freshwater strain were grown either in 0% or 20% ESAW medium.

In general, strains were maintained by transferring cultures ca. every two weeks into sterile medium in a 1 to 10 or 1 to 100 dilution. Incubation vessels were either 175 cm^2 vented cap, rectangular, polyethylene tissue culture flasks (Sarstedt, Nümbrecht, Germany) or T-

25 or T-225 CytoOne® vented filter cap, rectangular polyethylene tissue culture flasks (Starlab International, Hamburg, Germany). Each transfer was performed under a clean bench. Moreover, the positions of culture flasks were rotated clockwise after each measurement.

Strains were maintained at 25 °C under constant illumination at approximately 26 µmol photons m^{-2} s^{-1} of cool white fluorescent light (Master TL-D Super 80 36W/840 LED tube light, Philips, Amsterdam, Netherlands) at the Alfred Wegener Institute. For experiments samples were incubated at 30 °C at a 12:12 diurnal cycle at ca. 100 µmol photons m^{-2} s^{-1} in a growth chamber. The intensity of photosynthetically active radiation was measured with a LI-1000 light meter (LI-COR, Lincoln, NE, USA). All strains both during maintenance and experiments were grown in a growth chamber at the University of Bremen at 30 °C and ca. 130 µmol photons m^{-2} s^{-1} on a 12:12 hour light cycle (18 W/840 TL-D LED, Philips, Netherlands). The intensity of photosynthetically active radiation was measured with a LI-250A light meter (LI-COR, USA).

3.1.2. Growth Kinetics

The potential for quick adaptability of *Synechococcus* strain RCC2384 to lower osmolarity than 100% ESAW medium was tested in several small experiments which also served the purpose of establishing protocols, timescales necessary for analysis and templates e.g., for flow cytometry.

In the first quick adaptation test, the conditions tested were 100% and 29% osmolarity with five replicates each. The samples were inoculated with cell material from a three-week old starter culture grown at 25 °C, in a ca. 1:100 dilution by adding 3.5 mL to 350 mL of sterile medium. Growth was monitored by flow cytometry over 13 days (BD Accuri™ C6 Cytometer (Becton Dickinson, Franklin Lakes, NJ, USA). In the second test, the conditions tested were 100% to 40% osmolarity in 10% steps, with three replicates per condition. The cultures were each inoculated with 4 mL of a one-week old starter culture, in a 1:10 dilution into sterile ESAW medium of the respective osmolarity. Cells were counted with a CyFlow Cube8 flow cytometer (Sysmex Partec, Görlitz, Germany) and the pH was also measured at each time-point.

The possible effect of different suppliers of the major salts and nutrients of the ESAW medium was tested by inoculating duplicates in media prepared with two different sets of

ingredients. The starter culture of RCC2384 was one week old and the cell material was diluted 1:2 with the respective medium. The growth was monitored by flow cytometry.

A centrifugation protocol for the transfer and inoculation of cultures was established with *Synechococcus* RCC2384. The cells were grown at two different osmolarity regimes: 60% and 100% of ESAW. Out of the six replicates per condition, half were centrifuged for 15 min at 10,000 relative centrifugal force (x *g*) (Eppendorf Centrifuge 5810 R, Eppendorf, Germany) in conical centrifugation tubes (Sarstedt, Germany). For these samples, six times 8 mL of a one-and-a-half-week-old starter culture were centrifuged as described above. The supernatant was removed and the pellet was resuspended in 4 mL of ESAW medium of the corresponding osmolarity. Both centrifuged and uncentrifuged samples were transferred into 36 mL of sterile ESAW medium. Over the next seven days, the cultures were counted by flow cytometry and the pH was measured at each time point.

The adaptability of the freshwater strain PCC7942 to conditions of higher osmolarity and lower pH was tested in 10 conditions (Table 1), with four replicates per condition. Replicates were inoculated with cell material from a three-week old starter culture, that was grown in 20% ESAW and incubated at 30 °C. For this purpose, 10x 16 mL of the starter culture were centrifuged for 15 min at 10,000 x *g* in conical centrifugation tubes. Subsequently, the supernatant was removed and the pellet was resuspended in 1.6 mL sterile medium of the respective condition. The four replicates were each inoculated with 300 µL of the resuspended pellet. The growth of the cultures was monitored over 17 days, including flow cytometry counts and pH measurements. Moreover, the oxygen production of the cyanobacteria was measured in one replicate for conditions 1 and 10 (see section 3.4).

Table 1 Condition scheme for the growth curve of *Synechococcus* PCC7942. The adaptability of the strain to conditions of higher osmolarity and lower pH was monitored over 17 days. The number of the condition is indicated in the respective square.

	0 %	10 %	20 %	30 %
pH 8.2	1	5	6	7
pH 7.4	2			8
pH 7.2	3			9
pH 7.0	4			10

The growth rates were calculated based on the time intervals of exponential growth or decrease identified as linear increase or decrease in the natural logarithmic projection of the counts with the formula (2):

$$(2)\ \mu = \frac{(n_1 - n_0)}{n_0 \times (t_1 - t_0)}$$

Where μ is the specific growth rate which is calculated by subtracting the cell number (n_0) from that of a later time-point (n_1) and normalizing for time (t) and cell concentration at t_0 (n_0). All graphs were created with the R software (2008), including the packages cowplot, doBy, ggplot2, scales and viridis. The statistical analysis was also performed with R (2008) with the packages vegan, stats and ICS. The homogeneity of variances was tested with Bartlett's, Levene's and Fligner-Killeen tests with increasing robustness against non-normally distributed data. Subsequently, a one-way analysis of variance (ANOVA) was performed on each data set.

3.2. Flow Cytometry

3.2.1. General Measurements

Growth of cultures was measured with a BD Accuri™ C6 Cytometer (Becton Dickinson, USA) with yellow green beads (1.0 µm diameter microspheres; Fluoresbrite, Warrington, PA, USA) as volume control. The bead solution was calibrated after the fact, with BD Trucount™ beads (Becton Dickinson, USA) with a defined concentration of 41.92 beads μL^{-1}. Samples were stored at 4 °C in the dark until analysis to inhibit further activity and preserve the auto-fluorescence of the pigments. If necessary, dilutions were done with sterile 100% ESAW medium. Samples were vortexed, after which 490 µL of the sample or of the diluted sample were transferred into sample holders (Sarstedt, Germany). The yellow-green bead solution was vortexed as well, after which 10 µL were added to each sample holder. The solution was vortexed again before placement on the holdfast of the flow cytometer. The volume was set to 250 µL, with a flow rate of 66 µL min^{-1}, a core size of 22 µm and the threshold was set to 10 for forward scatter. The concentration of cells was determined based on the height of the fluorescent emission of phycoerythrobilin (FL2, 575 nm) plotted against forward scatter (height) after excitation at 488 nm (Figure 7). After each sample, the system was flushed for 2 min with ddH_2O. The beads were counted in a separate gate in the projection FL1 (525 nm, height) over forward scatter (Figure 7). To compare the counts, 1 mL of each culture was fixed by adding 0.1 mL of 10% paraformaldehyde solution (AppliChem, Darmstadt, Germany), followed by an incubation of at least 15 min at room temperature (RT) after which samples were diluted with 5 mL sterile filtered 1x phosphate buffered saline (tablets, VWR, Radnor, PA, USA). The samples were filtered individually (column diameter: 2.1 cm) onto polycarbonate filters (0.22 µm pore diameter; GE Osmonics Lenntech, Delfgauw, Netherlands). The filters were stained with DAPI OIL (1% (v/v) 4',6-diamidino-2-phenylindole, 100 µg mL^{-1} (Sigma-Aldrich, USA), 85% (v/v) Citifluor AF1 (Electron Microscopy Sciences, Hatfield, PA, USA) and 14% (v/v) Vectashield (Vector Laboratories, Burlingame, CA, USA)), placed onto microscope slides and covered. Finally, the slides were observed under an Axioskop 2 plus epifluorescence microscope with integrated AxioCam MRc 5 camera under 1000x magnification and the pictures were processed with the AxiovisionLE software (all Carl Zeiss, Oberkochen, Germany).

Cultures were counted with a CyFlow Cube8 flow cytometer (Sysmex Partec, Germany) at the University of Bremen. For this purpose, samples were kept at 4 °C in the dark until

Table 2 Settings for flow cytometry counts with a BD Accuri™ C6 Cytometer (Becton Dickinson, USA), including parameters recorded, excitation and recorded emission as well as the measured fluorophores. The system records forward scatter (FSC) and side scatter (SSC) and fluorescent emission for different wavelength spectra.

Channel	Excitation Wavelength (nm)	Emission (nm)	Wavelength Spectrum	Fluorophores
FSC	488			
SSC	488			
FL1	488	525	green	
FL2	488	575	orange	Phycoerythrobilin,
FL3	488	767	red	Chlorophyll a
FL4	633 - 635	660	far red	

further processing. Moreover, samples were vortexed briefly prior to transfer into individual sample holders (Sarstedt, Germany), and vortexed again before placement onto the sample holdfast. If necessary, samples were diluted with sterile medium of the same osmolarity. The volume was set to 30 µL with a pre-flow of 5 µL (or 30 µL for the second quick adaptation, medium and centrifugation tests of RCC2384) at a flow rate of 1 µL s^{-1}. The actual sampled volume was read out from the information provided by the own brand software of the cytometer. The wavelengths of the lasers were 488 nm and 638 nm at 50 mW and 25 mW power respectively. Additionally, a UV light emitting LED (365 nm) was switched on during all measurements. For RCC2384, the concentration of cells was determined based on the fluorescent emission of phycoerythrobilin (PEB, channel FL2) plotted against phycocyanobilin (PCB, channel FL5) as well as forward and side scatter (Figure 8 and Table 3). For the two PCC strains, fluorescent emission of PCB (FL5) was plotted against PEB (FL2), channel FL6 (far-red) as well as forward and side scatter (Figure 10 and Figure 37 in the Appendix). The system was flushed with autoclaved ddH_2O between conditions. All files were exported as fcs files from the own brand software of each flow cytometer and analysed with the FCS Express 6 Plus software (research version, De Novo Software, Glendale, CA; USA).

Table 3 Settings for flow cytometry counts with a CyFlow Cube8 flow cytometer (Sysmex Partec, Germany), including parameters recorded, filters, excitation and recorded emission of the filters, the measured fluorophores as well as the gains and thresholds. The system records forward scatter (FSC) and side scatter (SSC) and fluorescent emission with cut-off filters for specific wavelength spectra.

Channel	Excitation Wavelength (nm)	Filter	Wavelength Spectrum	Fluorophores	Gain (V)	Threshold (V)
FSC	488	Ex 488 ↑			226	0.00193
SSC	488	Ex 488 ↑			275	0.00023
FL1	488	536 ± 20 nm ↑	yellow-green		256	0.00023
FL2	488	590 ± 25 nm ↑	orange	Phyco-erythrobilin, Propidium Iodide	465	0.00023
FL3	488	675 ± 10 nm ↓	red		216	0.0002
FL4	488	455 ± 25 nm ↑	blue		463	0.00023
FL5	638	675 ± 10 nm ↓	red	Phycocyano-bilin	483	0.00023
FL6	638	ILP 748 ↑	far-red		547	0.00023

3.2.2. Propidium Iodide Staining & Pigment Content

For the growth curve of PCC7942, samples were stained with 1.5 µL of propidium iodide (1.0 mg mL^{-1} in water, Sigma-Aldrich, USA) from time-point 4 onwards. Propidium iodide (PI) is a nuclear counterstain that cannot penetrate intact cell envelopes (Xiao *et al.*, 2011) and can therefore stain dead cells. To compare the effect of PI staining on the number of particles counted, subsamples from the same sample were run both unstained and stained at time-point 5 (Figures 11 - 12). The pigment content of the PCC7942 strain was also monitored over time during the growth curve, by subtracting the background (identified with a histogram of sterile medium of the same osmolarity) from the histogram of the counts plotted against phycocyanobilin signal strength for each sample (Figure 13). The geometric mean, arithmetic mean and median of the remaining peak were then each divided by the number of events and plotted per condition against time and the pH at t_0.

3.3. Pulse Amplitude Modulation Fluorometry

Pulse-amplitude modulated fluorometry is a commonly used method for measuring photosynthetic health of higher plants and algae. The method takes advance of the fact that photosynthetic organisms can only direct light energy into three directions, into the photosynthetic reactions, emission as heat or fluorescent emission. F_V/F_M measures the maximum efficiency of PSII based on fluorescent emission with the formula (3):

$$(3) \qquad {F_V}/{F_M} = \frac{F_M - F_0}{F_M}$$

For the minimum fluorescence (F_0), dark adapted samples are exposed to modulated light intensity, too low to drive photosynthesis. A saturating pulse of light closes all reaction centres and maximum fluorescence is measured (F_M). Φ_{PSII} is another parameter to measure photosynthetic health and describes the efficiency of PSII at light adaptation (Mackey *et al.*, 2008).

F_V/F_M of the cyanobacterial cultures was determined with a Xenon Pulse Amplitude Modulation Fluorometer (PAM) (ED-101US/MP, Walz, Effeltrich, Germany). Prior to measurement samples were incubated in the dark at room temperature for ca. 15 min. The PAM was blanked with 2 mL of sterile filtered liquid from one of the samples. The measurements themselves were conducted in a 15 °C climate-controlled room, dark-adapted samples were well-mixed and transferred into quartz-cuvettes in the sample holder of the Xenon-PAM. Measurement delay was 1 µs, pre-flash measurement 20 µs, actinic and measuring flash duration were 3 µs each. The saturation pulse was set to INT. HALOGEN: 11 for 10000 ms at gain set to: 1, frequency: 2 and damping: 2.

3.4. Oxygen Measurements with the µRespirometer

This project also included first tests of the viability of a newly developed microfluidic µRespirometer (Bunge, 2018; Bunge *et al.*, 2017) for the observation of cyanobacterial cells, specifically for *Synechococcus*. Testing of experimental protocols included changing incubation times, light intensity and time until the light was first switched on. The µRespirometer consists of a microfluidic chip with a chamber (length: 12.3 mm, width: 2.5 mm and height: 200 µm) encased in silica gel and glass (Figure 5). Temperature in the measurement chamber can be controlled via the two integrated platinum conductors that function both as electrical heaters and temperature sensors measured by resistance.

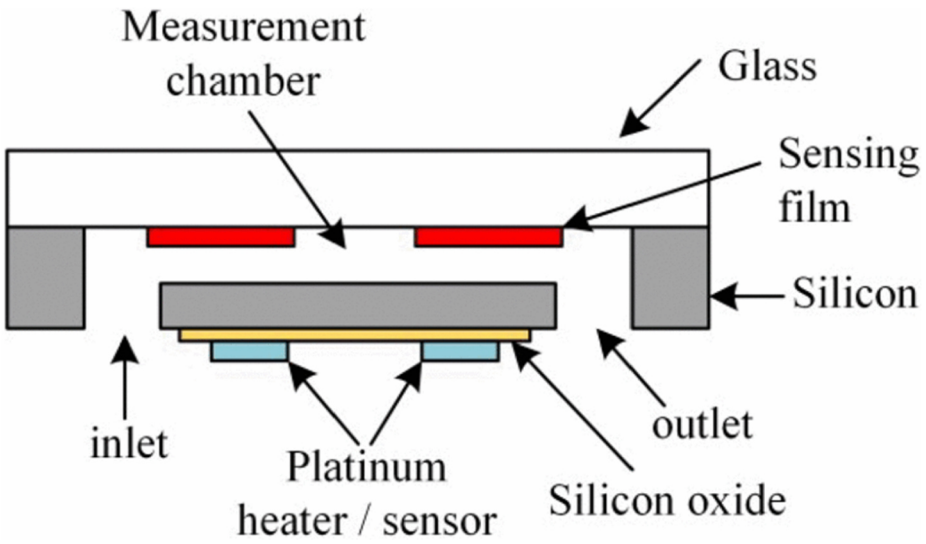

Figure 5 Schematic structure of the microfluidic chip of the µRespirometer. The measurement chamber (61.5 mm^3) is connected to the outside with an inlet and outlet of 0.7 mm diameter each. A heating module and a temperature sensor made out of platinum are integrated into the chip. The chamber is sealed on the sides and bottom by silica gels and on the top by a glass layer. Five, circular oxygen sensing spots (1.3 mm diameter) are attached to the glass layer facing the measuring chamber (taken from Bunge *et al.* (2018b)).

The chamber is sealed air-tight during measurement. Oxygen production and consumption is recorded with the oxygen-sensitive phosphorescent dye Platinum(II)-5, 10, 15,20-tetrakis-(2,3,4,5,6-pentafluorphenyl)-porphyrin (PtTFPP) that is embedded in a hydrophobic silica matrix (Bunge *et al.*, 2018c). An excitation LED (395 nm) illuminates the sensing film, leading to a shift into an excited state. The energy is re-emitted as light of a higher wavelength. In contrast to fluorescent dyes, the transition back to ground state is slower in phosphorescent dyes. Oxygen quenches the excited molecules of PtTFPP, leading to the reduction of the intensity and lifetime of phosphorescence with increasing oxygen concentration. In order to reach and quench PtTFPP, oxygen has to diffuse out of the liquid sample into the hydrophobic silica matrix of the sensing spots. Thus, oxygen concentration can only be measured up to the maximal partial pressure of oxygen at the desired temperature, calculated in percent air saturation (with ± 1% accuracy) (Bunge, 2018). The intensity after excitation at 395 nm is measured by a Raspberry Pi camera (Raspberry Pi Foundation, Cambridge, United Kingdom) located behind an optical filter with a cut-off of 600 nm (Figure 6).

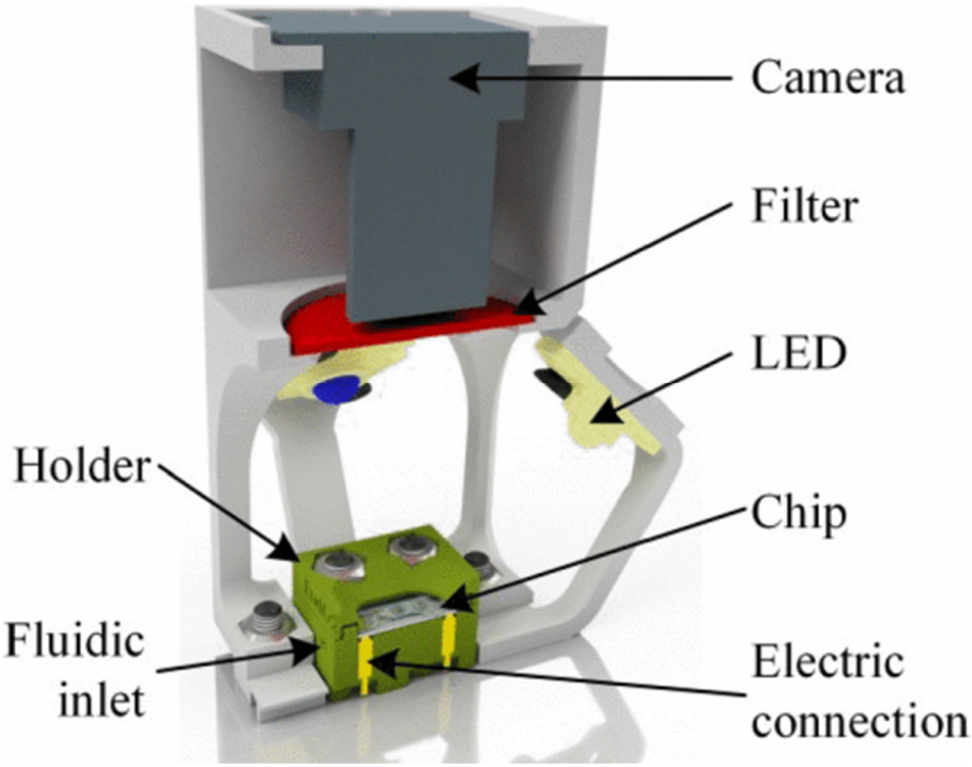

Figure 6 Setup of the µRespirometer. The microfluidic chip sits in a 3D printed holdfast and receives irradiance by an excitation LED and an illumination LED (not pictured here). A filter with a cut-off of 600 nm is mounted in front of the camera (taken from Bunge *et al.* (2018a)).

The microfluidic chip, the filter, the camera, the excitation LED as well as an illumination LED (not pictured here) are assembled in a 3D-printed casing. The camera takes a picture after excitation and the average intensity for each of the five oxygen sensing spots is calculated based on the detected image with the Stem-Volmer-Modell (4):

$$(4)\quad I(c,\Delta T) = I_0(1+\alpha_I \Delta T)\left(\frac{\gamma}{1+K_{SV}(1+\alpha_K \Delta T)c} + (1-\gamma)\right)$$

I being the intensity, ΔT the temperature difference to 20 °C, c the oxygen concentration, I_0 = 20.3 being the intensity at 20 °C with no oxygen present, α_I = - 0.016 K^{-1} is the temperature coefficient, γ = 0.09 being the portion of the dye that is quenched, the Stern-Volmer Constant K_{SV} = 0.084 % air saturation at 20 °C and α_K = - 0.015 K^{-1} the temperature coefficient of the Stern-Volmer Constant (Bunge *et al.*, 2018c).

For the oxygen measurements, the chamber was illuminated with a red-coloured LED at a current of 50 mA unless otherwise specified. The illumination LED was automatically switched off during excitation of the sensing spots and the time until the camera had taken a picture. Light and dark times as well as measuring time are indicated in the respective

graphs. In certain measurements the system was flushed with water with a defined low oxygen concentration and the measurement was continued. The water was bubbled with N_2 gas and the actual oxygen concentration was determined with a commercially available optical oxygen measurement device (Firesting O_2 Logger, Pyro Science, Aachen Germany). The data was analysed and the graphs were made with Matlab (Mathworks, Natick, MA. USA).

4. Results

4.1. Flow Cytometric Measurements & Method Development

4.1.1. *Synechococcus* RCC2384

The Red Sea strain RCC2384 was counted based on the fluorescent emission of phycoerythrin, the primary chromophore in the phycobilisome in *Synechococcus* of pigment type 3a either with a BD Accuri™ C6 Cytometer (Becton Dickinson, USA; Figure 7) or with a CyFlow Cube8 flow cytometer (Sysmex Partec, Germany; Figure 8). Furthermore, no difference between centrifugation protocols became apparent in both in the cell concentrations (Figure 9 and Figure 26 in the Appendix) and the pH values measured (Figure 27 in the Appendix). Therefore, this centrifugation protocol was applied to subsequent experiments with PCC7942.

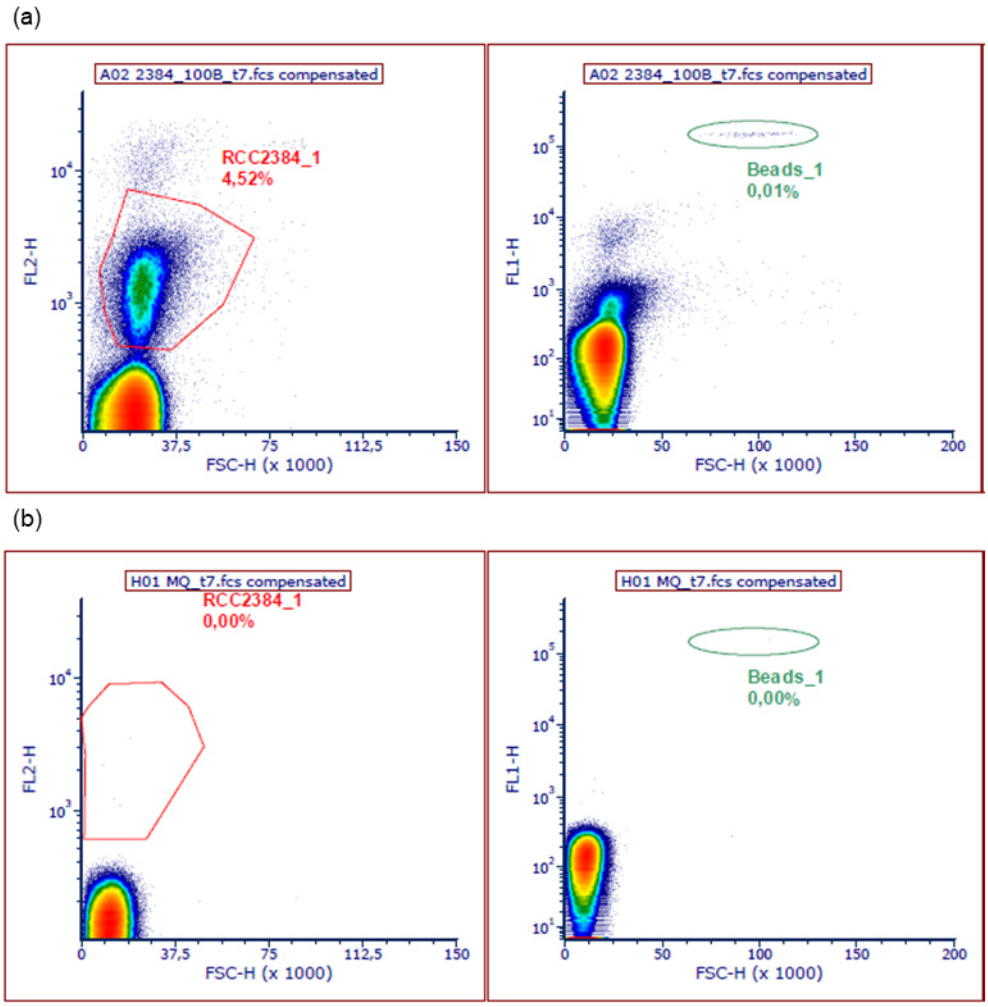

Figure 7 Exemplary presentation of the gates used to quantify the number of *Synechococcus* RCC2384 cells, for 100B at t_7 of the first quick adaptation test (a) and MilliQ as a control without beads on the same day (b). The number of cells was determined with the RCC2384_1 gate in the projection of the peak height of the fluorescent signal strength of phycoerythrobilin (FL2-H, 575 nm) plotted against peak height of side scatter after excitation at 488 nm (left). The beads for volume control were enumerated in gate Beads_1 by plotting FL1 (yellow-green, 525 nm) over forward scatter after excitation at 488 nm (right).

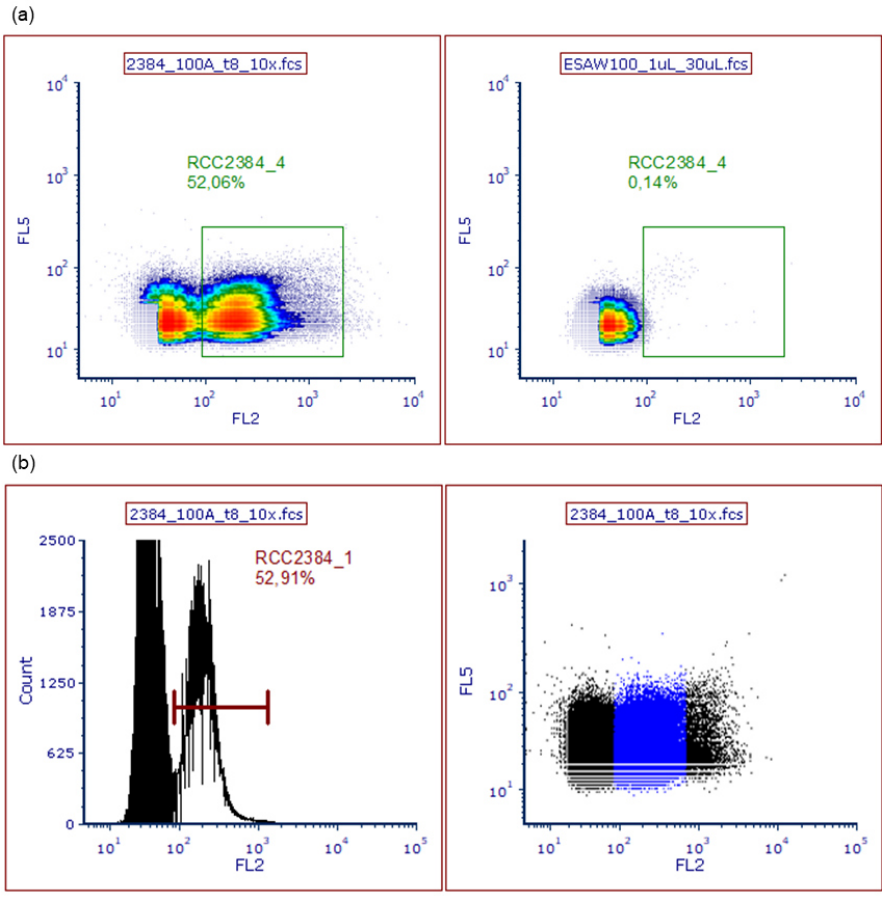

Figure 8 Exemplary presentation of the gates used to quantify the number of *Synechococcus* RCC2384 cells for 100A at t_8 (second quick adaptation test) and 100% ESAW medium as a control. The number of cells was determined with the RCC2384_4 gate in the projection of the fluorescent signal strength of phycocyanobilin (FL5) plotted against the fluorescent signal of phycoerythrobilin (FL2) after excitation at 638 and 488 nm respectively (a). The area of RCC2384_4 corresponded roughly to the peak area marked as Gate RCC2384_1 in the histogram of counts over signal intensity of FL2 (b).

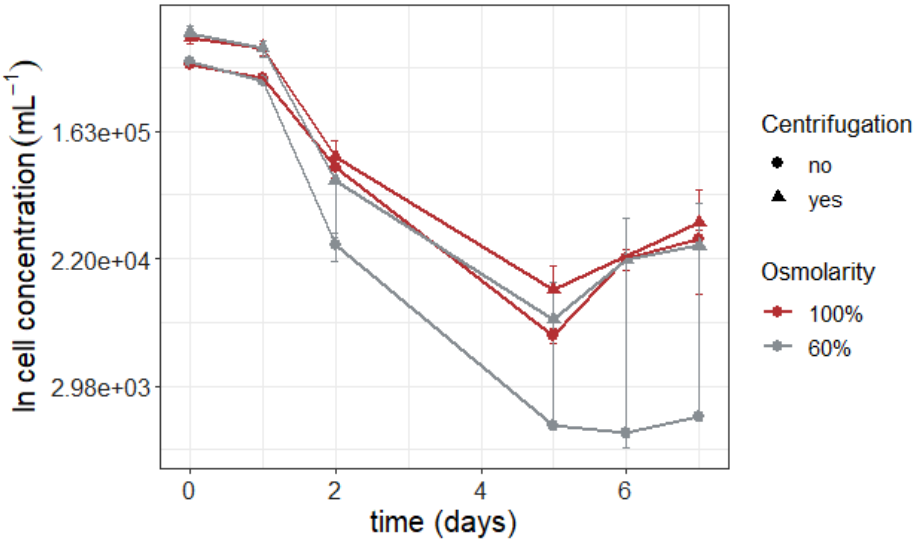

Figure 9 Cell concentrations of the centrifugation test with *Synechococcus* RCC2384 over seven days. The average cell concentrations (per mL, n = 3) with standard deviation for 100% and 60% osmolarity (indicated by colour) are shown over time (days) in natural logarithm projection of the y-axis. Centrifugation protocol is indicated by shape.

4.1.2. *Synechococcus* PCC7942

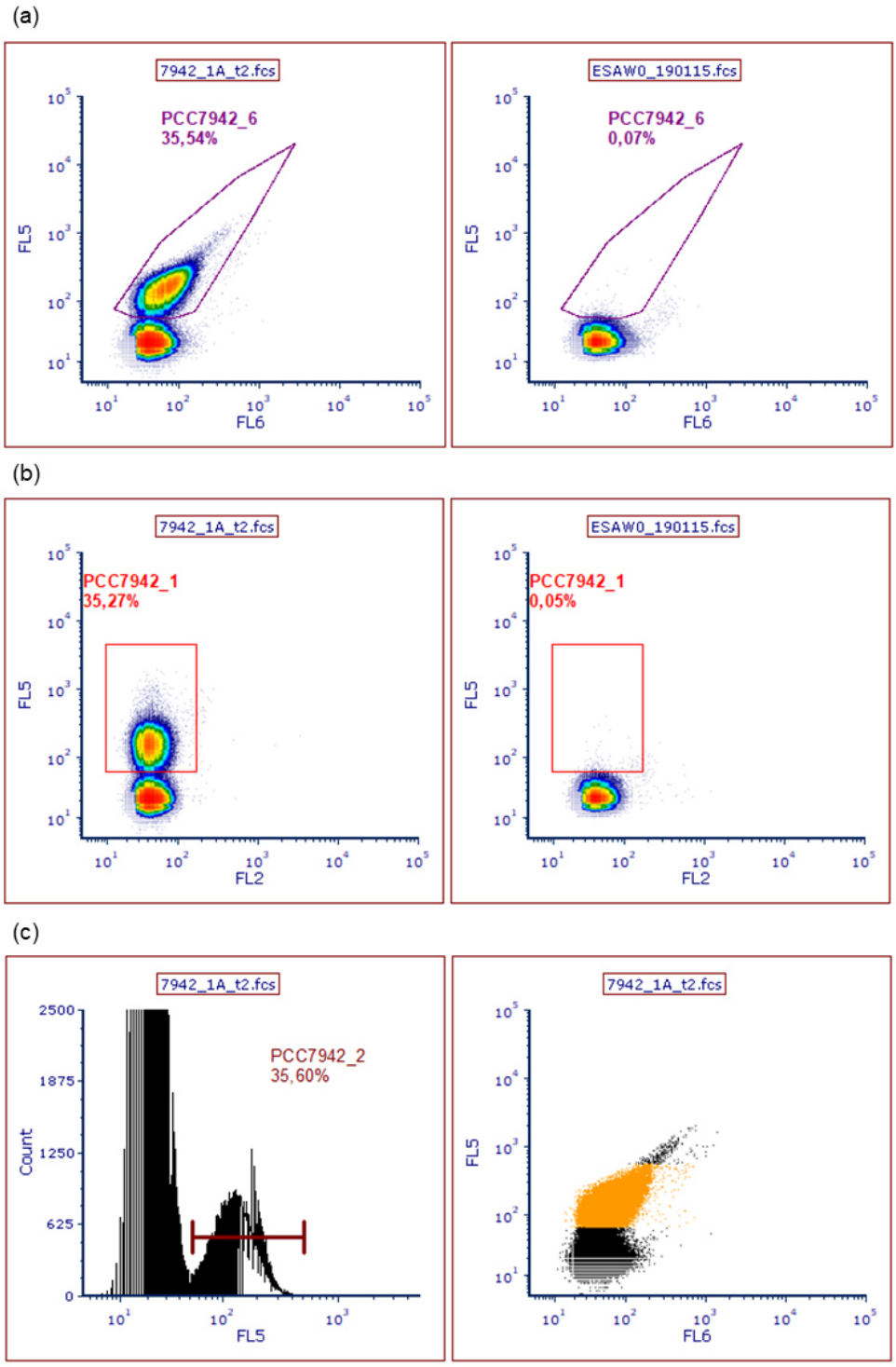

Figure 10 Exemplary presentation of the gates used to quantify the number of *Synechococcus* PCC7942 cells, for sample 1A at t_2 of the growth curve and 0% ESAW medium as a control. The number of cells was determined with the PCC7942_6 gate in the projection of the fluorescent signal strength of phycocyanobilin (FL5) plotted against the fluorescent signal in the far-red wavelength spectrum (FL6) after excitation at 638 nm (a). Additionally, PI-stained particles were enumerated in the gate PCC7942_1 in the projection of FL5 over the emission of phycoerythrobilin (FL2) after excitation at 638 and 488 nm respectively (Figure 11). The area of PCC7942_4 corresponded roughly to the peak area marked as Gate PCC7942_2 in the histogram of counts over signal intensity of FL5 (c).

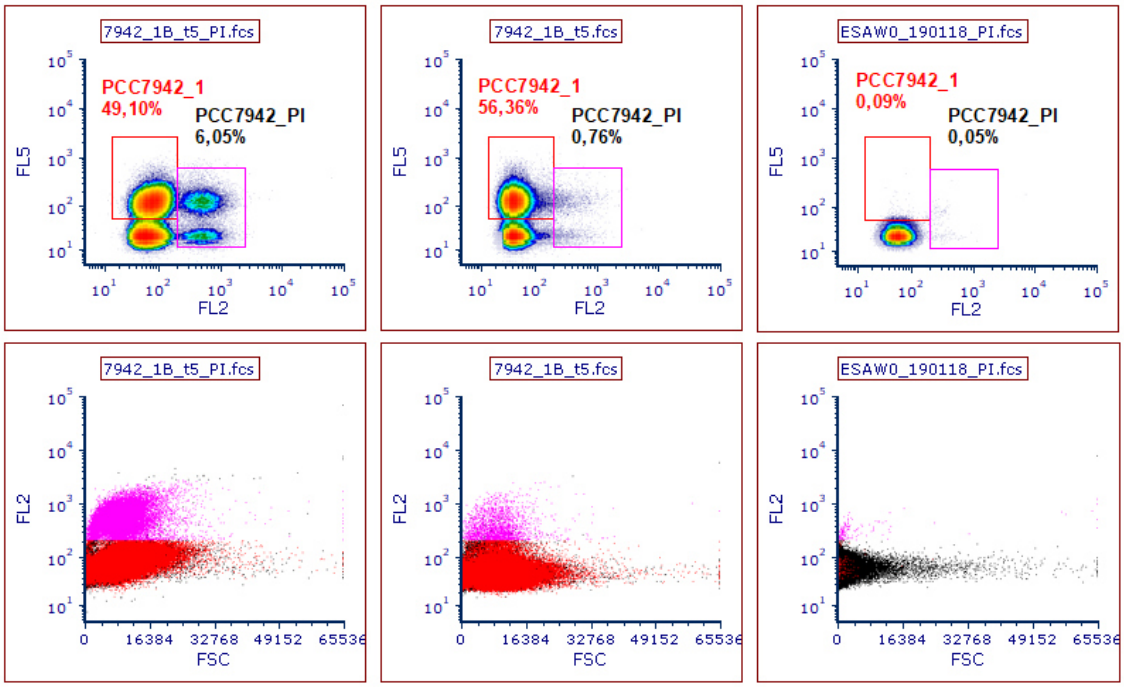

Figure 11 Exemplary presentation of the gates used to quantify the number of *Synechococcus* PCC7942 cells. The population was marked in gate PCC7942_1 and the population stained with PI was marked in Gate PCC7942_PI in the projection of the fluorescent signal strength of phycocyanobilin (FL5) plotted against PI (FL2) after excitation at 638 and 488 nm respectively. Shown here is sample 1B from the growth cycle experiment of PCC7942 (30% ESAW pH 8.2) at t_5 both stained with PI (left), unstained (middle) and sterile 0% ESAW medium as a control (right). The gates PCC7942_1 and PCC7942_PI were also marked in the FL2 over forward scatter plot with PCC7942_1 in red and pink respectively.

The freshwater strain PCC7942 was enumerated with the fluorescent emission of phycocyanobilin (Figure 10) with a CyFlow Cube8 flow cytometer (Sysmex Partec, Germany). Phycocyanobilin is the primary chromophore in this strain as the phycobilisome of the strain includes no phycoerythrin. This allowed for the addition of propidium iodide (PI), whose fluorescent emission is in the range of phycoerythrin, to the samples to enumerate dead cell material. The staining protocol had no significant effect on the number of living cells counted by phycocyanobilin fluorescence (Figures 11 - 12 and page 97 in the Appendix). The observation of growth by pigment auto-fluorescence also enabled simultaneous measurements of the pigment content as signal strength per fluorescent particle (Figure 13).

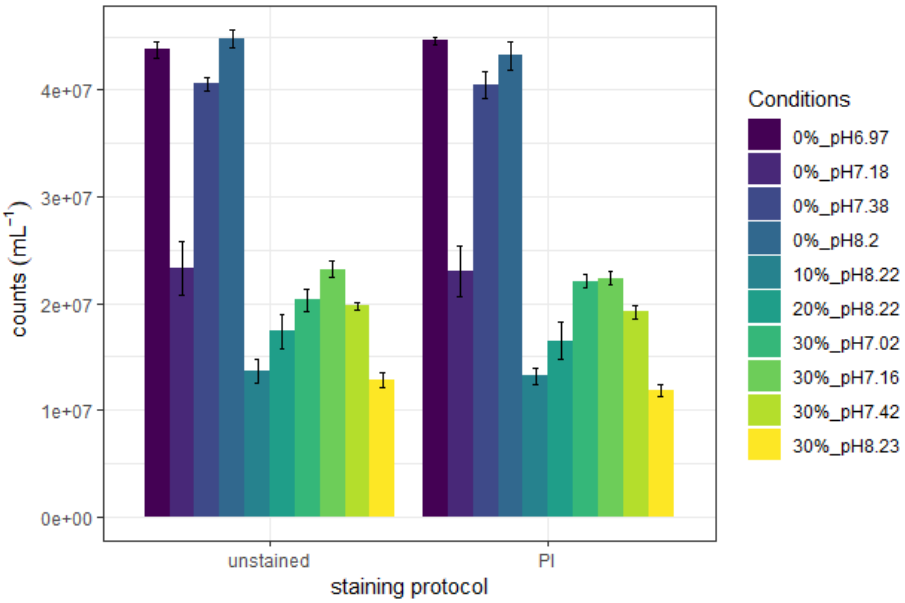

Figure 12 Comparison of cell concentrations from unstained and propidium iodide (PI) stained samples seven days after inoculation recorded at t_4 of the growth curve of *Synechococcus* PCC7942. Shown here are the average cell concentrations (n = 4) with standard deviations per condition and ordered by staining protocol.

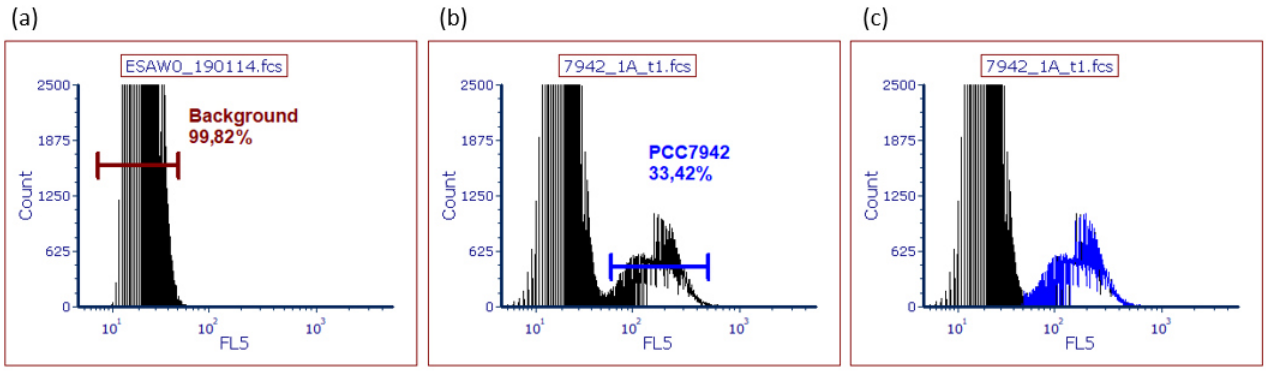

Figure 13 Exemplary presentation of the gates used to quantify the pigment content of *Synechococcus* PCC7942 cells. The background signal was identified in the histogram of counts over phycocyanobilin (FL5) signal strength for sterile medium of the respective osmolarity (a). This area marked in the background gate was then subtracted from the sample, shown here for 1A at t_1 of the growth curve. Pigment content was enumerated based on the statistics of the remaining peak (marked in blue in (c)).

4.2. Initial Trials with *Synechococcus* RCC2384

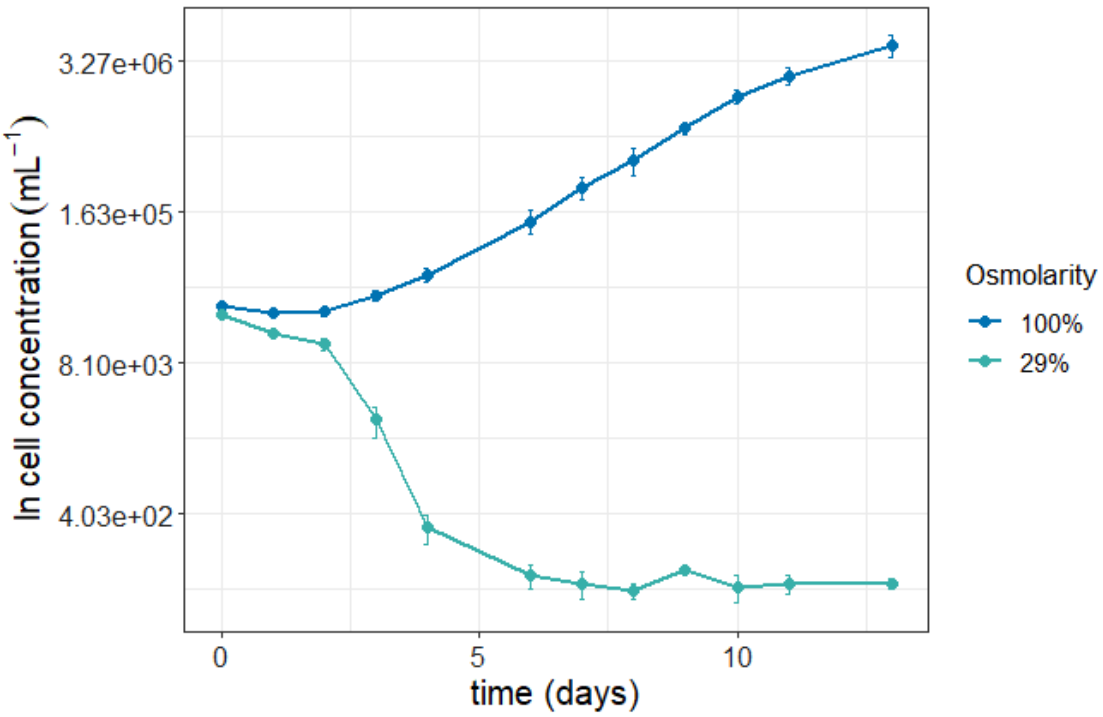

Figure 14 First quick adaptation test with *Synechococcus* RCC2384 over two weeks. Average cell concentrations (per mL, n = 5) with standard deviation are shown over time (days) for both 100% and 29% cultures in natural logarithm projection of the y-axis.

In the first quick adaptation test, the cell concentration per mL (Figure 14 and Figure 28 in the Appendix) of the 29% cultures started to decrease in number already one day after inoculation. After 4 days, all populations of the 29% cultures were undetectable in the flow cytometer, whereas the 100% control showed a visible increase from day 2 onwards, reaching a maximum of $> 5.0 \cdot 10^6$ cells mL^{-1} after 13 days. After nine days, auto-fluorescent bacteria were visible in all replicates of the control when viewed in the red filter of the epifluorescence microscope. However, counting was impossible as the DAPI staining had failed and the auto-fluorescent signal was not sufficient for quantification. No or very few particles were visible in the replicates of 29%.

Replicate 100D followed a different growth cycle as the other replicates of the control (Figure 29 the Appendix) as the culture reached its maximum cell density while the other replicates were still growing exponentially and subsequently started to decrease in cell concentration. The control cultures reached an average growth rate of 7.56 ± 2.7 day^{-1} between days 3 to 10, whereas the decrease of the 29% ESAW cultures reached -0.88 ± 0.04 day^{-1} between days 3 and 4. Furthermore, the F_V/F_M values were determined for the starter culture (average of 0.105 at t_0) as well as for the control cultures (average of 0.118 at t_{10}) since at that time cells were not detectable anymore in the 29% cultures. As the cells were not able to recover and adapt to medium of 29% osmolarity after the shock of inoculation, the range of adaptability was tested further in the second quick adaptation test.

Cell concentrations reduced drastically in every condition between the measured timepoints t_0 and t_1 (Figures 30 - 31 in the Appendix). As the populations were undetectable in the flow cytometer from the third day after inoculation onwards, only the control condition was recorded further until the end of the experiment 12 days after inoculation, apart from the 90% cultures on day 10. The 100% control cultures recovered by day 7 and reached cell densities of $1 \cdot 10^5$ cells mL^{-1} by day 12. Nevertheless, such a recovery was not visible in the 90% cultures after 10 days and the experiment could not be continued further due to time constraints. The rapid decrease in cell concentration per mL was accompanied by an increase in pH in the subsamples taken out from each culture for flow cytometric measurements (Figure 32 in the Appendix). The cause for the rapid decrease in cell concentrations was tested with ESAW medium prepared with salts by different suppliers as the medium for the second quick adaptation and subsequent tests was prepared with components from another supplier than the first test with RCC2384. However, observation over eight days showed that the duplicates inoculated in medium with components from Supplier II increased in cell density over time, whereas the cell density of cultures inoculated in medium with ingredients from Supplier I was below the detection limit of the flow cytometer from 24 hours after inoculation until the end of the experiment (Figures 33 - 34 in the Appendix). Similar decreases in cell concentration were again measured during the development of the centrifugation protocol (Figure 9). Therefore, as RCC2384 did not survive the transfer to 29% osmolarity and the failed experiments gave no indication that growth would be possible under low osmolarity conditions between 100% - 40% ESAW, the focus was subsequently shifted to the freshwater strain PCC7942.

4.3. Characterisation of *Synechococcus* PCC7942

4.3.1. Cell Concentrations & pH

For the freshwater strain PCC7942, maximum cell density was reached one week after inoculation in all conditions, except in condition 3 (Figure 15 and Figure 38 in the Appendix). In this condition (0% and pH 7.18), the maximum cell concentration was reached on day 10 of the growth curve. The control conditions of the lowest osmolarity showed the highest cell concentrations, reaching maximal concentrations of approximately $4 \cdot 10^7$ cells mL^{-1}, whereas, the maximum values ranged between $1 - 2 \cdot 10^7$ cells mL^{-1} in the other conditions. However, after the initial increase, the cell concentrations decreased rapidly regardless of condition. No condition showed a characteristic stationary phase after a sigmoid shaped curve. This decrease in cell concentrations was accompanied by an increase in PI stained events suggesting rapid cell mortality in the cultures. Moreover, the decrease continued in the second week of incubation into the last measured time-point 17 days after inoculation in control conditions 0% ESAW and pH 8.2 and 7.4. The cultures entered a second cycle of cell growth in 0% ESAW, pH 7.2 and 7.0 while the cultures of higher osmolarity reached a steady state at $< 1 \cdot 10^7$ cells mL^{-1}.

The number of PI-stained events surpassed the number of events recorded in the PCC7942 gate during the phase of rapid cell mortality in conditions 0% ESAW pH 7.4 and 7.2. This was not the case in conditions 0% pH 7.0, where the number events in the PI gate never surpassed the number of events in the PCC7942 gate until the last measured time-point and condition 0% ESAW pH 8.2 where the number of PI stained particles followed the shape of the curve of the cell particles. In general, the concentrations in higher osmolarities were lower than those in conditions of 0% osmolarity which was also reflected in the number of events recorded in the PI gate. The concentration of PI stained particles exceeded those recorded in Gate PCC7942 in the 10% and 20% conditions on day 11 of the growth curve. Yet, whereas the PI stained particle concentration rose in conditions of 30% osmolarity, their number was never greater than the cell concentration. Thus, high cell densities were accompanied by higher number of PI-stained particles.

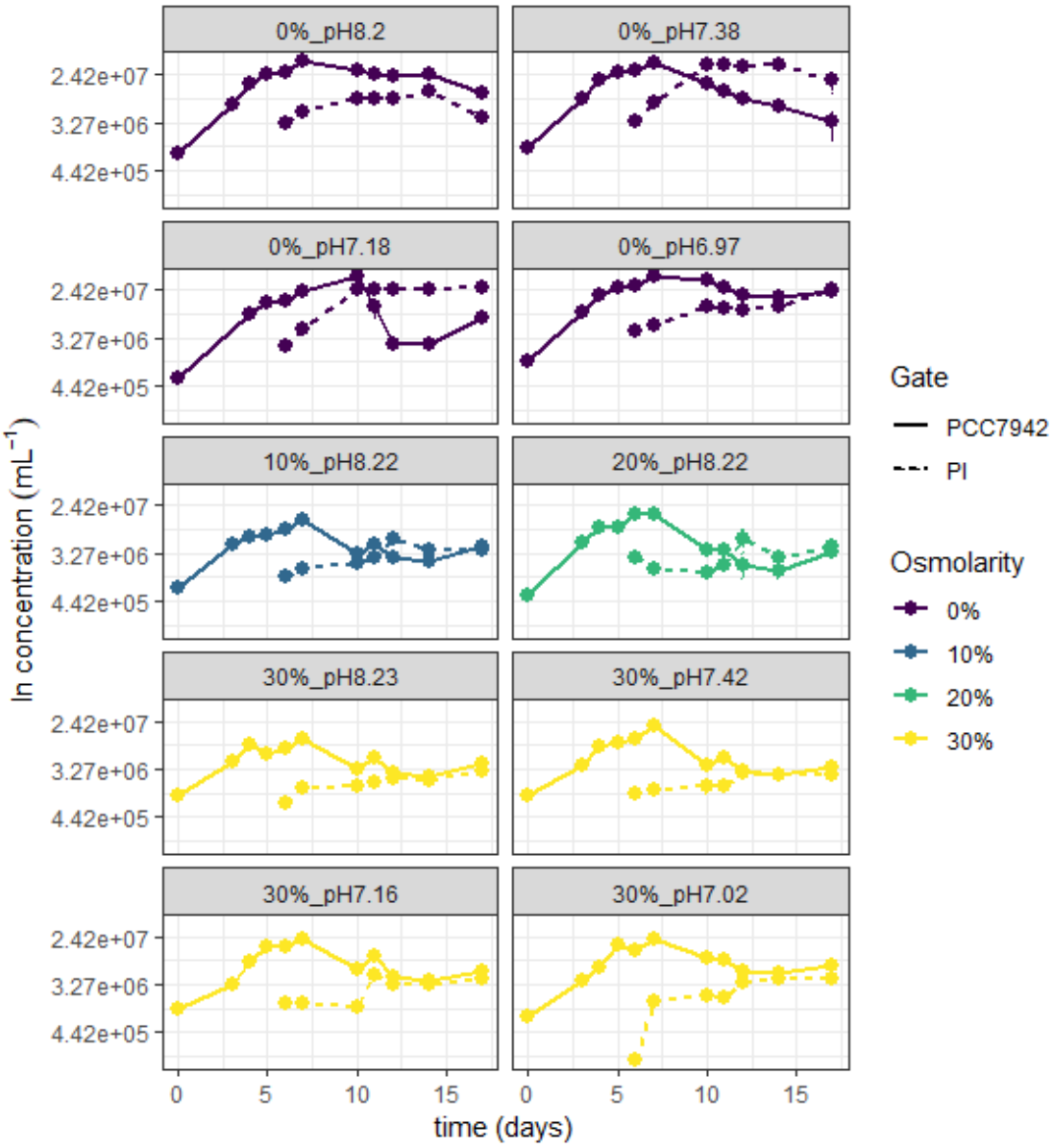

Figure 15 Growth curve of *Synechococcus* PCC7942 over 17 days. Shown here are the averages (n = 4) with standard deviations for the concentrations (mL^{-1}) of PCC7942 cells (solid line) and PI stained particles (dashed line) over time (days). The osmolarity condition of the medium is indicated by colour and the cell concentrations are shown in natural logarithm projection on the y-axis.

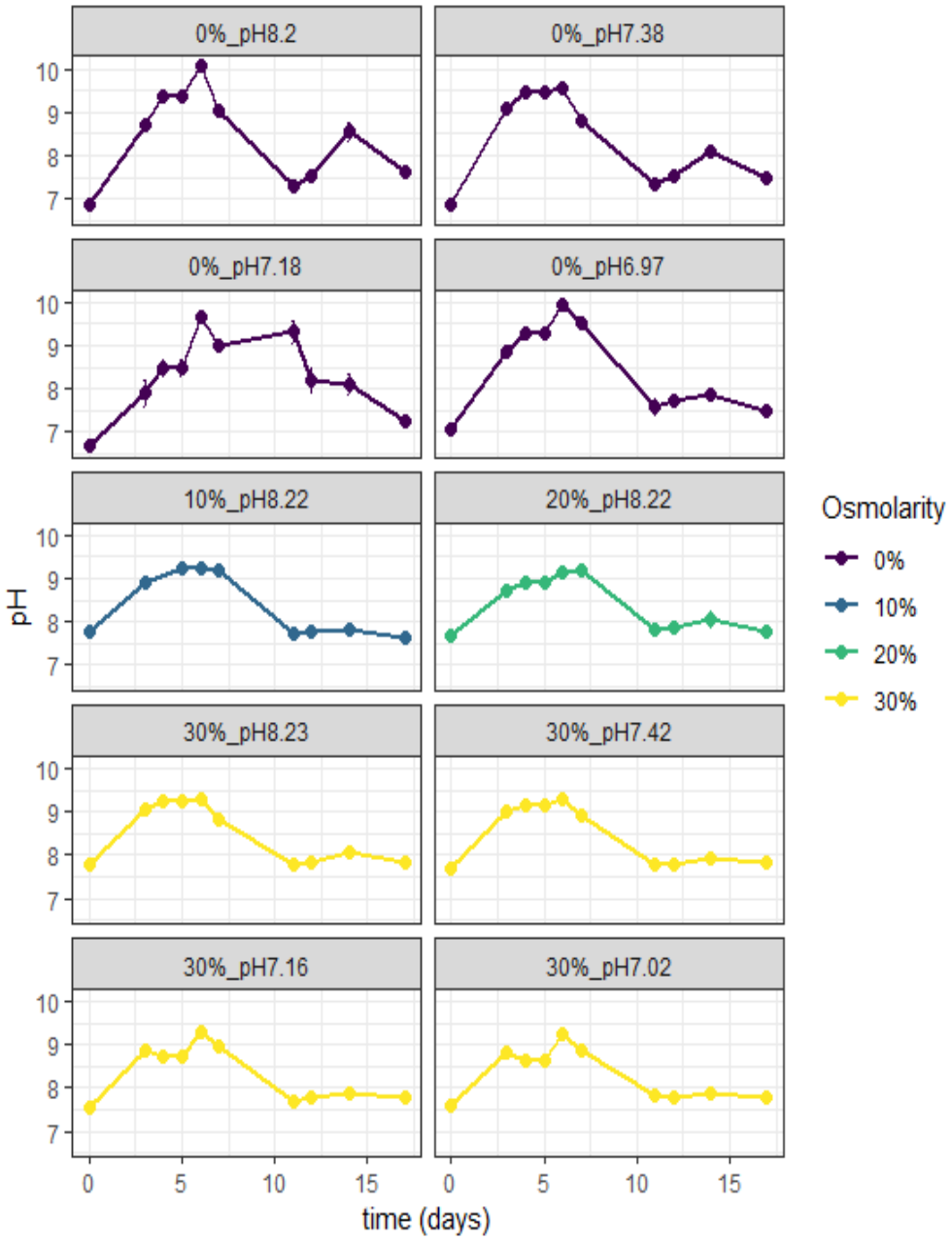

Figure 16 Growth curve of *Synechococcus* PCC7942 over 17 days. Average pH measurements (n = 4) with standard deviations are plotted against time (days). The osmolarity condition of the medium is indicated by colour.

The pH values measured in subsamples of the cultures mirrored the development of cell concentration per mL over time (Figure 16). The maximal pH values were recorded a day before the cultures reached their maximal cell concentration. In general, the pH range was wider in the control conditions of 0% ESAW, ranging from < pH 7 at t_0 and up to pH 10 at its highest. In contrast, the pH ranges were between pH 7.5 and 9.5 for replicates in conditions of higher osmolarity. The pH dropped after the initial peak around the 6th day and stayed around pH 8 after that.

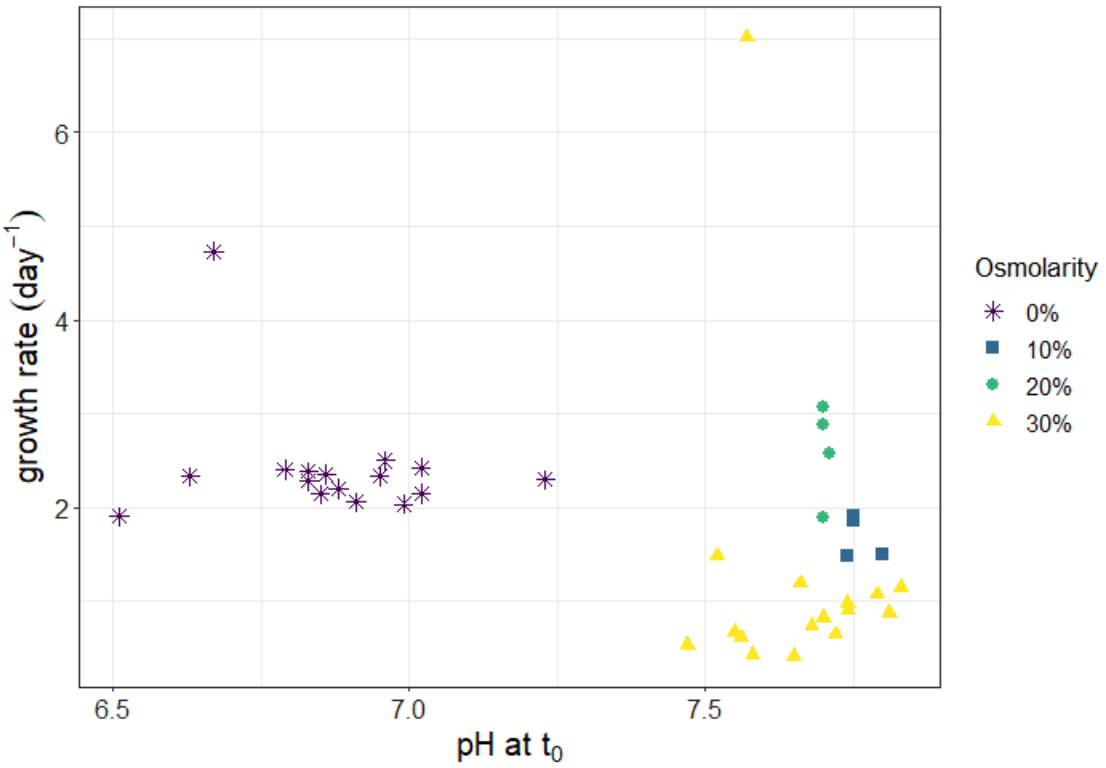

Figure 17 Growth rates of *Synechococcus* PCC7942 in different osmolarity conditions ($t_0 - t_1$) plotted against pH values measured at t_0. The osmolarity of the growth medium is indicated by shape and colour.

The growth rates measured during exponential growth were 2.4 ± 0.64 day^{-1} for 0% salinity, 1.7 ± 0.23 (10%), 2.6 ± 0.51 (20%) and 0.84 ± 0.3 day^{-1} (30%), respectively (Table 4). For the purpose of comparison only the growth rates of each condition between the time period $t_0 - t_1$ (three days) was taken into account. A clear separation between samples of 0% ESAW and those of higher osmolarities was visible, when plotted against pH at time t_0 (Figure 17). Apart from one possible outlier, all samples of 0% osmolarity showed growth rates around 2 - 2.5 day^{-1}. In general, the pH measured at t_0 was lower in 0% osmolarity samples than in samples of higher osmolarity. For these conditions the replicates grouped closely together, at high pH and relatively low growth rates. The growth rates of conditions 10 and 20% osmolarity were < 2 day^{-1} and 2 - 3 day^{-1} respectively. The 30% osmolarity samples showed the lowest growth rates of ca. 0.5 – 1.5 day^{-1} apart from one outlier.

The analysis of variance showed no significant effect of either the adjusted pH nor the osmolarity of the medium on the growth rates (page 98 in the Appendix), although the pH at t_0 did have a significant effect ($p = 0.0482$, $n = 40$).

Table 4 Growth rates recorded for *Synechococcus* PCC7942. Average pH values measured at t_0 of the growth curve (n = 4) are given per condition. Average growth rates (day^{-1}, n = 4) from four replicates per condition are given for $t_0 - t_1$ (3 days) and for other time-points, which are specified in the fourth column.

Condition	pH at t_0	Growth Rate ($t_0 - t_1$) (day^{-1})	Time-points	Time (days)	Growth Rate (day^{-1})
0% pH 8.2	6.87	2.22 ± 0.13	$t_0 - t_2$	4	4.46 ± 0.66
0% pH 7.4	6.89	2.33 ± 0.2	$t_0 - t_2$	4	4.3 ± 0.24
0% pH 7.2	6.67	2.78 ± 1.31	$t_1 - t_3$	2	0.85 ± 0.15
0% pH 7.0	7.05	2.3 ± 0.11	$t_0 - t_2$	4	3.79 ± 0.42
10% pH 8.2	7.76	1.69 ± 0.23	$t_0 - t_2$	4	1.88 ± 0.25
20% pH 8.2	7.70	2.61 ± 0.52	$t_0 - t_2$	4	3.94 ± 0.44
30% pH 8.2	7.79	1.02 ± 0.12	$t_0 - t_2$	4	1.80 ± 0.26
30% pH 7.4	7.69	0.92 ± 0.2	$t_0 - t_1$	3	0.92 ± 0.2
30% pH 7.2	7.56	0.72 ± 0.51	$t_0 - t_1$	3	0.72 ± 0.51
30% pH 7.0	7.60	0.64 ± 0.03	$t_0 - t_2$	4	1.16 ± 0.07

4.3.2. Pigment Content

Additionally, the pigment content of the cultures was monitored over time and the general pattern remained the same, irrespective which type of average was considered (Figure 18 and Figures 39 - 40 in the Appendix). The average normalised fluorescent signal decreased during the first week of incubation. A recovery was visible in the second week of incubation in the control conditions of 0% ESAW. However, this was not mirrored in the conditions of higher osmolarity, where the pigment content increased, even surpassing the value measured at t_0 on day 10 in the conditions 10% ESAW, 30% pH 8.2 and 30% pH 7.4. Nevertheless, the normalised values of these time-points also had a high standard deviation.

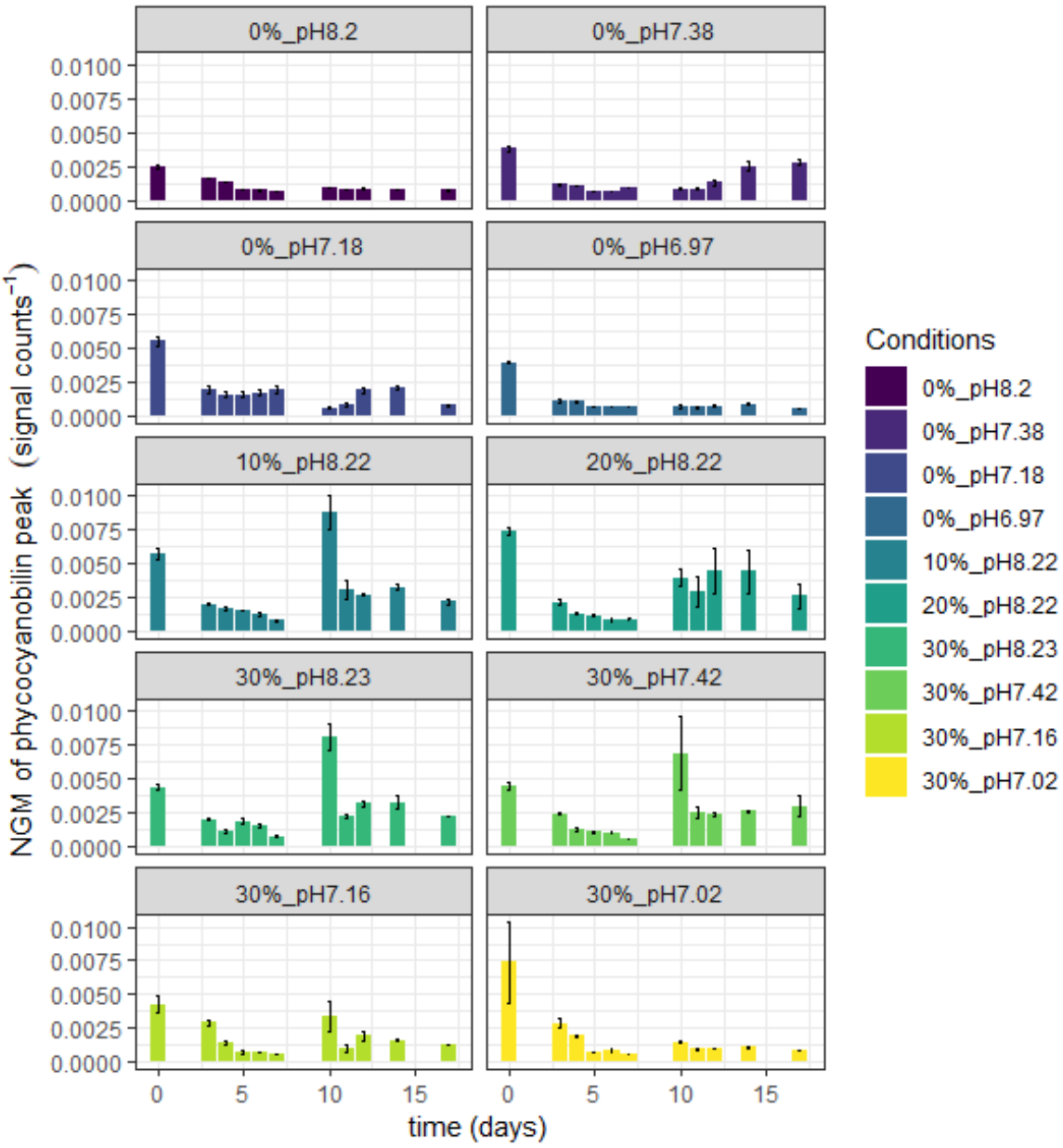

Figure 18 Normalised geometric means (NGM, signal counts^{-1}) of the phycocyanobilin peaks of *Synechococcus* PCC7942 plotted against time (days) and ordered by condition (indicated by colour).

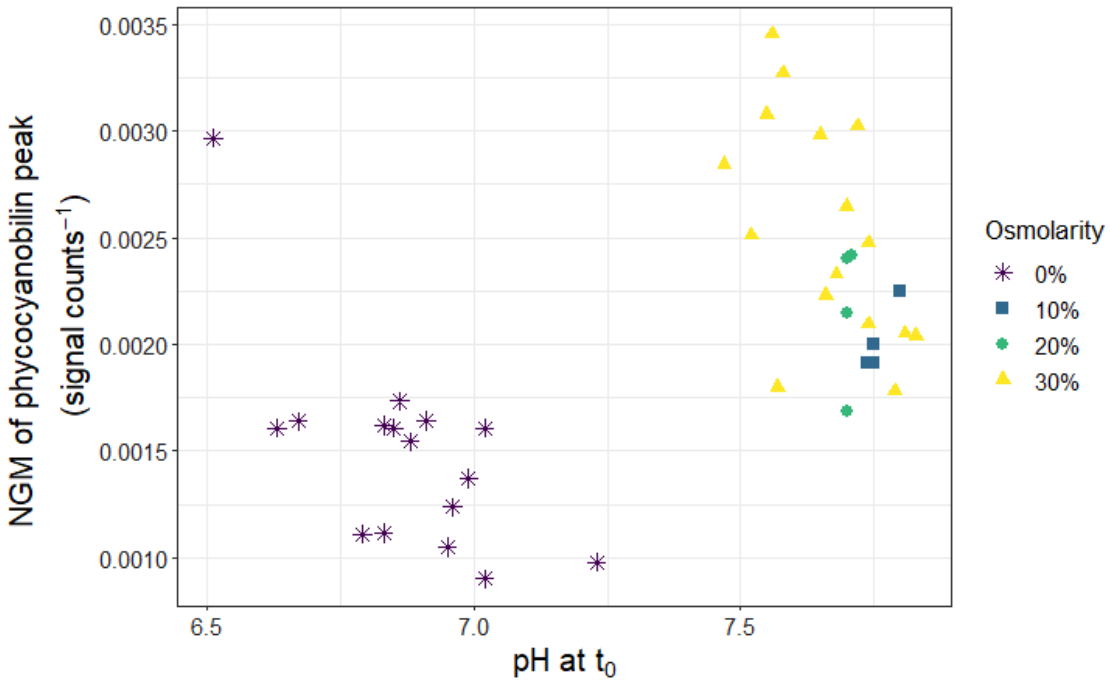

Figure 19 Normalised geometric means of the phycocyanobilin peaks of *Synechococcus* PCC7942 at t_1 (signal counts^{-1}) plotted against pH values measured at t_0. The osmolarity of the medium is indicated by shape and colour.

A clear grouping of the normalised geometric means of the FL5 peaks at t_1 by osmolarity also became visible when plotted against pH at t_0 (Figure 19). Samples of 0% osmolarity showed lower initial pH values and lower normalised geometric means than those of higher osmolarities. The replicates of 10 and 20% osmolarity grouped tightly together, whereas those of 30% osmolarity were scattered more. The analysis of variance showed that both the pH at t_0 ($p = 3.18 \cdot 10^{-5}$, $n = 40$) and the osmolarity ($p = 1.58 \cdot 10^{-5}$, $n = 40$) of the medium had a significant effect on the normalised geometric means (page 100 in the Appendix). The interaction of the two explanatory variables was not found to be significant.

4.4. Testing of the µRespirometer

The oxygen production of RCC2384 was monitored over 24 h under constant illumination with the µRespirometer, however, oxygen production could only be measured from the tenth hour onwards as the oxygen concentration first decreased although the chamber was illuminated. Then, presumably an air bubble managed to get into the measurement chamber and disrupted the oxygen measurements (Figure 20). Both the inlet and outlet

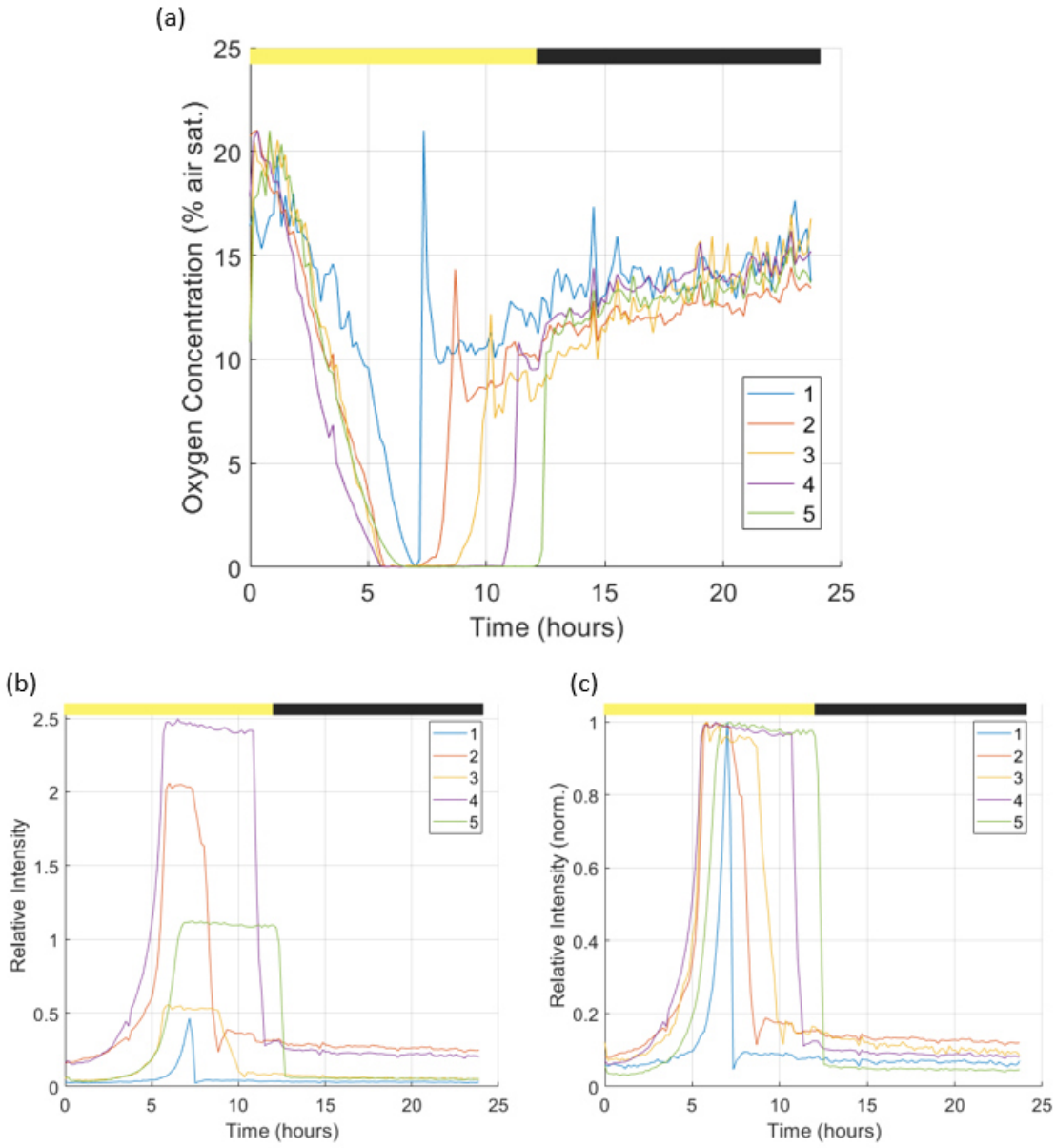

Figure 20 Oxygen measurement of *Synechococcus* RCC2384 over 24 hours in the µRespirometer. The oxygen concentration (% air sat., a) relative (b) normalised relative intensity (c) recorded by the camera are plotted against time (hours). Shown here are the values from the five oxygen sensing spots (indicated in the legend) of the microfluidic chip. Pictures were taken every 10 min and the temperature was set to 30 °C. The measurement chamber was illuminated in a 12:12 hour diurnal cycle from the start of the measurement (as indicated by the bar at the top) and the light was provided by a red-coloured LED at a current of 50 mA.

were sealed air-tight during subsequent measurements. Moreover, a slight increase in oxygen production was visible when the chamber was not illuminated, when oxygen consumption was expected. A control measurement with sterile 100% ESAW showed a steady oxygen concentration over 4 h under constant illumination (Figure 35 in the Appendix). The concentration only changed once the system was flushed with water of a defined oxygen concentration of around 5% air saturation (air sat.), four hours into the measurement. Subsequently, the µRespirometer was tested with the two PCC strains.

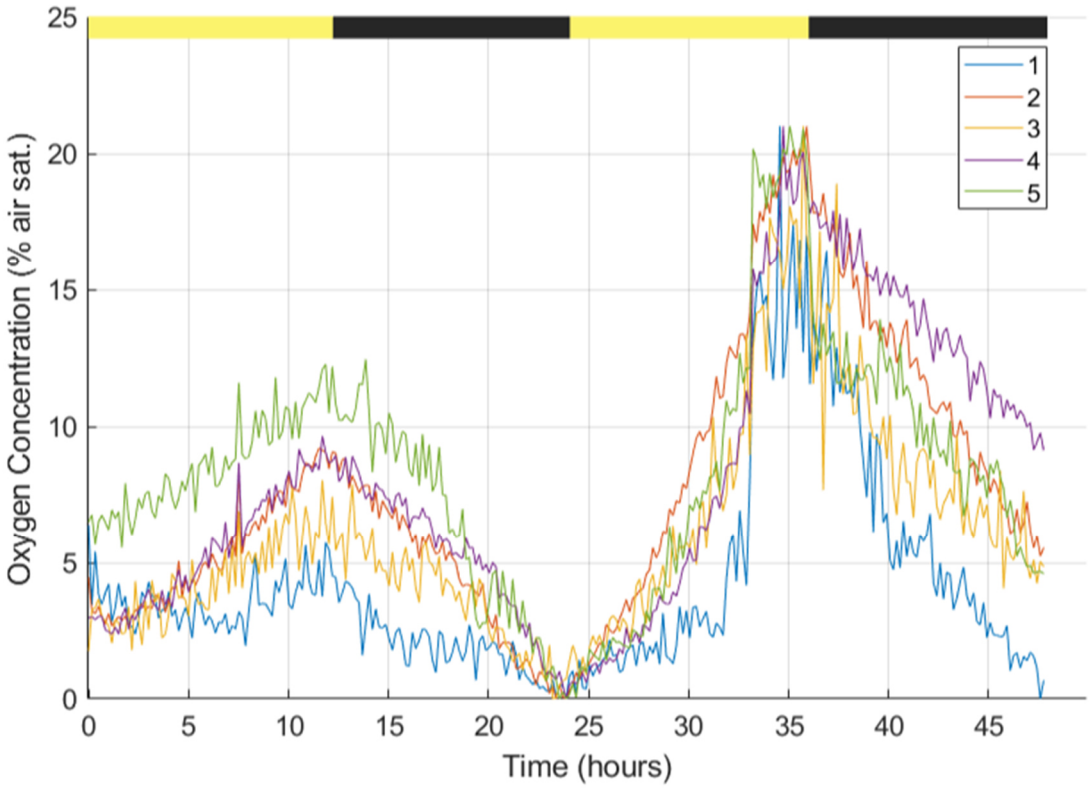

Figure 21 Oxygen measurement with *Synechococcus* PCC7002 in the µRespirometer over 48 hours. The oxygen concentration (% air sat.) calculated from the intensity of the phosphorescent signal is plotted against time (hours). Shown here are the values from the five oxygen sensing spots (indicated in the legend) of the microfluidic chip. Pictures were taken every 10 min and the temperature was set to 30 °C. The measurement chamber was illuminated in a 12:12 hour diurnal cycle from the start of the measurement (indicated by the bar at the top) and the light was provided by a red-coloured LED at a current of 50 mA.

Due to time constraints, PCC7002 could not be characterised in detail. However, the optimal conditions for the maintenance of the strain were determined to be 25 °C, ca. 26 µmol photons m^{-2} s^{-1} of cool white fluorescent light and 100% ESAW medium. The oxygen production of the strain was measured once over 48 hours, and the culture produced oxygen during intervals of illumination (Figure 21 and Figure 36 in the Appendix). Moreover, the air saturation with oxygen increased in the second light-dark cycle, indicating an increase in cell numbers.

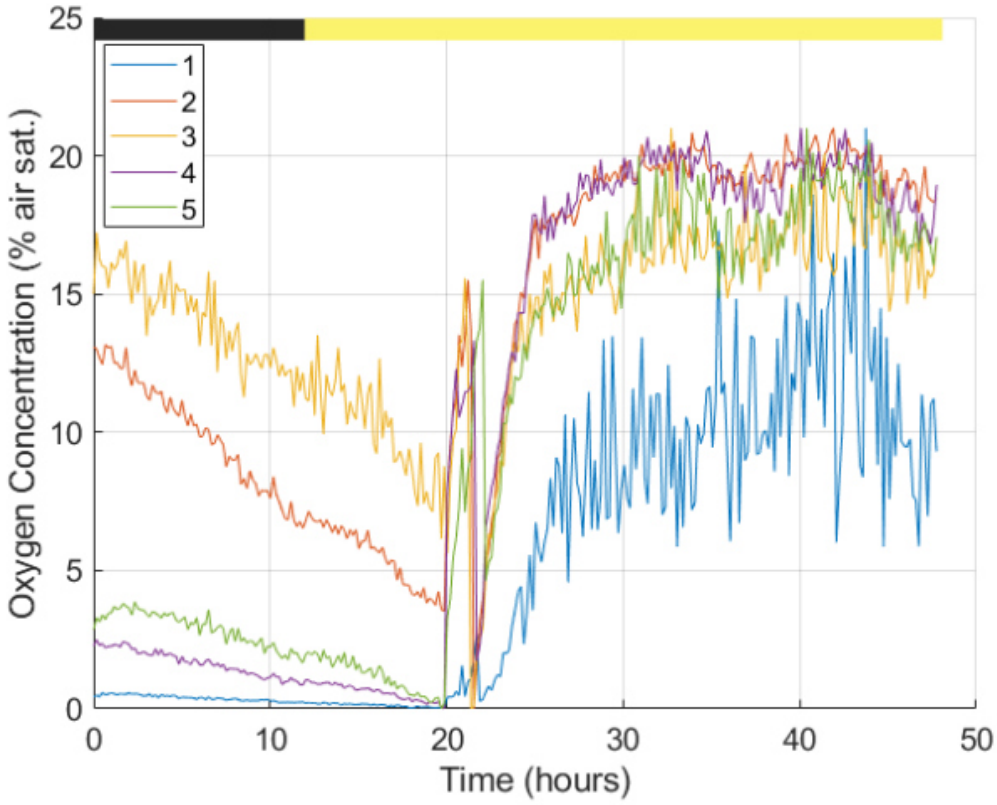

Figure 22 Oxygen measurement with *Synechococcus* PCC7942 in the µRespirometer over 48 hours. The oxygen concentration (% air sat.) calculated from the intensity of the phosphorescent signal is plotted against time (hours). Shown here are the values from the five oxygen sensing spots (indicated in the legend) of the microfluidic chip. Pictures were taken every 10 min and the temperature was set to 30 °C. The timespans of darkness and illumination are indicated by the bar at the top. The light was provided by a red-coloured LED at a current of 50 mA.

A photosynthesis versus irradiance curve was attempted for PCC7942, in that after 12 hours of darkness the light intensity would be increased every 9 hours in 50 mA steps up to 200 mA (Figure 22 and Figure 41 in the Appendix). However, the program continued illumination at 50 mA and just printed the set values in the measurement protocol. Moreover, the oxygen concentration initially continued to decrease even when the illumination LED was switched on 12 h into the measurement. At around 20 h, the oxygen concentration in all sensing spots except the first increased, which was rapidly followed by a decrease to ca. 0% air sat. This shows some similarities to Figure 20, where an air bubble likely disturbed the measurement. The oxygen levels remained constant after ca. 24 h, although spot 1 recorded noticeably lower concentrations than the other sensing spots.

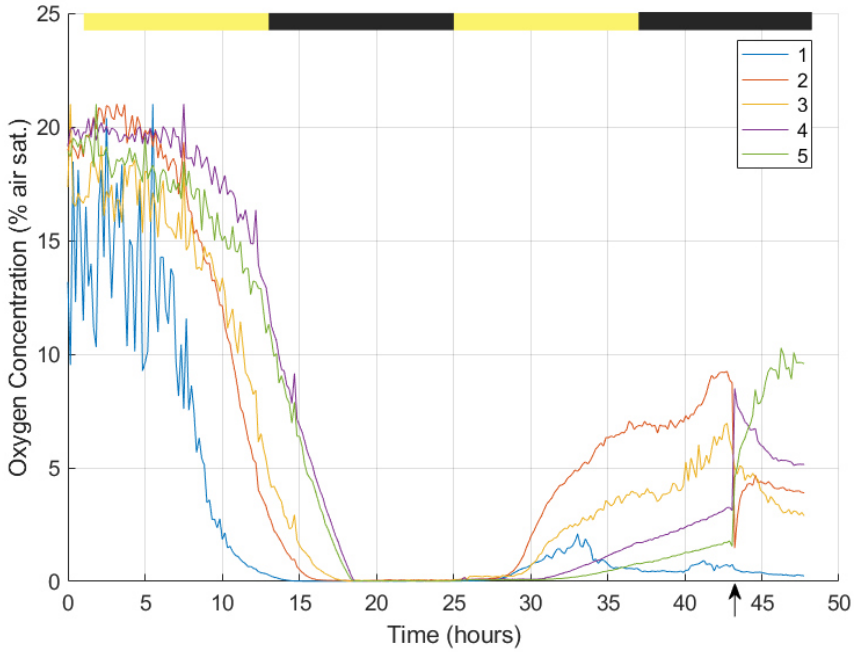

Figure 23 Oxygen measurement of *Synechococcus* PCC7942 over 48 hours in the µRespirometer as part of the growth curve (0% ESAW pH 8.2) 4 days after inoculation. The oxygen concentration (% air sat.) was calculated from the intensity of the phosphorescent signal is plotted against time (hours). Shown here are the values from the five oxygen sensing spots (indicated in the legend) of the microfluidic chip. Pictures were taken every 10 min and the temperature was set to 30 °C. The measurement chamber was illuminated in a 12:12 hour diurnal cycle shifted one hour from the start of the measurement (as indicated by the bar at the top) and the light was provided by a red-coloured LED at a current of 50 mA. At 43 h and 20 min the system was flushed with water with an oxygen concentration of 3% air sat. (indicated by the arrow on the x-axis). The cell density was ca. $1.32 \cdot 10^7$ cells mL^{-1} at the start of measurement.

In the first measurement during the growth curve of the control condition (0% ESAW pH 8.2) four days after inoculation, an increase on oxygen concentration was visible in the second day cycle (Figure 23 and Figure 42 in the Appendix). Nevertheless, decrease of oxygen level already started during the first light period. Flushing with water of a defined low oxygen concentration (3% air sat.) only affected the oxygen concentration momentarily. Furthermore, the concentrations recorded at spot 1 were again lower than those at other sensing spots.

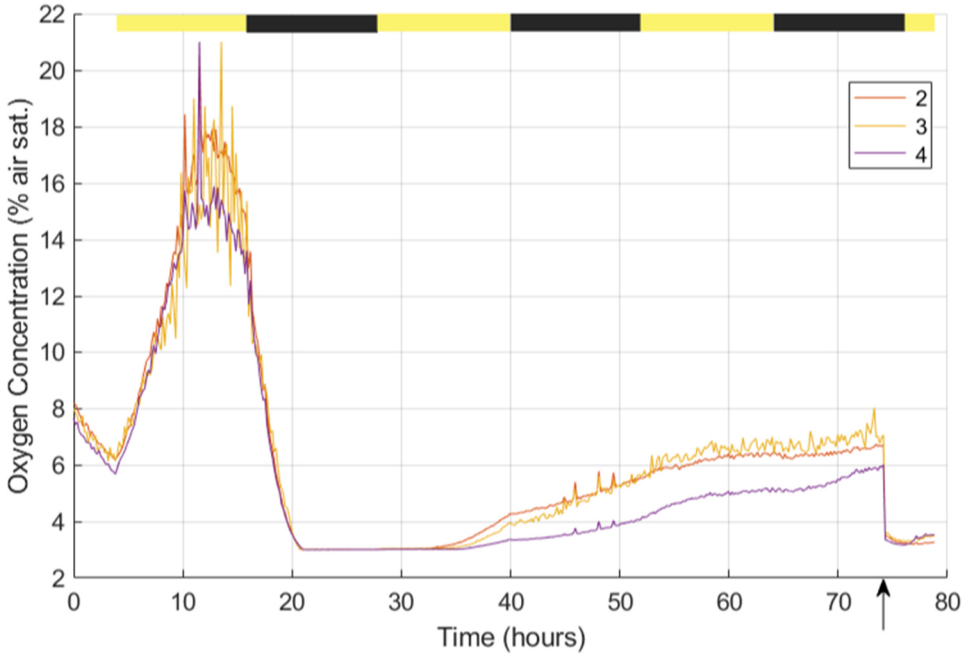

Figure 24 Oxygen measurement of *Synechococcus* PCC7942 over 79 hours in the µRespirometer as part of the growth curve (30% ESAW pH 7.0). The oxygen concentration (% air sat.) was calculated from the intensity of the phosphorescent signal is plotted against time (hours). Shown here are the values from the three oxygen sensing spots (indicated in the legend) of the microfluidic chip. Pictures were taken every 10 min and the temperature was set to 30 °C. The measurement chamber was illuminated in a 12:12 hour diurnal cycle shifted four hours from the start of the measurement (as indicated by the bar at the top) and the light was provided by a red-coloured LED at a current of 50 mA. At 74 h and 10 min the system was flushed with water with an oxygen concentration of 3% air sat. (indicated by the arrow on the x-axis). The data from spots 1 and 5 were removed from the graph for clarity. The cell density was ca. $1.85 \cdot 10^7$ cells mL^{-1} at the start of measurement.

In contrast to the control, the oxygen concentration in a sample of condition 30% pH 7.0 seven days after inoculation, followed the timespans of illumination and darkness for the first 24 h (Figure 24 and Figure 43 in the Appendix). However, a steady increase was recorded over the subsequent day cycles regardless of whether the chamber was illuminated or not. Flushing with water (3% air sat.) led to an immediate decrease in oxygen concentration.

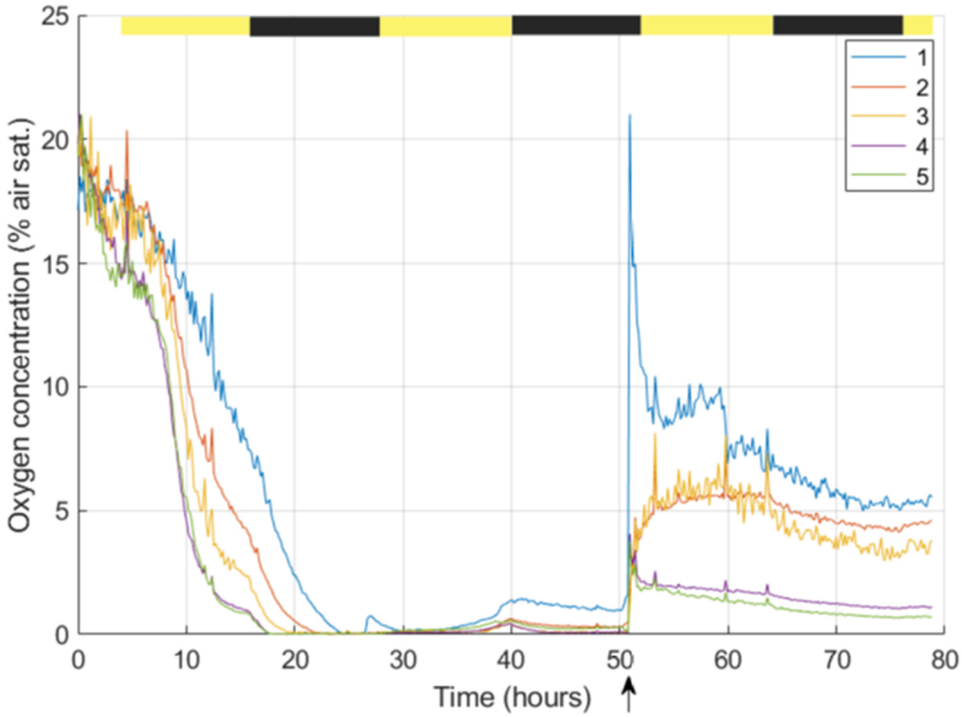

Figure 25 Oxygen measurement of *Synechococcus* PCC7942 over 79 hours in the µRespirometer as part of the growth curve (30% ESAW pH 7.0). The oxygen concentration (% air sat.) was calculated from the intensity of the phosphorescent signal is plotted against time (hours). Shown here are the values from the five oxygen sensing spots (indicated in the legend) of the microfluidic chip. Pictures were taken every 10 min and the temperature was set to 30 °C. The measurement chamber was illuminated in a 12:12 hour diurnal cycle shifted four hours from the start of the measurement (as indicated by the bar at the top) and the light was provided by a red-coloured LED at a current of 50 mA. At 74 h and 10 min the system was flushed with water with an oxygen concentration of 3% air sat. (indicated by the arrow on the x-axis). The data from spots 1 and 5 were removed from the graph for clarity. The cell density was ca. $2.12 \cdot 10^7$ cells mL^{-1} at the start of measurement.

When the control was measured again on the 12th day of the growth curve, no clear patterns of oxygen production and consumption were visible (Figure 25 and Figure 46 in the Appendix). Not only did the oxygen concentration decrease continuously during the first 24 h of measurement, but flushing with water (3% oxygen) led to a sharp increase in oxygen concentration. Both 0% and 30% of sterile ESAW medium showed a steady decrease in oxygen concentration when measured over 24 h (Figures 47 - 48 in the Appendix).

5. Discussion

The short-term adaptability of the two *Synechococcus* strains RCC2384 and PCC7942 was determined for a range of abiotic factors such as salinity/osmolarity, light level, temperature and pH. In the following section, the obtained growth rates will be compared to the available literature and possible adaptive processes will be discussed. The time scales of acclimatisation and growth will then be compared to common estuarine residence times to identify possible windows of time where adaptation and acclimatisation are possible. The strains will also be evaluated based on their suitability as endosymbionts for the treatment of chronic and slow-healing wounds. Furthermore, the applicability of the µRespirometer for continuous oxygen measurements with cyanobacterial cultures will be discussed.

5.1. Analysis of Initial Trials & Methodological Drawbacks

5.1.1. Initial Trials with *Synechococcus* RCC2384

Synechococcus RCC2384 was not able to cope with the osmotic shock of direct transfer into medium of lower osmolarity. While the cells did not immediately lyse, the cell concentrations started to decrease at once and the population was not detectable in the flow cytometer anymore after 4 days. The attempts to further clarify the osmotic tolerance range of RCC2384 failed, as all samples decreased in cell density regardless of condition. This may have been a side-effect of the move of the cultures into a new incubator with higher light levels than they were acclimatised to (130 µmol m^{-2} s^{-1} vs 26 or 100 µmol m^{-2} s^{-1}). The starter culture had been incubating in the new growth chamber for 4 days prior to inoculation of the second quick adaptation test and longer for the following experiments. However, the possibility cannot be discounted that the higher irradiance level led to fluorescent threshold changes in the cultures due to reduction of the photosynthetic apparatus. Kana & Glibert (1987) reported no photoinhibition of growth up to 2000 µmol m^{-2} s^{-1} for *Synechococcus* sp. WH7803. Pigment content was negatively correlated to growth irradiance and phycoerythrin was the most affected out of the pigments (Kana & Glibert, 1987). Like RCC2384, *Synechococcus* WH7803 is also classified under pigment type 3a (Grébert *et al.*, 2018b). Therefore, it is plausible that the increased light level would have led to lower pigment content per cell during the second quick adaptation test and subsequent experiments. The pigment content was essential to enumerate cells in these experiments as no dye was added and cells were counted based on auto-fluorescence

with flow cytometry. Nevertheless, such a rapid decrease and complete disappearance of the population in the flow cytometer suggests that the cells did not have enough time to acclimatise to the light levels and perished. Kana & Glibert (1987) raised irradiance levels stepwise and over several days, presumably giving the populations enough time to adapt to the higher light levels. However, Barlow & Alberte (1985) recorded an increase of in-vivo fluorescence of phycoerythrin after excitation at 560 nm in WH7803 as part of photoinhibition of cells which were not acclimatised to high levels of irradiation (≤ 250 µmol m^{-2} s^{-1}). As phycoerythrin auto-fluorescence was mainly used for counting cells here, photoinhibition alone is not likely to have led to such a rapid decrease in cell concentrations as was recorded here. The flow cytometer (CyFlow Cube8) is not optimized for auto-fluorescent phytoplankton and could have distorted the counted concentrations. Another explanation for the observed cell mortality could have been some component of the medium prepared with components from different suppliers. Nevertheless, the cell concentrations from the medium test firmly indicate that the medium components were not the cause.

The decrease in cell concentrations as counted by flow cytometry together with the increase in pH is contrary to expectations, and suggests three possibilities. First, the cell concentrations obtained may have been incorrect and some undetected cells caused the increase in pH by removing dissolved inorganic carbon from the medium for photosynthesis. Second, the cell concentrations may have been correct but a small population not detectable by flow cytometry survived and was very photosynthetically active, driving the pH increase. Third, the cell concentrations may have been valid and the increase in pH was caused by other processes e.g. cell lysis, which could explain the stationary pH towards the end of the second quick adaptation test as no new cells were lysed.

While the definite cause of the decreased cell concentrations could not be established in this project, there are indications that *Synechococcus* RCC2384 is sensitive to changes in light level and needs to be acclimatised slowly. Furthermore, temperatures of 30 °C, 100% salinity ESAW medium and irradiance levels of ca. 100 µmol m^{-2} s^{-1} were found to be optimal conditions for growth with growth rates of 7.56 day^{-1} during the initial exponential growth phase. To date, little has been published about this strain, however, this growth rate is a lot higher than those recorded for other strains of the same pigment type e.g. 0.5 - 2.0 day^{-1} for WH7803 first isolated from the Sargasso Sea recorded at irradiance up to 2000 µmol $m^{-2}s^{-1}$ (Kana & Glibert, 1987), > 2 day^{-1} for environmental

Synechococcus samples in the Arabian Sea (Liu *et al.*, 1998), ca. 1 day^{-1} for isolates from the coastal and pelagic Arabian Sea (Bemal & Anil, 2016). Moreover, a growth rate of ca. 0.5 day^{-1} has been reported for the Caribbean strain WH8102 (Mackey *et al.*, 2013a) as well as ca. 1 - 2 day^{-1} for *Synechococcus* strains of tropical North Atlantic origin at 30 °C (Pittera *et al.*, 2014). This suggests that the control culture conditions were close to the optimal growth conditions of the strain.

Some of the unique characteristics of the cyanobacterial photosystem impede traditional measurements of photosynthetic parameters such as F_V/F_M. The main difference to the photosynthetic apparatus of higher plants is that photosynthesis and respiration occur within the same membranes. The Phycobilisome (PBS) associates either with Photosystem I (PSI) or Photosystem II (PSII), allowing the organism to avoid photodamage and the accumulation of electrons at either point of the electron transport chain (Mackey *et al.*, 2013a). When PSI is preferentially excited and electron carriers are mostly oxidized, the photosystem is in state I and the PBS binds to PSII thus increasing the electron flow (Figure 1). During dark-adaptation and when PSII is preferentially excited, the plastoquinone pool is in reduced state and the PBS binds to the PSI (Kirilovsky, 2015; Mackey *et al.*, 2013a). The exact mechanism of energy transfer is still unclear, theories include spill over from PSII to PSI and or the reversible migration of the phycobilisome, however, recent evidence suggests that the core of PSII may become quenched in state II to compensate for the excess of reduced electron carriers (Ranjbar Choubeh *et al.*, 2018).

In contrast, during high light conditions photoprotective reactions include redirection of the electron pathway (Mackey *et al.*, 2008), redirection of light energy to specific photosystems (Campbell *et al.*, 1998) and nonphotochemical-quenching. Here, electrons are removed from PSII and funnelled into reducing oxygen (Bailey *et al.*, 2008). Mackey *et al.* (2013a) showed a temperature dependence of the PBS association in several strains of *Synechococcus.* When temperatures neared those optimal for growth, the PBS associated with PSII thus increasing the flux into the linear electron pathway. At lower temperatures, PBS associated with PSI which could increase cyclic electron flow. Moreover, the researchers also showed an increased synthesis of proteins associated with the photosynthetic apparatus when *Synechococcus* sp. WH8102 was grown at higher temperatures. This might partly explain the wide geographic distribution of *Synechococcus* in contrast to *Prochlorococcus* which lacks a phycobilisome (Mackey *et al.*, 2013a). All of these characteristics have been known to lead to artificially low measurements of Fv/F_M or other

photosynthetic health parameters for *Synechococcus* (Campbell *et al.*, 1998) and could help explain the low values of ca. 0.1 for Fv/F_M in the control cultures of RCC2384. Campbell *et al.* (1998) proposed the addition of 3-(3,4-dichlorophenyl)-1,1-dimethylurea (DCMU) in order to keep the reaction centres of PSII closed. Published F_V/F_M data of other *Synechococcus* cultures ranges between 0.41 - 0.56 for environmental populations (Fu *et al.*, 2007), 0.15 - 0.35 for *Synechococcus* sp. PCC7002 (Mou *et al.*, 2017), ca. 0.77 for environmental *Synechococcus* isolates from the Arabian Sea (Bemal & Anil, 2016), and 0.090 – 0.2 for thermophilic *Synechococcus lividus* isolates (Liao *et al.*, 2006). These values strongly suggest that the low values F_V/F_M measured in this study may not provide an accurate estimate of the photosynthetic health of the cultures. PAM measurements were also attempted for the two PCC strains; however, measurements could not be conducted successfully as the measured values were too low to proceed to large-scale measurements as additional data to a growth curve without first establishing a specific protocol for F_V/F_M or Φ_{PSII} measurements for these strains.

5.1.2. Applicability of the µRespirometer for Oxygen Measurements with *Synechococcus*

The applicability of the novel microfluidic chamber for measurements of oxygen fluxes in photosynthetic organisms has not yet been determined. Here, the aim was to identify the limits of the method as well as to propose improvements to the experimental protocol. Improvements included, identifying reasonable timeframes of analysis, prevention of air bubbles by sealing the chamber during the measurements, as well as calibration of the system with water of a defined oxygen concentration. The current set-up of the µRespirometer is not very well suited for measurements over 24 h, as the measured oxygen concentrations become uncoupled to the expected patterns following illumination protocol after one day in most cases. Presumably the chamber volume is too small to sustain cyanobacterial populations over that time frame, becoming depleted of nutrients and dissolved gases. Moreover, recovery of oxygen production was not visible after 12 hours of darkness, indicating that all oxygen was consumed in the chamber and that the cyanobacterial cells likely perished. In some cases, no increases in oxygen concentration were visible during the first 12 h of illumination. As the system can only record changes in oxygen concentration up to 21% air sat. the effect of photosynthesis on oxygen concentration could presumably not be recorded. In order to circumvent this problem, the cultures were first incubated in the dark to induce respiration and decrease the oxygen concentration

before the first light cycle was started. However, one hour of darkness evidently was not long enough to see an effect but 4 h proved sufficient to record clear increases in oxygen after the light was switched on.

As the system calculates oxygen concentration based on the relative fluorescence intensity, flushing the system with water of a defined oxygen concentration is necessary to give a defined low point against which to calculate the oxygen concentration. This improves the system accuracy; nevertheless, quantitative oxygen measurements are not yet possible and increases and decreases of oxygen concentration should always only be compared relative to other datapoints measured in the curve in order to avoid misinterpretation of the results. Moreover, flushing the system also carries with it the danger of introducing air bubbles into the chamber which could lead to sharp spikes in the oxygen concentration. The increase in biomass during measurement was not monitored in these datasets, however, this additional information could be very useful to correlate growth rate more clearly with photosynthesis as represented by O_2 production here. In general, the µRespirometer has the potential to be a very useful tool for monitoring oxygen evolution in picophytoplankton species. The small size of the measurement chamber as well as the possibility to measure samples continuously under defined temperature and irradiance conditions, circumvents many of the drawbacks of current commercial oxygen sensing methods.

5.2. Characterisation of *Synechococcus* PCC7942

5.2.1. Temperature and Irradiance Dependence of Growth

Temperature acclimatisation and adaptation were not tested comprehensively in this project, however, the freshwater strain PCC7942 was grown successfully at 30 °C regardless of osmolarity or pH regime. This was expected, as the strain is commonly cultivated in temperatures between 30 - 37 °C (Billini *et al.*, 2008; Porankiewicz *et al.*, 1998; Scanlan *et al.*, 1995).

Although the stock cultures were maintained in the same growth chamber over several weeks, the phycocyanobilin signals decreased over time when normalised to cell concentrations. The normalised geometric means increased in certain conditions after the two days when the cultures were not sampled in the middle of the experiment. This recovery is intriguing and suggests two possibilities; first, that the incubator may have switched

off or reduced illumination level over the weekend and/or second, that the accuracy of the flow cytometer decreased over the course of the experiment. Furthermore, adaptation to irradiance levels appears to happen only on the individual cell level, since the cultures reduced their pigment content to cope with excess light even after the stock cultures presumably had had time to adapt to the light conditions over several weeks. A similar decrease in pigment content over time at higher light levels has been shown in environmental *Synechococcus* populations in *in situ* incubations in the North Atlantic near Bermuda co-occurring with changes in irradiance (Lomas *et al.*, 2012). The fact that PCC7942 was better able to cope with the higher light intensity than RCC2384 is presumably due to the different pigment types of the two strains. The rods of the phycobilisome type 1 are shorter compared to other pigment types, which is considered to be beneficial at high irradiance levels by allowing the cyanobacteria to minimize the absorption of excess light (Mackey *et al.*, 2017).

5.2.2. Osmolarity Dependence of Growth

PCC7942 was also able to cope well with the osmolarities up to 30% ESAW medium. Growth rates reached up to 2.4 ± 0.64 day^{-1} (0% ESAW), 1.7 ± 0.23 (10%), 2.6 ± 0.51 (20%) and 0.84 ± 0.3 day^{-1} (30%) during initial exponential growth. Whereas the growth rates were noticeably lower in the conditions 10 and 30%, the growth rate recorded in 20% osmolarity even exceeded that of the control (0%). Therefore, the optimal conditions for the maintenance of the strain would be 20% ESAW medium, 30 °C and 130 µmol m^{-2} s^{-1}, and not 0% ESAW as expected. The lowered growth rates indicate salinity stress; nevertheless, all growth rates were positive irrespective of condition and pH at t_0, which suggests that the strain has a wide salinity tolerance. Indeed, the upper salinity tolerance limit for PCC7942 has been described as ≤0.4 M NaCl (Ladas & Papageorgiou, 2000a), which is much higher than the conditions tested here as 30% ESAW roughly equals to 0.11 M NaCl.

The growth rates recorded here were higher than the ca. 0.77 day^{-1} shown for PCC7942 cultures (Scanlan *et al.*, 1995). Presumably this was due to the lower irradiance level during cultivation in that study. Higher growth rates (3.6 day^{-1}) were shown for PCC7942 cultures grown at both higher temperature and lower irradiance than the conditions in the present study (Porankiewicz *et al.*, 1998). Bernal & Anil (2017) reported growth rates of ca. 0.36 day^{-1} (salinity 10) and 0.19 day^{-1} (salinity 30) for the freshwater strain

Synechococcus sp. CCAP1405. Growth rate, photosynthetic efficiency (F_V/F_M) and phase duration of cell cycle were significantly lower and slower in conditions higher than 10 salinity. To the best of my knowledge, the highest recorded growth rates at ambient CO_2 levels for a *Synechococcus* strain were ca. 10.4 day^{-1} for the freshwater cyanobacterium *S. elongatus* PCC 11801 first isolated from a lake in Mumbai, India (Jaiswal *et al.*, 2018). This novel strain outperformed the common cyanobacterial model strains of PCC7942 and *Synechocystis* sp. PCC 6803. Therefore, the growth rates recorded for PCC7942 in the preferred conditions 0% and 20% osmolarity fall within the upper range of previously published data.

In the 2017 study, CCAP1405 cells reacted to salinity stress by increasing production and secretion of exopolysaccharides, presumably transferring energy from growth into an increased surrounding exopolysaccharide layer in order to protect against hypersaline environments (Bemal & Anil, 2017; Rosales *et al.*, 2005; Sheng *et al.*, 2006). Qiu *et al.* (2012) also showed that increased extracellular polymeric substance (EPS) production and desaturation of membrane lipids were correlated to increasing salinity in a salinity tolerant *Synechococcus* strain.

Apart from the increased exopolymeric layer, osmoregulation in cyanobacterial cells is mediated by either ion exchanges over the cell wall or by the synthesis of organic solutes in the cytosol to maintain turgor. In the first instance, the first protection against desiccation or cell lysis in an osmotic shock is mediated by Na^+/H^+ antiporters and Na^+/ATP pumps until cells reach their new equilibrium (Nitschmann & Packer, 1992; Ritchie, 1992). Under hypersaline conditions, the cells are not able to compensate Na^+ influx by transport processes and stop growing (Waditee *et al.*, 2002). In freshwater cyanobacteria, this process is followed by the synthesis of sucrose and other disaccharides which increase cell turgor, whereas a heteroside and glycine betaine are the main osmolytes in marine and hypersaline cyanobacteria respectively (Mackay *et al.*, 1984). Under hypersaline conditions, freshwater cyanobacteria are not able to synthesize high enough concentrations of sucrose to maintain cell turgor and cease to proliferate. Moreover, high internal sucrose concentrations have toxic effects which further limits the salinity tolerance (Ladas & Papageorgiou, 2000a; 2000b). Another limiting factor is the reduction of the photosynthetic apparatus during salinity stress as energy is diverted into production of osmolytes and exopolymers at the expense of e.g. chlorophyll a and phycocyanin content (Ladas & Papageorgiou, 2000b; Papageorgiou *et al.*, 1998). Although lower growth rates were

recorded in hypersaline conditions in this study, the pigment content itself, as measured by fluorescent emission of phycocyanobilin, was in fact higher in conditions 10 - 30% osmolarity. More quantitative and precise measures of pigment content would be necessary to further investigate the salinity stress response of PC7942.

Efforts have been made to improve the salinity tolerance of PCC7942 by genetic transformation, for example, in order to introduce the capability to synthesize glycine betaine. However, this did not lead to osmoregulation with glycine betaine but instead enhanced cell metabolism, leading to increased intracellular sucrose concentrations that enabled growth under hypersaline conditions but did not widen the salinity tolerance of the strain (Ladas & Papageorgiou, 2000a). Waditee *et al.* (2002) acclimatised PCC7942 to growth in salt water by overexpressing Na^+/H^+ antiporters. Whereas the basic salinity tolerance may not be broadened by these strategies, salinity stress might be alleviated under hypersaline conditions that limit growth for the freshwater cyanobacterium *Synechococcus* PCC7942.

5.2.3. pH Dependence of Growth

The pH tolerance was only tested for strain PCC7942, but in this case the initial adjusted pH of the medium had no effect on the subsequent pH values measured in the cultures. All measured values at t_0 differed considerably from the targeted pH and it became quickly apparent that within a few days of inoculation, the pH was controlled by the cultures and not the other way around. For instance, the pH increased rapidly up to pH 10 in conditions of 0% osmolarity and < pH 9.5 in conditions of higher osmolarity. The maximum pH values also roughly coincided with maximal cell concentrations. Carbon is taken up from the surrounding medium for photosynthesis in the form of CO_2 or CO_3^-, which shifts the bicarbonate buffering system towards consuming free H^+. Therefore, the pH is expected to rise with photosynthetic activity. Thus, only the pH values measured at t_0 were considered in subsequent analysis of impact on other parameters. The larger range of pH values in 0% osmolarity cultures likely is a reflection of the lack of native buffer system, apart from hydrogen carbonate, in the recipe of ESAW medium. As sodium hydrogen carbonate was listed under anhydrous salts in the recipe, it was excluded from the 0% osmolarity media. Although the pH was adjusted prior to sterile filtration for each medium, the unstable carbonate system may have caused the changes in the two days between preparation and inoculation. Furthermore, a spill-over effect from the starter

culture is unlikely as the cultures were resuspended in medium of the target osmolarity and pH prior to inoculation. However, the cultures themselves could have had an influence on the pH by switching their metabolism towards increased respiration due to the osmotic shock caused by the transfer into new medium. In future, the addition of a separate buffer system (e.g. Tris-HCl) or continuous adjustments of the pH would be necessary to observe adaptation and acclimatisation to constant pH values in the range of human physiological conditions.

Strain PCC7942 has shown remarkable tolerance to pH ranges from below pH 7 up to pH 10, and the high pH is a clear indication that photosynthesis took place in the cultures during the first half of the growth curve. No clear stationary phase was recorded during the growth curve; however, the decrease in cell concentration at later time-points is likely to have been due to age of the culture and depletion of nutrients. Stressful conditions cause a shift towards increased respiration and lower photosynthesis rates in *Synechococcus* (Billis *et al.*, 2014). Consequently, the decrease in cell concentration likely caused the decrease in pH due to increased respiration in the culture as well as the release of cytosol components by cell lysis. If carbon in the form of CO_2 and bicarbonate ions was the limiting nutrient, placing culture bottles on a shaker, or bubbling with CO_2 enriched or 'normal' air may be necessary to properly aerate the cultures. Thus far, the only exchange of air was through the vented filter cap and diffusion into the medium in vertically erected bottles. As no organic carbon sources, apart from the vitamins, were added to the artificial sea water medium the cyanobacterial cells would have had to live on organic carbon compounds or CO_2 produced by the culture itself.

Cyanobacteria are considered to be alkaliphilic in general, preferring conditions from neutral up to pH 10 (Summerfield & Sherman, 2008); the lower limit of pH tolerance has been reported as being below pH 5 (Brock, 1973). During the growth curve, pH values reached up to pH 10 roughly at the same time-points as the maximal cell densities. In shallow lakes, photosynthetic activity can drive the pH even above pH 10 at which point the alkalophilic cyanobacteria outcompete other phytoplankton species (Lopez-Archilla *et al.*, 2004). While high pH puts the organism under stress, high pH is also indicative of high biomass and high activity levels during cyanobacterial blooms.

As with salinity tolerance, bacteria maintain pH equilibrium with Na^+/H^+ antiporters in the cell walls. At alkaline pH of the surrounding medium, the cytoplasm becomes

acidified (Padan *et al.*, 2005). Under alkalinity stress, cyanobacteria scavenge and accumulate CO_2 and bicarbonate by investing more energy into metabolism. Moreover, cell wall biosynthesis is upregulated, potentially in order to increase tolerance to alkaline conditions (Billis *et al.*, 2014). In contrast to *Prochlorococcus*, *Synechococcus* has been reported to react positively to pCO_2 and temperature conditions predicted by climate change models. Growth rates as well as photosynthetic capacity (F_V/F_M) and pigment content were increased significantly under these conditions (Fu *et al.*, 2007). The growth rates were ca. 0.3 day^{-1} (present day control) and ca. 0.75 day^{-1} (greenhouse conditions) for *Synechococcus* sp. CCMP1334 (Fu *et al.*, 2007). However, on the individual cell level changes to pCO_2 levels are likely compensated by adjustments of the photosynthetic apparatus, thus decoupling pCO_2 from growth rates, which are instead more influenced by nutrient availability (Beardall *et al.*, 2009).

The pH measured at t_0 had statistically significant effects on both the growth rates ($t_0 - t_1$) as well as the pigment signal strength at t_1. In general, growth rates were higher at lower pH although as the samples clearly grouped by osmolarity it may have indirectly influenced the growth rates. The pigment content was also significantly influenced by the pH at t_0, lower pH values lead to lower geometric means when normalised for counts. Again, osmolarity presumably played an indirect role, due to its influence on the possible pH ranges. Lomas *et al.* (2012) recorded a similar decrease in pigment fluorescence (Chlorophyll a and phycoerythrin) as measured by flow cytometry correlated to pH values for environmental *Synechococcus* populations in *in situ* incubation experiments in the Northern Atlantic near Bermuda. However, this effect was only apparent in September and during other months decrease in pigment content was not related to pH treatment but instead influenced by irradiance levels. Both the growth rates and pigment fluorescence data demonstrate that pH does have an influence on both growth and physiological health.

5.3. Environmental Relevance

Hitherto, adaptation and acclimatisation of *Synechococcus* were only considered in the context of the very specific abiotic conditions imposed by the targeted application as endosymbionts. Due to the very different environmental conditions present at the original sites of isolation of the strains, only general comparisons can be made between the two strains evaluated in this work. In the following section, the adaptation time scales of

marine and freshwater *Synechococcu*s will be put into an environmental context e.g., physical mixing in an estuarine system.

Estuarine systems exist on the interface between marine and freshwater aqueous ecosystems. Here, water masses converge and microbes and other organisms that are transported passively by water flow are suddenly subjected to conditions that may be unfavourable to them. If a model of a large river plume under climate change is considered, then the system is enriched with nutrients, subject to increasing sea surface temperatures and exhibits conditions of varying salinity and changing pH, acidic at oxygen minimum zones where organic matter is respired and alkaline in phytoplankton blooms. Higher temperatures are expected to stimulate primary production by phytoplankton, however, this effect can only be observed when nutrients are not limiting (Marañón *et al.*, 2018). Moreover, anthropogenic eutrophication is likely to overload estuaries with nitrates and phosphates. Therefore, growth should in theory not be limited with respect to major nutrients. This set up shows certain similarities to the culture conditions in this project as the nitrate and phosphate concentrations in ESAW are within the range of those measured in the eutrophic Scheldt estuary in Belgium and the Netherlands (Soetaert *et al.*, 2006).

Cyanobacteria are key primary producers in both marine and freshwater ecosystems. The unique adaptive capabilities of *Synechococcus* allow the cyanobacteria to thrive in habitats of widely differing conditions. While *Synechococcus* is generally considered to be non-toxic, research on the bloom dynamics of cyanobacteria in estuaries is in most cases related to the study of harmful cyanobacterial blooms. Particularly, since they are expected to spread and increase in frequency with climate change (O'Neil *et al.*, 2012; Paerl *et al.*, 2011). Therefore, it is imperative to study survival times of cyanobacteria in estuarine waters. For picoplankton estuarine survival is dependent on the residence times inside of the system, this value measures the length of time spent in a predefined area of water (de Brauwere *et al.*, 2011; Zimmerman, 1976). Longer residence times would give phytoplankton populations time to adapt and grow to a certain cell density so that a stable estuarine population could establish itself and evolve. This relationship between residence time and the doubling time of phytoplankton has been described in several studies (Crump *et al.*, 2004; Wang *et al.*, 2004).

Here, marine and freshwater cyanobacteria were represented by *Synechococcus* RCC2384 (pigment type 3a) and PCC7942 (pigment type 1) respectively. This follows

observations that low salinity microenvironments in estuaries are dominated by *Synechococcus* with phycocyanin as their main pigment of the phycobilisome, whereas *Synechococcus* with phycoerythrin are mainly present in higher salinity environments (Rajaneesh & Mitbavkar, 2013; Xia *et al.*, 2015). *Synechococcus* RCC2384 cell concentrations started to decrease immediately after transfer into medium of osmolarity lower than 100% and became undetectable in the flow cytometer on day 4. This would indicate that the residence time in an estuary would have to be longer than 4 days in order for the population to have a fighting chance to survive. The four days estimate is of course based on transfer into 29% ESAW medium which would be a dramatic shift unlikely to occur in nature without intermediate steps. The second quick adaptation test would need to be repeated to obtain a clearer picture of the lower limit of salinity tolerance for this marine strain. However, due to its origin from the high salinity and oligotrophic Red Sea it is not likely that the cyanobacterium would encounter these conditions in the natural environment.

Starting from the opposite end of the spectrum the freshwater cyanobacterium was successfully acclimatised to conditions up to 30% osmolarity from the original 0%, reflecting data obtained for similar salinity ranges in another freshwater strain (Bemal & Anil, 2017). This of course does not represent the whole spectrum from freshwater until full marine sea water, which would be full-strength ESAW medium in this case. Nevertheless, since t_1 was sampled three days after inoculation the possibility cannot be discounted that exponential growth began after a 1 - 2 day lag phase whose length may have been dependant on osmolarity regime. While the exact freshwater lake in California from which the strain was first isolated is not known, it follows that unless the strain is endemic to a particular closed lake system some cells will inevitably be transported into more saline environments. However, this potential adaptation time would still be less than half than that shown for RCC2384. In the context of osmotic stress, it would also be worth to consider that the secretion of carbon to strengthen the exopolymeric layer around the cyanobacteria (Bemal & Anil, 2017) could have implications for the availability of carbon for heterotrophic bacteria and grazers.

Estuarine systems each have their own characteristics such as volume, shape, tidal range etc. making general statements about what these adaptation times could mean in an actual estuary, difficult. Published data for residence times ranges e.g. from approximately 1 - 2 days for the Danshuei River estuary in Taiwan (Wang *et al.*, 2004), ca. 1 - 4 days for

the Mersey estuary in the United Kingdom (Yuan *et al.*, 2007), ca. 7 – 20 days for the Parker River estuary in the north-eastern United States (Crump *et al.*, 2004) and approximately 10 - 75 days for the Scheldt estuary in the Netherlands (de Brauwere *et al.*, 2011). In light of these highly variable timescales, the short potential lag phase and adaptation to both higher salinity and a wide pH range shown for PCC7942 here, would serve members of that strain very well in an estuarine system. In contrast, the exact limits of tolerance still need to clarified for RCC2384, although the strain appears to be less well equipped for handling brackish waters.

Synechococcus is widely considered to be non-toxic yet the genus is also rarely investigated for toxicity. However, Martins *et al.* (2005) reported toxic activity of *Synechococcus* which had been isolated from the Portuguese coast against the liver, kidneys, lungs and intestines of mice. In a follow up study, the authors showed a apoptotic effect of marine *Synechococcus* and *Synechocystis* on human leukaemia cell lines and primary rat hepatocytes (Martins *et al.*, 2008). Microcystins, hepatotoxic cyanobacterial toxins, were also detected in *Synechococcus* isolates from the Salton Sea, a lake in California (Carmichael & Li, 2006). Moreover, extracts of isolates of *Synechocystis* and *Synechococcus* off the coast of Portugal had negative impacts on marine invertebrates, particularly on the embryogenesis in a sea urchin and a mussel species (Martins *et al.*, 2007). However, in another study screening of axenic cyanobacterial strains showed no genomic markers for oligopeptide cyanobacterial toxins (Jakubowska & Szeląg-Wasielewska, 2015). In addition to the commonly referenced cyanobacterial hepatotoxins and neurotoxins, lipopolysaccharides (LPS), part of the external cell wall of gram-negative bacteria are also known to cause inflammation (Wiegand & Pflugmacher, 2005). Whereas LPS do not by themselves have a strong toxic effect, they do enhance the effect of other toxins (Alves-Rosa *et al.*, 2001). The LPS structure of *Synechococcus* deviates from the common structure of the compound in other gram-negative bacteria, which may be the cause of the lower toxigenic effect compared to LPS from *E. coli* (Jakubowska & Szeląg-Wasielewska, 2015; Snyder *et al.*, 2009; Stewart, 2005).

Although not generally deemed to be toxic, exposure and adaptation to environmental conditions may induce the production of toxins and allelochemicals in *Synechococcus*. For instance, the strength of allelopathic activity of a Baltic *Synechococcus* strain against a Baltic diatom has been shown to depend on light, temperature and salinity conditions (Śliwińska-Wilczewska *et al.*, 2016). Filtrates from cyanobacterial cultures grown at

higher temperatures and higher illumination inhibited the growth of the diatom *Navicula perminuta*. Similar behaviour has been shown for toxigenic cyanobacteria from the Baltic (Lehtimaki *et al.*, 1997) and in an Argentinian Water Reservoir (Amé *et al.*, 2003). The induction of toxicity in normally non-toxic species could have fatal effects on human health and economy.

5.4. Application as an Endosymbiont in Biomedical Research

The primary goal of this work was to find and characterise *Synechococcus* strains that are suitable for the application in a novel therapeutic method for human skin tissues where impaired perfusion of oxygen inhibits proper wound healing. Work was started on the already available Red Sea strain RCC2384, which to the best of my knowledge has not been characterised in great detail regarding adaptation to salinity, temperature and pH. Based on the available literature, the Caribbean strain PCC7002 and the freshwater strain PCC7942 were selected as candidates for examining survival and growth under conditions mimicking certain aspects of the cytosol of human cells.

Unfortunately, the Caribbean strain *Synechococcus* PCC7002 could not be further characterised in this study. However, the strain may present an intermediate between the two characterised strains. Its coastal marine habitat places it near RCC2384 yet the composition of the phycobilisome is much closer to PCC7942.

The initial trails with RCC2384 quickly showed that the lowered salinity would present an insurmountable hurdle in the survival of the cultures when the cells were shocked in the quick transfer from 100% ESAW to medium of lower osmolarity. Potentially the cells might be able to adapt if the basic set up of the second quick adaptation was taken and the cells were successively transferred into medium of lower osmolarity once exponential growth had been established at a certain salinity level. Since the decrease in cell concentration was almost immediate after transfer into 29% ESAW medium, the lower limit of salinity tolerance would presumably be easily identified in this set-up. As growth was recorded at 30 °C, temperature would surely not impede RCC2384's survival under human physiological conditions. pH adaptation and acclimatisation were not tested here but osmotic concentration would presumably be more of a problem since cultures would control the pH themselves past a certain level of biomass.

Conceptually, if salinity or osmotic concentration of the medium is the biggest hurdle for the adaptation of a marine strain, it follows logically that freshwater strains would have a higher success rate. This expectation was proven in the positive growth rates regardless of osmolarity condition shown for PCC7942. Moreover, selected samples also showed oxygen production at 30 °C. Although the adaptation to pH could not be shown comprehensively in this work, growth was not impeded by pH < 7.0 < 8.0 at t_0 which is promising for survival inside the cytosol of human keratinocytes. Keeping the cultures at steady pH would of course be important with respect to their potential biomedical application. The buffer capabilities of the cytosol of human keratinocytes would need to be tested once cyanobacterial cells have been successfully introduced into the cells. However, any changes in pH due to photosynthesis of the endosymbionts could have adverse consequences for the skin cells in the tissues that are supposed to benefitted by the treatment method. Intracellular pH in eukaryotic cells influences metabolism, growth, proliferation, differentiation as well as induction of cancer and is thought to act as signal for other effectors (Busa & Nuccitelli, 1984; Harguindey *et al.*, 1995).

In conclusion, the freshwater strain *Synechococcus* sp. PCC7942 was able to adapt to a range of salinities from 0 - 30% ESAW. However, adaptation of the Red Sea strain RCC2384 to salinities below the control (100% ESAW) was not possible. The pH measured at t_0 did have a significant effect on both the growth rates ($t_0 – t_1$) and the phycocyanobilin fluorescence at t_1 which leads to the conclusion that the pH of the medium does influence both growth and physiology of *Synechococcus* during initial exponential growth.

Due to the demonstrated adaptability to environmental conditions mimicking certain aspects of the cytosol of human keratinocytes the freshwater strain *Synechococcus* PCC7942 is, to date, the best candidate for potential future medical application out of the strains evaluated in this work.

6. Outlook & Future Perspectives

The limits of tolerance for RCC2384 could not yet be determined in detail. While unlikely to be suitable as an endosymbiont, *Synechococcus* of pigment type 3 are still important primary producers in marine ecosystems and should therefore be considered with respect to their adaptability to changing environmental conditions. However, any experiments should be implemented with stock cultures that have had enough time to adapt to any changes in irradiance levels and in growth curves of over more than two weeks. Moreover, *Synechococcus* PCC7002 would need to characterised with respect to temperature, salinity and pH tolerance. The strain may present an intermediate between RCC2384 and PCC7942 as a coastal marine strain of pigment type 1 and could provide further insights into the adaptation and acclimatisation processes in cyanobacteria.

Furthermore, work should focus on the freshwater strain PCC7942 as it is the most promising candidate for future medical application as part of the Endosymbiont project. Although the pH tolerance of PCC7942 could not be tested for the targeted conditions here, the results obtained are promising nevertheless. The pH tolerance could be further determined by adding a buffer system other than hydrogen carbonate to the growth medium as this was not considered during the initial experiments. Another possibility could be the continued adjustment of pH during a growth curve as the cyanobacteria are likely to influence the pH with photosynthetic activity even within the narrower ranges imposed by the buffer system. Therefore, it would also be essential to determine the cell density at which the cyanobacteria start to control the pH, particularly as changes of intracellular pH could have fatal consequences inside keratinocytes.

More frequent sampling in the first 72 h of a growth curve would be necessary to get an idea of how fast the pH changes from the initial values as well as to determine if there is a lag phase before the cells go on into exponential growth. The length of this lag phase could be crucial for adaptation and acclimatisation. Moreover, cell counting by flow cytometry offers the possibility to track changes in cell sizes caused by osmotic stress by adding size standards to the measured samples as described by Lomas *et al.* (2012). The pulse amplitude modulation fluorometry protocol also needs to be optimized for *Synechococcus* cells if large-scale measurements as part of growth curves are to be implemented. For instance, 3-(3,4-dichlorophenyl)-1,1-dimethylurea (DCMU) could be added to keep the reaction centres of PSII closed (Campbell *et al.*, 1998).

Future improvements with the µRespirometer including quantitative O_2 measurements and measurements at defined light intensities could be used to make photosynthesis vs irradiance curves in small sample volumes. O_2 production would here serve as a proxy for photosynthetic activity in contrast to the conventional biomass or carbon uptake measurements. This would allow for shorter measurement times at each light intensity since changes in O_2 production will be much faster than biomass increase. As the five sensing spots in the chamber are at different angles to the light source, oxygen measurements could theoretically be done simultaneously for five light intensities. This could help optimize culture conditions by identifying optimal irradiance levels for different strains as well as the maximal obtainable oxygen production rates. Oxygen production data could then be corroborated with cell concentrations before and after the measurements.

In the future, toxicity screening of the candidate strains will be necessary. Whereas *Synechococcus* is generally considered to be non-toxic, the chance remains that the strain would react to the close contact to mammalian cells necessary for the application as endosymbionts. This co-culture and eventual endosymbiosis could trigger defensive reactions in the cyanobacteria such as the production of toxins and allelochemicals. Apart from liquid chromatography – mass spectrometry (LC-MS) screening against known cyanobacterial toxins, the effect on human keratinocytes in co-cultures could be assessed with a testing protocol partially based on Kozdęba *et al.* (2014). For this purpose, cultures of keratinocytes would be observed over 96 h in co-culture with cyanobacterial cultures in four conditions. These conditions could include incubation with whole cells, ultra-sonicated cells, the filtrate of ultra-sonicated cells, and sterile medium as the control. The main objective would be to assess any adverse effects of the cell cultures against each other. The proliferation of both organisms would need to be tracked in order to detect e.g. any inhibition of the growth, actin cytoskeleton formation and cell migration as described for long-term incubations of 96 h of primary human keratinocytes with microcystin extracts (Kozdęba *et al.*, 2014). Further tests could include, live-dead staining with propidium iodide, lactate dehydrogenase assays to test for cell lysis and bromodeoxyuridine incorporation assays to track cell proliferation. If cytotoxic or inhibitory effects are recorded the effective dose (EC50) would need to be determined.

Further in the future, appropriate nitrogen and phosphorus supply would need to be established for the cyanobacteria in the cytosol. The demonstrated genetic transformability of the PCC7942 strain could also allow for genetic modifications to add functions to

the future endosymbionts such as e.g. increased salinity tolerance (Ladas & Papageorgiou, 2000a; Waditee *et al.*, 2002), as well as increased glucose production and export (Niederholtmeyer *et al.*, 2010).

In conclusion, while the groundwork has been laid regarding the osmolarity and pH tolerance of *Synechococcus* PCC7942, further characterisation is necessary with regards to oxygen production under the targeted conditions, photosynthetic efficiency and potential toxicity for future medical application.

7. References

Alves-Rosa, F., Beigier-Bompadre, M., Fernández, G., Barrionuevo, P., Mari, L., Palermo, M., & Isturiz, M. n. (2001). Tolerance to lipopolysaccharide (LPS) regulates the endotoxin effects on Shiga toxin-2 lethality. *Immunology letters, 76*(2), 125-131. doi: 10.1016/S0165-2478(01)00177-8.

Amé, M. V., del Pilar Díaz, M., & Wunderlin, D. A. (2003). Occurrence of toxic cyanobacterial blooms in San Roque Reservoir (Córdoba, Argentina): A field and chemometric study. *Environmental Toxicology, 18*(3), 192-201. doi: 10.1002/tox.10114

Bailey, S., Melis, A., Mackey, K. R. M., Cardol, P., Finazzi, G., van Dijken, G., Berg, G. M., Arrigo, K., Shrager, J., & Grossman, A. (2008). Alternative photosynthetic electron flow to oxygen in marine *Synechococcus*. *Biochimica et Biophysica Acta - Bioenergetics, 1777*(3), 269-276. doi: 10.1016/j.bbabio.2008.01.002

Bandyopadhyay, A., Stockel, J., Min, H., Sherman, L., & Pakrasi, H. (2010). High rates of photobiological H_2 production by a cyanobacterium under aerobic conditions. *Nature communications, 1*(139). doi: 10.1038/ncomms1139

Barlow, R. G., & Alberte, R. S. (1985). Photosynthetic characteristics of phycoerythrin-containing marine *Synechococcus* spp. *Marine Biology, 86*(1), 63-74. doi: 10.1007/bf00392580

Beardall, J., Stojkovic, S., & Larsen, S. (2009). Living in a high CO_2 world: impacts of global climate change on marine phytoplankton. *Plant Ecology & Diversity, 2*(2), 191-205. doi: 10.1080/17550870903271363

Bemal, S., & Anil, A. C. (2016). Genetic and ecophysiological traits of *Synechococcus* strains isolated from coastal and open ocean waters of the Arabian Sea. *FEMS microbiology ecology, 92*(11). doi: 10.1093/femsec/fiw162

Bemal, S., & Anil, A. C. (2017). Effects of salinity on cellular growth and exopolysaccharide production of freshwater *Synechococcus* strain CCAP1405. *Journal of Plankton Research, 40*(1), 46-58. doi: 10.1093/plankt/fbx064

Berges, J. A., Franklin, D. J., & Harrison, P. J. (2001). Evolution of an artificial seawater medium: improvements in enriched seawater, artificial water over the last two decades. *Journal of phycology, 37*(6), 1138-1145. doi: 10.1046/j.1529-8817.2001.01052.x

Bernstein, H. C., Konopka, A., Melnicki, M. R., Hill, E. A., Kucek, L. A., Zhang, S., Shen, G., Bryant, D. A., & Beliaev, A. S. (2014). Effect of mono- and dichromatic light quality on growth rates and photosynthetic performance of *Synechococcus* sp. PCC 7002. *Frontiers in microbiology, 5*(488). doi: 10.3389/fmicb.2014.00488

Berube, P. M., Biller, S. J., Hackl, T., Hogle, S. L., Satinsky, B. M., Becker, J. W., Braakman, R., Collins, S. B., Kelly, L., & Berta-Thompson, J. (2018). Single cell genomes of *Prochlorococcus*, *Synechococcus*, and sympatric microbes from diverse marine environments. *Scientific data, 5*. doi: 10.1038/sdata.2018.154

Bierman, W. (1936). The temperature of the skin surface. *Journal of the American Medical Association, 106*(14), 1158-1162. doi: 10.1001/jama.1936.02770140020007

Billini, M., Stamatakis, K., & Sophianopoulou, V. (2008). Two members of a network of putative Na^+/H^+ antiporters are involved in salt and pH tolerance of the freshwater cyanobacterium *Synechococcus elongatus*. *Journal of bacteriology, 190*(19), 6318-6329. doi: 10.1128/JB.00696-08

Billis, K., Billini, M., Tripp, H. J., Kyrpides, N. C., & Mavromatis, K. (2014). Comparative transcriptomics between *Synechococcus* PCC 7942 and *Synechocystis* PCC 6803 provide insights into mechanisms of stress acclimation. *PloS one, 9*(10), e109738. doi: 10.1371/journal.pone.0109738

Blondin, P. A., Kirby, R. J., & Barnum, S. R. (1993). The Heat Shock Response and Acquired Thermotolerance in Three Strains of Cyanobacteria. *Current Microbiology, 26*(2), 79-84. doi: 10.1007/bf01577340

Boylan, A., Martin, C., & Gardner, G. (1992). Infrared emissivity of burn wounds. *Clinical Physics and Physiological Measurement, 13*(2), 125. doi: 10.1088/0143-0815/13/2/003

Brock, T. D. (1973). Lower pH limit for the existence of blue-green algae: evolutionary and ecological implications. *Science, 179*(4072), 480-483. doi: 10.1126/science.179.4072.480

Brown, G. D., Wong, H.-F., Hutchinson, N., Lee, S.-C., Chan, B. K., & Williams, G. (2004). Chemistry and biology of maculalactone A from the marine cyanobacterium *Kyrtuthrix maculans*. *Phytochemistry Reviews, 3*(3), 381-400. doi: 10.1007/s11101-004-6552-5

Bunge, F. (2018). *On-chip Mammalian Cell Cultivation and Monitoring.* (Doktor-Ingenieur Dissertation), University of Bremen, Bremen.

Bunge, F., van den Driesche, S., Waite, A., Mirastschijski, U., & Vellekoop, M. J. (2017). *µRespirometer to determine the oxygen consumption rate of mammalian cells in a microfluidic cell culture.* Paper presented at the 2017 IEEE 30th International Conference on Micro Electro Mechanical Systems (MEMS), Las Vegas, NV, USA

Bunge, F., van den Driesche, S., Waite, A., Mirastschijski, U., & Vellekoop, M. J. (2018a). Microfluidic oxygen sensor based on silica gels for longterm experiments. Cross-section of the entire assembly consisting of the sensing chip, the holder with the electric and fluidic connections, the excitation LED, a filter and the camera (the assembly is symmetrical regarding the cross-section surface. Retrieved from: https://ieeexplore.ieee.org/ielx7/8339522/8346457/08346783.pdf?tp=&arnumber=8346783&isnumber=8346457

Bunge, F., van den Driesche, S., Waite, A., Mirastschijski, U., & Vellekoop, M. J. (2018b). Microfluidic oxygen sensor based on silica gels for longterm experiments. Design of the microfluidic chip to determine the concentration of dissolved oxygen in the measurement chamber (height: 200f.201m) with an integrated temperature sensor and heater out of platinum. Retrieved from: https://ieeexplore.ieee.org/ielx7/8339522/8346457/08346783.pdf?tp=&arnumber=8346783&isnumber=8346457

Bunge, F., van den Driesche, S., Waite, A., Mirastschijski, U., & Vellekoop, M. J. (2018c). *Microfluidic oxygen sensor based on silica gels for longterm experiments.* Paper presented at the 2018 IEEE 31th International Conference on Micro Electro Mechanical Systems (MEMS), Belfast, United Kingdom.

Busa, W., & Nuccitelli, R. (1984). Metabolic regulation via intracellular pH. *American Journal of Physiology-Regulatory, Integrative and Comparative Physiology, 246*(4), R409-R438. doi: 10.1152/ajpregu.1984.246.4.R409

Cai, W.-J., Hu, X., Huang, W.-J., Murrell, M. C., Lehrter, J. C., Lohrenz, S. E., Chou, W.-C., Zhai, W., Hollibaugh, J. T., Wang, Y., Zhao, P., Guo, X., Gundersen, K., Dai, M., & Gong, G.-C. (2011a). Acidification of subsurface coastal waters enhanced by eutrophication. 766. Retrieved from: https://www.nature.com/articles/ngeo1297.pdf

Cai, W.-J., Hu, X., Huang, W.-J., Murrell, M. C., Lehrter, J. C., Lohrenz, S. E., Chou, W.-C., Zhai, W., Hollibaugh, J. T., Wang, Y., Zhao, P., Guo, X., Gundersen, K., Dai, M., & Gong, G.-C. (2011b). Acidification of subsurface coastal waters enhanced by eutrophication. *Nature Geoscience, 4*, 766. doi: 10.1038/ngeo1297

Campbell, D., Hurry, V., Clarke, A. K., Gustafsson, P., & Öquist, G. (1998). Chlorophyll Fluorescence Analysis of Cyanobacterial Photosynthesis and Acclimation. *Microbiology and Molecular Biology Reviews, 62*(3), 667-683

Carmichael, W. W., & Li, R. (2006). Cyanobacteria toxins in the Salton Sea. *Saline systems, 2*(1), 5. doi: 10.1186/1746-1448-2-5

Caro-Diaz, E. J., Valeriote, F. A., & Gerwick, W. H. (2019). Highly Convergent Total Synthesis and Assignment of Absolute Configuration of Majusculamide D, a Potent and Selective Cytotoxic Metabolite from *Moorea sp*. *Organic letters, 21*(3), 793–796. doi: 10.1021/acs.orglett.8b04050

Castenholz, R. W., Wilmotte, A., Herdman, M., Rippka, R., Waterbury, J. B., Iteman, I., & Hoffmann, L. (2001). Phylum BX. *cyanobacteria*. In *Bergey's Manual® of Systematic Bacteriology* (pp. 473-599): Springer.

Chen, M., Schliep, M., Willows, R. D., Cai, Z.-L., Neilan, B. A., & Scheer, H. (2010). A red-shifted chlorophyll. *Science, 60*(329), 1318-1319. doi: 10.1126/science.1191127

Chou, W.-C., Gong, G.-C., Hung, C.-C., & Wu, Y.-H. (2013). Carbonate mineral saturation states in the East China Sea: present conditions and future scenarios. *Biogeosciences, 10*(10), 6453-6467. doi: 10.5194/bg-10-6453-2013

Chynoweth, D. P. (2005). Renewable Biomethane From Land and Ocean Energy Crops and Organic Wastes. *HortScience, 40*(2), 283-286. doi: 10.21273/hortsci.40.2.283

Cohen, J. E., Goldstone, A. B., Paulsen, M. J., Shudo, Y., Steele, A. N., Edwards, B. B., Patel, J. B., MacArthur, J. W., Hopkins, M. S., & Burnett, C. E. (2017). An innovative biologic system for photon-powered myocardium in the ischemic heart. *Science advances, 3*(6), e1603078. doi: 10.1126/sciadv.1603078

Collier, J. L., & Grossman, A. R. (1992). Chlorosis induced by nutrient deprivation in *Synechococcus* sp. strain PCC 7942: not all bleaching is the same. *Journal of bacteriology, 174*(14), 4718-4726. doi: 10.1128/jb.174.14.4718-4726.1992

Converti, A., Oliveira, R. P. S., Torres, B. R., Lodi, A., & Zilli, M. (2009). Biogas production and valorization by means of a two-step biological process. *Bioresource Technology, 100*(23), 5771-5776. doi: 10.1016/j.biortech.2009.05.072

Crump, B. C., Hopkinson, C. S., Sogin, M. L., & Hobbie, J. E. (2004). Microbial Biogeography along an Estuarine Salinity Gradient: Combined Influences of Bacterial Growth and Residence Time. *Applied and environmental microbiology, 70*(3), 1494-1505. doi: 10.1128/aem.70.3.1494-1505.2004

Dahms, H.-U., Ying, X., & Pfeiffer, C. (2006). Antifouling potential of cyanobacteria: a mini-review. *Biofouling, 22*(5), 317-327. doi: 10.1080/08927010600967261

de Brauwere, A., de Brye, B., Blaise, S., & Deleersnijder, E. (2011). Residence time, exposure time and connectivity in the Scheldt Estuary. *Journal of Marine Systems, 84*(3), 85-95. doi: 10.1016/j.jmarsys.2010.10.001

Doney, S. C., Fabry, V. J., Feely, R. A., & Kleypas, J. A. (2009). Ocean acidification: the other CO_2 problem. *Annual Review of Marine Science, Volume 1*, 169-192. doi: 10.1146/annurev.marine.010908.163834

El Semary, N. A., & Fouda, M. (2015). Anticancer activity of *Cyanothece* sp. strain extracts from Egypt: First record. *Asian Pacific Journal of Tropical Biomedicine, 5*(12), 992-995. doi: 10.1016/j.apjtb.2015.09.004

Fatima, N., Ahmad, I. Z., & Chaudhry, H. (2017). Alterations in the antibacterial potential of *Synechococcus* spp. PCC7942 under the influence of UV-B radiations on skin pathogens. *Saudi Journal of Biological Sciences, 24*(7), 1657-1662

Feely, R. A., Sabine, C. L., Hernandez-Ayon, J. M., Ianson, D., & Hales, B. (2008). Evidence for upwelling of corrosive 'acidified' water onto the continental shelf. *Science, 320*(5882), 1490-1492. doi: 10.1126/science.1155676

Flombaum, P., Gallegos, J. L., Gordillo, R. A., Rincón, J., Zabala, L. L., Jiao, N., Karl, D. M., Li, W. K., Lomas, M. W., & Veneziano, D. (2013). Present and future global distributions of the marine Cyanobacteria *Prochlorococcus* and *Synechococcus*. *Proceedings of the National Academy of Sciences, 110*(24), 9824-9829. doi: 10.1073/pnas.1307701110

Fu, F. X., Warner, M. E., Zhang, Y., Feng, Y., & Hutchins, D. A. (2007). Effects of Increased temperature and CO_2 on photosynthesis, growth, and elemental ratios in marine *Synechococcus* and *Prochlorococcus* (cyanobacteria). *Journal of phycology, 43*(3), 485-496. doi: 10.1111/j.1529-8817.2007.00355.x

Gao, Z., Zhao, H., Li, Z., Tan, X., & Lu, X. (2012). Photosynthetic production of ethanol from carbon dioxide in genetically engineered cyanobacteria. *Energy & Environmental Science, 5*(12), 9857-9865. doi: 10.1039/C2EE22675H

Geraghty, T., & LaPorta, G. (2019). Current health and economic burden of chronic diabetic osteomyelitis *Expert Review of Pharmacoeconomics & Outcomes Research*, 1-8. doi: 10.1080/14737167.2019.1567337

Gerwick, W. H., Roberts, M. A., Proteau, P. J., & Chen, J.-L. (1994). Screening cultured marine microalgae for anticancer-type activity. *Journal of Applied Phycology, 6*(2), 143-149. doi: 10.1007/BF02186068

Golden, S. S., Johnson, C. H., & Kondo, T. (1998). The cyanobacterial circadian system: a clock apart. *Current opinion in microbiology, 1*(6), 669-673. doi: 10.1016/S1369-5274(98)80113-6

Grébert, T., Doré, H., Partensky, F., Farrant, G. K., Boss, E. S., Picheral, M., Guidi, L., Pesant, S., Scanlan, D. J., & Wincker, P. (2018a). Fig. S1. Biochemical

composition and biooptical properties of phycobilisomes (PBSs) of the main *Synechococcus* pigment types (PTs). (A) Models of PBS structure, highlighting the conserved core and variable rods of increasing complexity from PT1 to PT3 [redrawn after Six *et al.* (4)]. (B) Whole-cell absorption spectra of the different PTs [reproduced after Six *et al.* (4)]. Chromophores responsible of each absorption peaks are indicated. (C) Whole-cell fluorescence excitation spectra with emission at 680 nm. Note that, for chromatic acclimaters (PT 683d), the PBS structure is similar to other PT 683 but that the excitation ratio at 495 and 545 nm (Ex495:545) varies from 680.686 in green light to 681.686 in blue light (685). Retrieved

Grébert, T., Doré, H., Partensky, F., Farrant, G. K., Boss, E. S., Picheral, M., Guidi, L., Pesant, S., Scanlan, D. J., & Wincker, P. (2018b). Light color acclimation is a key process in the global ocean distribution of *Synechococcus* cyanobacteria. *Proceedings of the National Academy of Sciences*, 201717069. doi: 10.1073/pnas.1717069115

Gunasekera, S. P., Li, Y., Ratnayake, R., Luo, D., Lo, J., Reibenspies, J. H., Xu, Z., Clare-Salzler, M. J., Ye, T., & Paul, V. J. (2016). Discovery, total synthesis and key structural elements for the immunosuppressive activity of cocosolide, a symmetrical glycosylated macrolide dimer from marine cyanobacteria. *Chemistry – A European Journal, 22*(24), 8158-8166. doi: 10.1002/chem.201600674

Harguindey, S., Pedraz, J. L., Canero, R. G., de Diego, J. P., & Cragoe Jr, E. J. (1995). Hydrogen ion-dependent oncogenesis and parallel new avenues to cancer prevention and treatment using a H^+-mediated unifying approach: pH-related and pH-unrelated mechanisms. *Critical Reviews™ in Oncogenesis, 6*(1). doi: 10.1615/CritRevOncog.v6.i1.20

Harrison, P. J., Waters, R. E., & Taylor, F. (1980). A broad spectrum artificial sea water medium for coastal and open ocean phytoplankton. *Journal of phycology, 16*(1), 28-35. doi: 10.1111/j.0022-3646.1980.00028.x

Hendry, E. B. (1961). Osmolarity of human serum and of chemical solutions of biologic importance. *Clinical chemistry, 7*(2), 156-164

Houghton, J. T., Ding, Y., Griggs, D., Noguer, M., Van der Linden, P., Dai, X., Maskell, K., & Johnson, C. (2001). *Climate change 2001: the scientific basis. Contribution of working group I to the third assessment report of the intergovernmental panel on climate change*. Retrieved from Cambridge, New York: https://www.osti.gov/etdeweb/biblio/20188640

Jaiswal, D., Sengupta, A., Sohoni, S., Sengupta, S., Phadnavis, A. G., Pakrasi, H. B., & Wangikar, P. P. (2018). Genome Features and Biochemical Characteristics of a Robust, Fast Growing and Naturally Transformable Cyanobacterium *Synechococcus elongatus* PCC 11801 Isolated from India. *Scientific reports, 8*(1), 16632. doi: 10.1038/s41598-018-34872-z

Jakubowska, N., & Szeląg-Wasielewska, E. (2015). Toxic picoplanktonic cyanobacteria. *Marine drugs, 13*(3), 1497-1518. doi: 10.3390/md13031497

Kana, T. M., & Glibert, P. M. (1987). Effect of irradiances up to 2000 μE m^{-2} s^{-1} on marine *Synechococcus* WH7803—I. Growth, pigmentation, and cell composition. *Deep Sea Research Part A. Oceanographic Research Papers, 34*(4), 479-495. doi: 10.1016/0198-0149(87)90001-X

Karatay, S. E., & Dönmez, G. (2011). Microbial oil production from thermophile cyanobacteria for biodiesel production. *Applied Energy, 88*(11), 3632-3635. doi: 10.1016/j.apenergy.2011.04.010

Khan, S. A., Sharma, G. K., Malla, F. A., Kumar, A., Rashmi, & Gupta, N. (2019). Microalgae based biofertilizers: A biorefinery approach to phycoremediate wastewater and harvest biodiesel and manure. *Journal of Cleaner Production, 211*, 1412-1419. doi: 10.1016/j.jclepro.2018.11.281

Kinmond, K., McGee, P., Gough, S., & Ashford, R. (2003). 'Loss of self': a psychosocial study of the quality of life of adults with diabetic foot ulceration. *Journal of tissue viability, 13*(1), 6-16. doi: 10.1016/S0965-206X(03)80025-6

Kirilovsky, D. (2015). Modulating energy arriving at photochemical reaction centers: orange carotenoid protein-related photoprotection and state transitions. *Photosynthesis Research, 126*(1), 3-17. doi: 10.1007/s11120-014-0031-7

Kleszczyński, K., Tukaj, S., Kruse, N., Zillikens, D., & Fischer, T. W. (2013). Melatonin prevents ultraviolet radiation-induced alterations in plasma membrane potential and intracellular pH in human keratinocytes. *Journal of pineal research, 54*(1), 89-99. doi: 10.1111/j.1600-079X.2012.01028.x

Koehn, F. E., Longley, R. E., & Reed, J. K. (1992). Microcolins A and B, new immunosuppressive peptides from the blue-green alga *Lyngbya majuscula*. *Journal of Natural Products, 55*(5), 613-619. doi: 10.1021/np50083a009

Koharudin, Leonardus M. I., & Gronenborn, Angela M. (2011). Structural Basis of the Anti-HIV Activity of the Cyanobacterial *Oscillatoria Agardhii* Agglutinin. *Structure, 19*(8), 1170-1181. doi: 10.1016/j.str.2011.05.010

Kozdęba, M., Borowczyk, J., Zimoląg, E., Wasylewski, M., Dziga, D., Madeja, Z., & Drukala, J. (2014). Microcystin-LR affects properties of human epidermal skin cells crucial for regenerative processes. *Toxicon, 80*, 38-46

Kruse, C. R., Singh, M., Targosinski, S., Sinha, I., Sørensen, J. A., Eriksson, E., & Nuutila, K. (2017). The effect of pH on cell viability, cell migration, cell proliferation, wound closure, and wound reepithelialization: In vitro and in vivo study. *Wound Repair and Regeneration, 25*(2), 260-269. doi: 10.1111/wrr.12526

Kuan, D., Duff, S., Posarac, D., & Bi, X. (2015). Growth optimization of *Synechococcus elongatus* PCC7942 in lab flasks and a 2-D photobioreactor. *The Canadian Journal of Chemical Engineering, 93*(4), 640-647. doi: 10.1002/cjce.22154

Kumar, J., Parihar, P., Singh, R., Singh, V. P., & Prasad, S. M. (2016). UV-B induces biomass production and nonenzymatic antioxidant compounds in three cyanobacteria. *Journal of Applied Phycology, 28*(1), 131-140. doi: 10.1007/s10811-015-0525-5

Ladas, N. P., & Papageorgiou, G. C. (2000a). Cell turgor: A critical factor for the proliferation of cyanobacteria at unfavorable salinity. *Photosynthesis Research, 65*(2), 155-164. doi: 10.1023/a:1006423221150

Ladas, N. P., & Papageorgiou, G. C. (2000b). The salinity tolerance of freshwater cyanobacterium *Synechococcus* sp. PCC 7942 is determined by its ability for osmotic adjustment and presence of osmolyte sucrose. *Photosynthetica, 38*(3), 343-348. doi: 10.1023/A:1010957117237

Landen, N. X., Li, D., & Stahle, M. (2016). Transition from inflammation to proliferation: a critical step during wound healing. *Cellular and Molecular Life Sciences, 73*(20), 3861-3885. doi: 10.1007/s00018-016-2268-0

Lau, K., Paus, R., Tiede, S., Day, P., & Bayat, A. (2009). Exploring the role of stem cells in cutaneous wound healing. *Experimental dermatology, 18*(11), 921-933. doi: 10.1111/j.1600-0625.2009.00942.x

Lehtimaki, J., Moisander, P., Sivonen, K., & Kononen, K. (1997). Growth, nitrogen fixation, and nodularin production by two baltic sea cyanobacteria. *Applied and environmental microbiology, 63*(5), 1647-1656

Liao, C. C., Liu, S. L., & Wang, W. L. (2006). Effects of temperature and pH on growth and photosynthesis of the thermophilic cyanobacterium *Synechococcus lividus* as measured by pulse-amplitude modulated fluorometry. *Phycological research, 54*(4), 260-268. doi: 10.1111/j.1440-1835.2006.00432.x

Liu, H., Campbell, L., Landry, M. R., Nolla, H. A., Brown, S. L., & Constantinou, J. (1998). *Prochlorococcus* and *Synechococcus* growth rates and contributions to production in the Arabian Sea during the 1995 Southwest and Northeast Monsoons. *Deep Sea Research Part II: Topical Studies in Oceanography, 45*(10), 2327-2352. doi: 10.1016/S0967-0645(98)00073-3

Lomas, M., Hopkinson, B., Ryan, J. L. D., Shi, D., Xu, Y., & Morel, F. (2012). Effect of ocean acidification on cyanobacteria in the subtropical North Atlantic. *Aquatic Microbial Ecology, 66*(3), 211-222. doi: 10.3354/ame01576

Lopez-Archilla, A. I., Moreira, D., López-García, P., & Guerrero, C. (2004). Phytoplankton diversity and cyanobacterial dominance in a hypereutrophic shallow lake with biologically produced alkaline pH. *Extremophiles, 8*(2), 109-115. doi: 10.1007/s00792-003-0369-9

Ludwig, M., & Bryant, D. A. (2012). *Synechococcus* sp. strain PCC 7002 transcriptome: acclimation to temperature, salinity, oxidative stress, and mixotrophic growth conditions. *Frontiers in microbiology, 3*, 14. doi: 10.3389/fmicb.2012.00354

Mackay, M. A., Norton, R. S., & Borowitzka, L. J. (1984). Organic Osmoregulatory Solutes in Cyanobacteria. *Microbiology, 130*(9), 2177-2191. doi: 10.1099/00221287-130-9-2177

Mackey, K. R. M., Paytan, A., Caldeira, K., Grossman, A., Moran, D., McIlvin, M., & Saito, M. (2013a). Effect of temperature on photosynthesis and growth in marine *Synechococcus*. *Plant physiology, 163*(2), 815-829. doi: 10.1104/pp.113.221937

Mackey, K. R. M., Paytan, A., Caldeira, K., Grossman, A., Moran, D., McIlvin, M., & Saito, M. (2013b). Figure 1. Phycobilisome (PBS) structure and linear photosynthetic electron flow in cyanobacteria. In this schematic the PBS is in "state 1," indicating it is associated with a PSII dimer. Photosynthetic electron flow pathways are indicated by black arrows and chemical reactions are indicated by blue arrows. Major ETC components include photosystem (PS)II, PSI, plastoquinone (PQ) /plastoquinol (PQH2), cytochrome b6f (Cyt b6f), plastocyanin (PLC), ferredoxin (FX), flavodoxin (FL), ferredoxin/flavodoxin NADP reductase (FNR). Other proteins depicted include the phycobiliproteins allophycocyanin (APC), phycocyanin (PC), two forms of phycoerythrin (PEI and PEII), PSII chlorophyll-binding proteins CP47 and CP43, the PSII core polypeptides D41 and D42, the PSI chlorophyll-binding core proteins PsaA and

PsaB, and the PSI reaction center subunit PsaD. . Retrieved from: http://www.plantphysiol.org/content/plantphysiol/early/2013/08/15/pp.113.221937.full.pdf

Mackey, K. R. M., Paytan, A., Grossman, A. R., & Bailey, S. (2008). A photosynthetic strategy for coping in a high-light, low-nutrient environment. *Limnology and Oceanography, 53*(3), 900-913. doi: 10.4319/lo.2008.53.3.0900

Mackey, K. R. M., Post, A. F., McIlvin, M. R., & Saito, M. A. (2017). Physiological and proteomic characterization of light adaptations in marine *Synechococcus*. *Environmental Microbiology, 19*(6), 2348-2365. doi: 10.1111/1462-2920.13744

Malinsky-Rushansky, N., Berman, T., Berner, T., Yacobi, Y. Z., & Dubinsky, Z. (2002). Physiological characteristics of picophytoplankton, isolated from Lake Kinneret: responses to light and temperature. *Journal of Plankton Research, 24*(11), 1173-1183. doi: 10.1093/plankt/24.11.1173

Marañón, E., Lorenzo, M. P., Cermeño, P., & Mouriño-Carballido, B. (2018). Nutrient limitation suppresses the temperature dependence of phytoplankton metabolic rates. *The ISME journal, 12*(7), 1836-1845. doi: 10.1038/s41396-018-0105-1

Martins, R., Fernandez, N., Beiras, R., & Vasconcelos, V. (2007). Toxicity assessment of crude and partially purified extracts of marine *Synechocystis* and *Synechococcus* cyanobacterial strains in marine invertebrates. *Toxicon, 50*(6), 791-799. doi: 10.1016/j.toxicon.2007.06.020

Martins, R., Pereira, P., Welker, M., Fastner, J., & Vasconcelos, V. M. (2005). Toxicity of culturable cyanobacteria strains isolated from the Portuguese coast. *Toxicon, 46*(4), 454-464. doi: 10.1016/j.toxicon.2005.06.010

Martins, R. F., Ramos, M. F., Herfindal, L., Sousa, J. A., Skærven, K., & Vasconcelos, V. M. (2008). Antimicrobial and cytotoxic assessment of marine cyanobacteria-*Synechocystis* and *Synechococcus*. *Marine drugs, 6*(1), 1-11. doi: 10.3390/md6010001

Mirastschijski, U., Waespy, M., Waite, A., Belge, G., Radtke, A., & Vellekoop, M. J. (2018). [Photosynthetic keratinocytes: light-powered oxygen for non-healing skin wounds].

Mou, S., Zhang, Y., Li, G., Li, H., Liang, Y., Tang, L., Tao, J., Xu, J., Li, J., & Zhang, C. (2017). Effects of elevated CO_2 and nitrogen supply on the growth and photosynthetic physiology of a marine cyanobacterium, *Synechococcus sp.* PCC7002. *Journal of Applied Phycology, 29*(4), 1755-1763

Niederholtmeyer, H., Wolfstädter, B. T., Savage, D. F., Silver, P. A., & Way, J. C. (2010). Engineering Cyanobacteria To Synthesize and Export Hydrophilic Products. *Applied and environmental microbiology, 76*(11), 3462-3466. doi: 10.1128/aem.00202-10

Nitschmann, W. H., & Packer, L. (1992). NMR studies on Na^+ transport in *Synechococcus* PCC 6311. *Archives of biochemistry and biophysics, 294*(2), 347-352. doi: 10.1016/0003-9861(92)90694-R

Nunan, R., Harding, K. G., & Martin, P. (2014). Clinical challenges of chronic wounds: searching for an optimal animal model to recapitulate their complexity. *Disease Models & Mechanisms, 7*(11), 1205-1213. doi: 10.1242/dmm.016782

O'Neil, J. M., Davis, T. W., Burford, M. A., & Gobler, C. J. (2012). The rise of harmful cyanobacteria blooms: The potential roles of eutrophication and climate change. *Harmful algae, 14*, 313-334. doi: 10.1016/j.hal.2011.10.027

OpenStax College, A. P. (2018). Figure 4. [Schematic Figure, Chapter 5.1 Layers of the Skin]. The epidermis of thick skin has five layers: *stratum basale, stratum spinosum*, *stratum granulosum*, *stratum lucidum*, and *stratum corneum*. Retrieved from: http://cnx.org/contents/14fb4ad7-39a1-4eee-ab6e-3ef2482e3e22@11.1

Padan, E., Bibi, E., Ito, M., & Krulwich, T. A. (2005). Alkaline pH homeostasis in bacteria: New insights. *Biochimica et Biophysica Acta - Biomembranes, 1717*(2), 67-88. doi: 10.1016/j.bbamem.2005.09.010

Paerl, H. W., Hall, N. S., & Calandrino, E. S. (2011). Controlling harmful cyanobacterial blooms in a world experiencing anthropogenic and climatic-induced change. *Science of The Total Environment, 409*(10), 1739-1745. doi: 10.1016/j.scitotenv.2011.02.001

Papageorgiou, G. C., Alygizaki-Zorba, A., Ladas, N., & Murata, N. (1998). A method to probe the cytoplasmic osmolality and osmotic water and solute fluxes across the cell membrane of cyanobacteria with chlorophyll a fluorescence: Experiments with *Synechococcus* sp. PCC7942. *Physiologia Plantarum, 103*(2), 215-224. doi: 10.1034/j.1399-3054.1998.1030209.x

Parmar, A., Singh, N. K., Pandey, A., Gnansounou, E., & Madamwar, D. (2011). Cyanobacteria and microalgae: A positive prospect for biofuels. *Bioresource Technology, 102*(22), 10163-10172. doi: 10.1016/j.biortech.2011.08.030

Percival, S. L., McCarty, S., Hunt, J. A., & Woods, E. J. (2014). The effects of pH on wound healing, biofilms, and antimicrobial efficacy. *Wound Repair and Regeneration, 22*(2), 174-186. doi: 10.1111/wrr.12125

Phillips, C. J., Humphreys, I., Fletcher, J., Harding, K., Chamberlain, G., & Macey, S. (2016). Estimating the costs associated with the management of patients with chronic wounds using linked routine data. *International Wound Journal, 13*(6), 1193-1197. doi: 10.1111/iwj.12443

Pittera, J., Humily, F., Thorel, M., Grulois, D., Garczarek, L., & Six, C. (2014). Connecting thermal physiology and latitudinal niche partitioning in marine *Synechococcus*. *The ISME journal, 8*(6), 1221. doi: 10.1038/ismej.2013.228

Porankiewicz, J., Selstam, E., Campbell, D., & Öquist, G. (1998). Membrane lipid composition and restoration of photosynthesis during low temperature acclimation in *Synechococcus* sp. strain PCC 7942. *Physiologia Plantarum, 104*(3), 405-412. doi: 10.1034/j.1399-3054.1998.1040316.x

Posnett, J., & Franks, P. (2007). The costs of skin breakdown and ulceration in the UK. *Skin Breakdown – the silent epidemic. Hull: The Smith and Nephew Foundation*

Posnett, J., & Franks, P. (2008). The burden of chronic wounds in the UK. *Nursing Times, 104*(3), 44-45

Priya, S. G., Jungvid, H., & Kumar, A. (2008). Skin Tissue Engineering for Tissue Repair and Regeneration. *Tissue Engineering Part B: Reviews, 14*(1), 105-118. doi: 10.1089/teb.2007.0318

Pushparaj, B., Pelosi, E., & Jüttner, F. (1998). Toxicological analysis of the marine cyanobacterium *Nodularia harveyana*. *Journal of Applied Phycology, 10*(6), 527-530

Qiu, X., Wang, H., Liu, D., Gong, L., Wu, X., & Xiang, X. (2012). The physiological response of *Synechococcus elongatus* to salinity: a potential biomarker for ancient salinity in evaporative environments. *Geomicrobiology Journal, 29*(5), 477-483. doi: 10.1080/01490451.2011.581331

Rai, A. N., Singh, A. K., & Syiem, M. B. (2019). Chapter 23 - Plant Growth-Promoting Abilities in Cyanobacteria. In A. K. Mishra, D. N. Tiwari, & A. N. Rai (Eds.), *Cyanobacteria* (pp. 459-476): Academic Press.

Rajaneesh, K., & Mitbavkar, S. (2013). Factors controlling the temporal and spatial variations in *Synechococcus* abundance in a monsoonal estuary. *Marine environmental research, 92*, 133-143. doi: 10.1016/j.marenvres.2013.09.010

Ranjbar Choubeh, R., Wientjes, E., Struik, P. C., Kirilovsky, D., & van Amerongen, H. (2018). State transitions in the cyanobacterium *Synechococcus elongatus* 7942 involve reversible quenching of the photosystem II core. *Biochimica et Biophysica Acta - Bioenergetics, 1859*(10), 1059-1066. doi: 10.1016/j.bbabio.2018.06.008

Ribeiro, K. F., Duarte, L., & Crossetti, L. O. (2018). Everything is not everywhere: a tale on the biogeography of cyanobacteria. *Hydrobiologia, 820*(1), 23-48. doi: 10.1007/s10750-018-3669-x

Rinnerthaler, M., Duschl, J., Steinbacher, P., Salzmann, M., Bischof, J., Schuller, M., Wimmer, H., Peer, T., Bauer, J. W., & Richter, K. (2013). Age-related changes in the composition of the cornified envelope in human skin. *Experimental dermatology, 22*(5), 329-335. doi: 10.1111/exd.12135

Rinnerthaler, M., & Richter, K. (2018). The influence of calcium on the skin pH and epidermal barrier during aging. In *pH of the Skin: Issues and Challenges* (Vol. 54, pp. 79-86): Karger Publishers.

Rippka, R. (2019). Pasteur culture collection of cyanobacterial strains in axenic culture. *Catalogue and taxonomic handbook, catalogue of strains.* Retrieved from https://catalogue-crbip.pasteur.fr/crbip_catalogue/faces/recherche_catalogue.xhtml

Rippka, R., & Cohen-Bazire, G. (1983). *The Cyanobacteriales: a legitimate order based on the type strain Cyanobacterium stanieri?* Paper presented at the Annales de l'Institut Pasteur/Microbiologie.

Ritchie, R. J. (1992). Sodium Transport and the Origin of the Membrane Potential in the Cyanobacterium *Synechococcus* R-2 (*Anacystis Nidulans*) PCC 7942. *Journal of Plant Physiology, 139*(3), 320-330. doi: 10.1016/S0176-1617(11)80345-7

Robertson, B. R., Tezuka, N., & Watanabe, M. M. (2001). Phylogenetic analyses of *Synechococcus* strains (cyanobacteria) using sequences of 16S rDNA and part of the phycocyanin operon reveal multiple evolutionary lines and reflect phycobilin content. *International journal of systematic and evolutionary microbiology, 51*(3), 861-871. doi: 10.1099/00207713-51-3-861

Rocks, B., Sherwood, R., & Cook, J. (1986). Whole blood osmolality. *Annals of Clinical Biochemistry: International Journal of Laboratory Medicine, 23*(1), 106-108. doi: 10.1177/000456328602300115

Romay, C., Gonzalez, R., Ledon, N., Remirez, D., & Rimbau, V. (2003). C-phycocyanin: a biliprotein with antioxidant, anti-inflammatory and neuroprotective effects. *Current protein and peptide science, 4*(3), 207-216. doi: 10.2174/1389203033487216

Rosales, N., Ortega, J., Mora, R., & Morales, E. (2005). Influence of salinity on the growth and biochemical composition of the cyanobacterium *Synechococcus* sp. *Ciencias marínas, 31*(2), 349-355. doi: 10.7773/cm.v31i2.59

Rubinstein, E. H., & Sessler, D. I. (1990). Skin-surface temperature gradients correlate with fingertip blood flow in humans. *Anesthesiology, 73*(3), 541-545

Scanlan, D. J., Sundaram, S., Newman, J., Mann, N. H., & Carr, N. G. (1995). Characterization of a zwf mutant of *Synechococcus* sp. strain PCC 7942. *Journal of bacteriology, 177*(9), 2550-2553. doi: 10.1128/jb.177.9.2550-2553.1995

Schneider, L. A., Korber, A., Grabbe, S., & Dissemond, J. (2007). Influence of pH on wound-healing: a new perspective for wound-therapy? *Archives of dermatological research, 298*(9), 413-420. doi: 10.1007/s00403-006-0713-x

Sen, C. K., Gordillo, G. M., Roy, S., Kirsner, R., Lambert, L., Hunt, T. K., Gottrup, F., Gurtner, G. C., & Longaker, M. T. (2009). Human skin wounds: A major and snowballing threat to public health and the economy. *Wound Repair and Regeneration, 17*(6), 763-771. doi: 10.1111/j.1524-475X.2009.00543.x

Sheng, G. P., Yu, H. Q., & Yue, Z. (2006). Factors influencing the production of extracellular polymeric substances by *Rhodopseudomonas acidophila*. *International Biodeterioration & Biodegradation, 58*(2), 89-93. doi: 10.1016/j.ibiod.2006.07.005

Shestakov, S., & Khyen, N. T. (1970). Evidence for genetic transformation in blue-green alga *Anacystis nidulans*. *Molecular and General Genetics, 107*(4), 372-375. doi: 10.1007/BF00441199

Shih, P. M., Zarzycki, J., Niyogi, K. K., & Kerfeld, C. A. (2014). Introduction of a synthetic CO_2-fixing photorespiratory bypass into a cyanobacterium. *J Biol Chem, 289*(14), 9493-9500. doi: 10.1074/jbc.C113.543132

Shimizu, H. (2017). *Shimizu's textbook of dermatology second edition*. Chichester, West Sussex; Hoboken, NJ: John Wiley & Sons, Ltd.

Show, K.-Y., Yan, Y.-G., & Lee, D.-J. (2019). Chapter 13 - Biohydrogen production from algae: Perspectives, challenges, and prospects. In A. Pandey, J.-S. Chang, C. R. Soccol, D.-J. Lee, & Y. Chisti (Eds.), *Biofuels from Algae (Second Edition)* (pp. 325-343): Elsevier.

Singh, R., Parihar, P., Singh, M., Bajguz, A., Kumar, J., Singh, S., Singh, V. P., & Prasad, S. M. (2017). Uncovering potential applications of cyanobacteria and algal metabolites in biology, agriculture and medicine: current status and future prospects. *Frontiers in microbiology, 8*, 515. doi: 10.3389/fmicb.2017.00515

Sinno, H., & Prakash, S. (2013). Complements and the wound healing cascade: an updated review. *Plastic surgery international, 2013*, 7. doi: 10.1155/2013/146764

Six, C., Thomas, J.-C., Garczarek, L., Ostrowski, M., Dufresne, A., Blot, N., Scanlan, D. J., & Partensky, F. (2007). Diversity and evolution of phycobilisomes in

marine *Synechococcus spp.*: a comparative genomics study. *Genome biology, 8*(12), 259. doi: 10.1186/gb-2007-8-12-r259

Śliwińska-Wilczewska, S., Pniewski, F., & Latała, A. (2016). Allelopathic activity of the picocyanobacterium *Synechococcus sp.* under varied light, temperature, and salinity conditions. *International Review of Hydrobiology, 101*(1-2), 69-77. doi: 10.1002/iroh.201501819

Snyder, D. S., Brahamsha, B., Azadi, P., & Palenik, B. (2009). Structure of Compositionally Simple Lipopolysaccharide from Marine *Synechococcus*. *Journal of bacteriology, 191*(17), 5499-5509. doi: 10.1128/jb.00121-09

Sobotta, J., & Welsch, U. (2006). *Lehrbuch Histologie*. München, Jena: Urban Fischer.

Soetaert, K., Middelburg, J. J., Heip, C., Meire, P., Van Damme, S., & Maris, T. (2006). Long-term change in dissolved inorganic nutrients in the heterotrophic Scheldt estuary (Belgium, The Netherlands). *Limnology and Oceanography, 51*(1 part2), 409-423. doi: 10.4319/lo.2006.51.1_part_2.0409

Soltani, N., Khavari-Nejad, R., Tabatabaei Yazdi, M., Shokravi, S., & Fernández-Valiente, E. (2005). Screening of soil cyanobacteria for antifungal and antibacterial activity. *Pharmaceutical biology, 43*(5), 455-459. doi: 10.1080/13880200590963871

Sorg, H., Tilkorn, D. J., Hager, S., Hauser, J., & Mirastschijski, U. (2017). Skin wound healing: an update on the current knowledge and concepts. *European surgical research, 58*(1-2), 81-94. doi: 10.1159/000454919

Stewart, I. (2005). *Recreational exposure to freshwater cyanobacteria: epidemiology, dermal toxicity and biological activity of cyanobacterial lipopolysaccharides*. University of Queensland, Australia.

Summerfield, T. C., & Sherman, L. A. (2008). Global Transcriptional Response of the Alkali-Tolerant Cyanobacterium *Synechocystis* sp. Strain PCC 6803 to a pH 10 Environment. *Applied and environmental microbiology, 74*(17), 5276-5284. doi: 10.1128/aem.00883-08

Tan, X., Yao, L., Gao, Q., Wang, W., Qi, F., & Lu, X. (2011). Photosynthesis driven conversion of carbon dioxide to fatty alcohols and hydrocarbons in cyanobacteria. *Metabolic engineering, 13*(2), 169-176. doi: 10.1016/j.ymben.2011.01.001

Team, R. D. C. (2008). R: A language and environment for statistical computing. Vienna, Austria. Retrieved from http://www.R-project.org.

Tenenhaus, M., & Rennekampff, H.-O. (2016). Current Concepts in Tissue Engineering: Skin and Wound. *Plastic and Reconstructive Surgery, 138*(3S), 42S-50S. doi: 10.1097/prs.0000000000002685

Theillet, F.-X., Binolfi, A., Frembgen-Kesner, T., Hingorani, K., Sarkar, M., Kyne, C., Li, C., Crowley, P. B., Gierasch, L., & Pielak, G. J. (2014). Physicochemical properties of cells and their effects on intrinsically disordered proteins (IDPs). *Chemical reviews, 114*(13), 6661-6714. doi: 10.1021/cr400695p

Vaulot, D., Le Gall, F., Marie, D., Guillou, L., & Partensky, F. (2004). The Roscoff Culture Collection (RCC): a collection dedicated to marine picoplankton. *Nova Hedwigia, 79*(1-2), 49-70. doi: 10.1127/0029-5035/2004/0079-0049

Vijayakumar, S., & Angione, C. (2017). *Multi-omic Data Integration Elucidates Synechococcus Adaptation Mechanisms to Fluctuations in Light Intensity and Salinity*. Paper presented at the IWBBIO 2017: Bioinformatics and Biomedical Engineering, Granada, Spain. https://link.springer.com/content/pdf/10.1007%2F978-3-319-56148-6_19.pdf. doi:10.1007/978-3-319-56148-6_19

Waditee, R., Hibino, T., Nakamura, T., Incharoensakdi, A., & Takabe, T. (2002). Overexpression of a Na^+/H^+ antiporter confers salt tolerance on a freshwater cyanobacterium, making it capable of growth in sea water. *Proceedings of the National Academy of Sciences, 99*(6), 4109-4114. doi: 10.1073/pnas.052576899

Wahlen, B. D., Willis, R. M., & Seefeldt, L. C. (2011). Biodiesel production by simultaneous extraction and conversion of total lipids from microalgae, cyanobacteria, and wild mixed-cultures. *Bioresource Technology, 102*(3), 2724-2730. doi: https://doi.org/10.1016/j.biortech.2010.11.026

Wang, C.-F., Hsu, M.-H., & Kuo, A. Y. (2004). Residence time of the Danshuei River estuary, Taiwan. *Estuarine, Coastal and Shelf Science, 60*(3), 381-393. doi: 10.1016/j.ecss.2004.01.013

Weller, R., Hunter, J., Savin, J., & Dahl, M. (2008). *Clinical Dermatology*. Oxford: Blackwell Publishing.

Werkneh, A. A., & Rene, E. R. (2019). Applications of Nanotechnology and Biotechnology for Sustainable Water and Wastewater Treatment. In X.-T. Bui, C. Chiemchaisri, T. Fujioka, & S. Varjani (Eds.), *Water and Wastewater Treatment Technologies* (pp. 405-430). Singapore: Springer Singapore.

Wiegand, C., & Pflugmacher, S. (2005). Ecotoxicological effects of selected cyanobacterial secondary metabolites a short review. *Toxicology and Applied Pharmacology, 203*(3), 201-218. doi: 10.1016/j.taap.2004.11.002

Xia, X., Vidyarathna, N. K., Palenik, B., Lee, P., & Liu, H. (2015). Comparison of the seasonal variation of *Synechococcus* assemblage structure in estuarine waters and coastal waters of Hong Kong. *Applied and environmental microbiology, 81*(21), 7644-7655. doi: 10.1128/AEM.01895-15

Xiao, X., Han, Z.-y., Chen, Y.-x., Liang, X.-q., Li, H., & Qian, Y.-c. (2011). Optimization of FDA–PI method using flow cytometry to measure metabolic activity of the cyanobacteria, *Microcystis aeruginosa*. *Physics and Chemistry of the Earth, Parts A/B/C, 36*(9), 424-429. doi: 10.1016/j.pce.2010.03.028

Xu, Y., Guerra, L. T., Li, Z., Ludwig, M., Dismukes, G. C., & Bryant, D. A. (2013). Altered carbohydrate metabolism in glycogen synthase mutants of *Synechococcus* sp. strain PCC 7002: cell factories for soluble sugars. *Metabolic engineering, 16*, 56-67. doi: 10.1016/j.ymben.2012.12.002

Yang, Y. H., Feng, J., Li, T., Ge, F., & Zhao, J. D. (2015). CyanOmics: an integrated database of omics for the model cyanobacterium *Synechococcus* sp. PCC 7002. *Database - the Journal of Biological Databases and Curation*, 9. doi: 10.1093/database/bau127

Yasuhara-Bell, J., Yang, Y., Barlow, R., Trapido-Rosenthal, H., & Lu, Y. (2010). In vitroevaluation of marine-microorganism extracts for anti-viral activity. *Virology Journal, 7*(1), 182. doi: 10.1186/1743-422X-7-182

Yosipovitch, G., Xiong, G. L., Haus, E., Sackett-Lundeen, L., Ashkenazi, I., & Maibach, H. I. (1998). Time-dependent variations of the skin barrier function in humans: transepidermal water loss, *stratum corneum* hydration, skin surface pH, and skin temperature. *Journal of investigative dermatology, 110*(1), 20-23. doi: 10.1046/j.1523-1747.1998.00069.x

Yuan, D., Lin, B., & Falconer, R. A. (2007). A modelling study of residence time in a macro-tidal estuary. *Estuarine, Coastal and Shelf Science, 71*(3), 401-411. doi: 10.1016/j.ecss.2006.08.023

Zhong, S. P., Zhang, Y. Z., & Lim, C. T. (2010). Tissue scaffolds for skin wound healing and dermal reconstruction. *Wiley Interdisciplinary Reviews: Nanomedicine and Nanobiotechnology, 2*(5), 510-525. doi: 10.1002/wnan.100

Zhu, Y., Graham, J. E., Ludwig, M., Xiong, W., Alvey, R. M., Shen, G., & Bryant, D. A. (2010). Roles of xanthophyll carotenoids in protection against photoinhibition and oxidative stress in the cyanobacterium *Synechococcus* sp. strain PCC 7002. *Archives of biochemistry and biophysics, 504*(1), 86-99. doi: 10.1016/j.abb.2010.07.007

Zimmerman, J. T. F. (1976). Mixing and flushing of tidal embayments in the western Dutch Wadden Sea part I: Distribution of salinity and calculation of mixing time scales. *Netherlands Journal of Sea Research, 10*(2), 149-191. doi: 10.1016/0077-7579(76)90013-2

8. Appendix

8.1. Figures

8.1.1. *Synechococcus* RCC2834

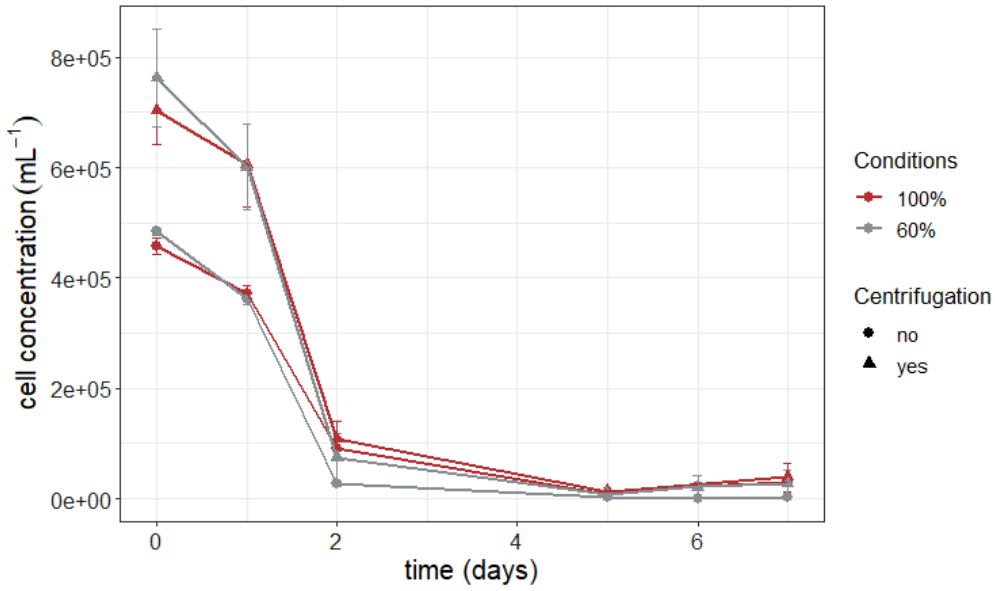

Figure 26 Cell concentrations of the centrifugation test with Synechococcus RCC2384 over seven days. The average cell concentrations (per mL, n = 4) with standard deviation for 100% and 60% osmolarity are shown over time (days). The osmolarity of the medium is indicated by colour, centrifugation protocol is indicated by shape.

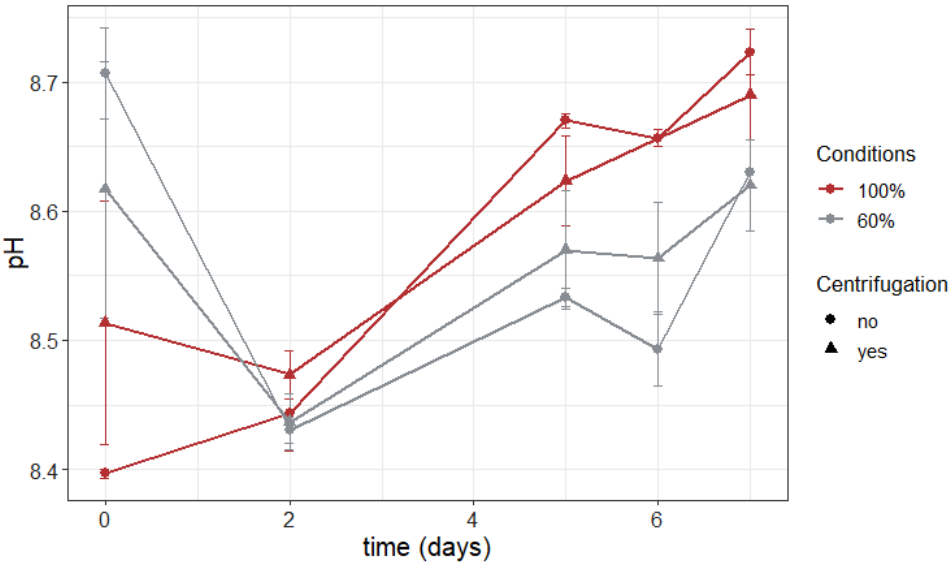

Figure 27 pH values measured as part of the centrifugation test with *Synechococcus* RCC2384 over seven days. The average pH values (n = 4) measured in every condition with standard deviation for conditions of 100% and 60% osmolarity are shown over time (days). The osmolarity of the medium is indicated by colour, centrifugation protocol is indicated by shape.

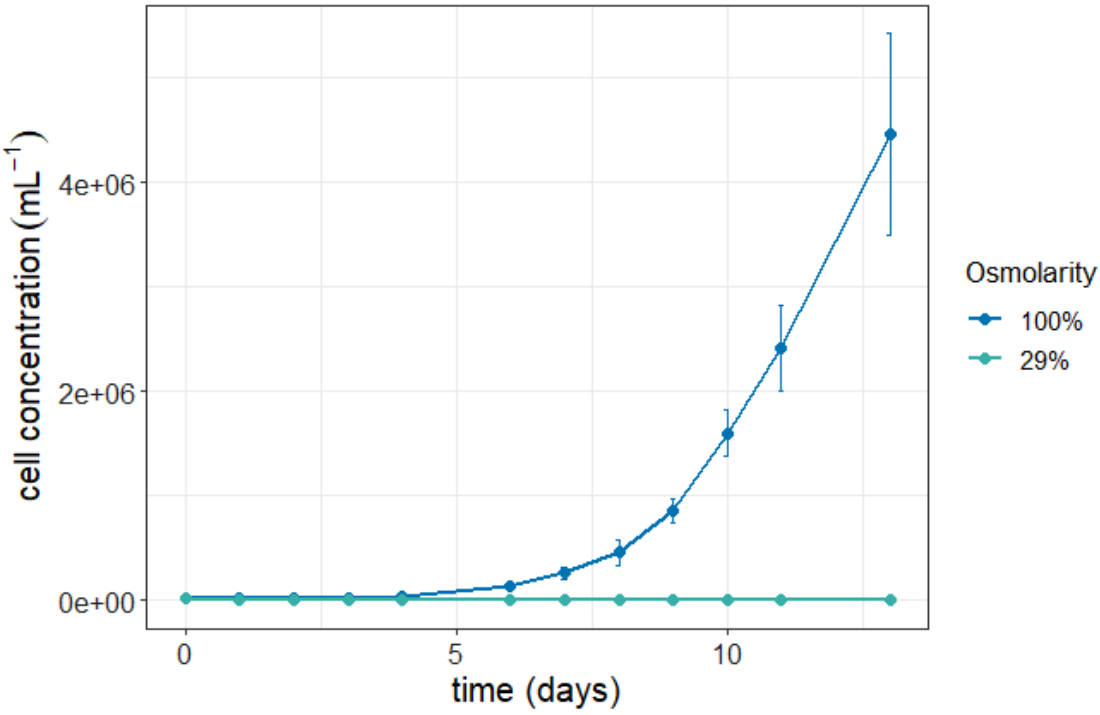

Figure 28 First quick adaptation test with *Synechococcus* RCC2384 over two weeks. Average cell concentrations (per mL, n = 5) with standard deviation are shown over time (days) for both 100% and 29% cultures. The osmolarity of the medium is indicated by colour.

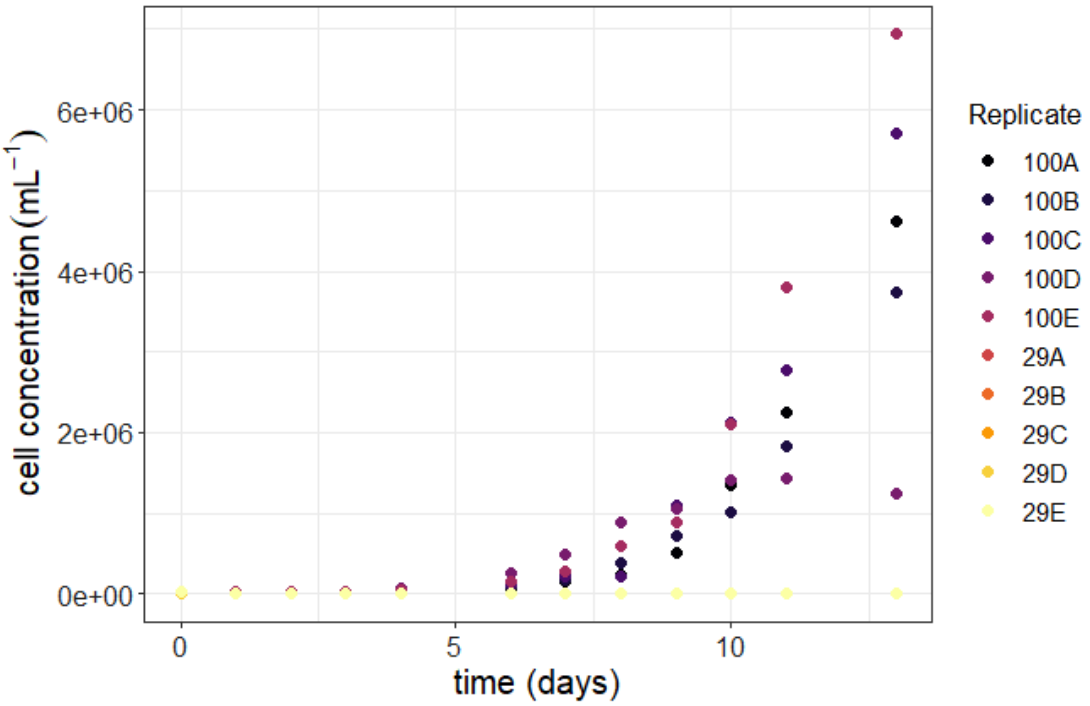

Figure 29 First quick adaptation test with Synechococcus RCC2384 over two weeks. Cell concentrations (per mL) for each of the five replicates of the osmolarity conditions 100% and 29% are shown over time (days). The number and condition of each replicate are indicated by colour.

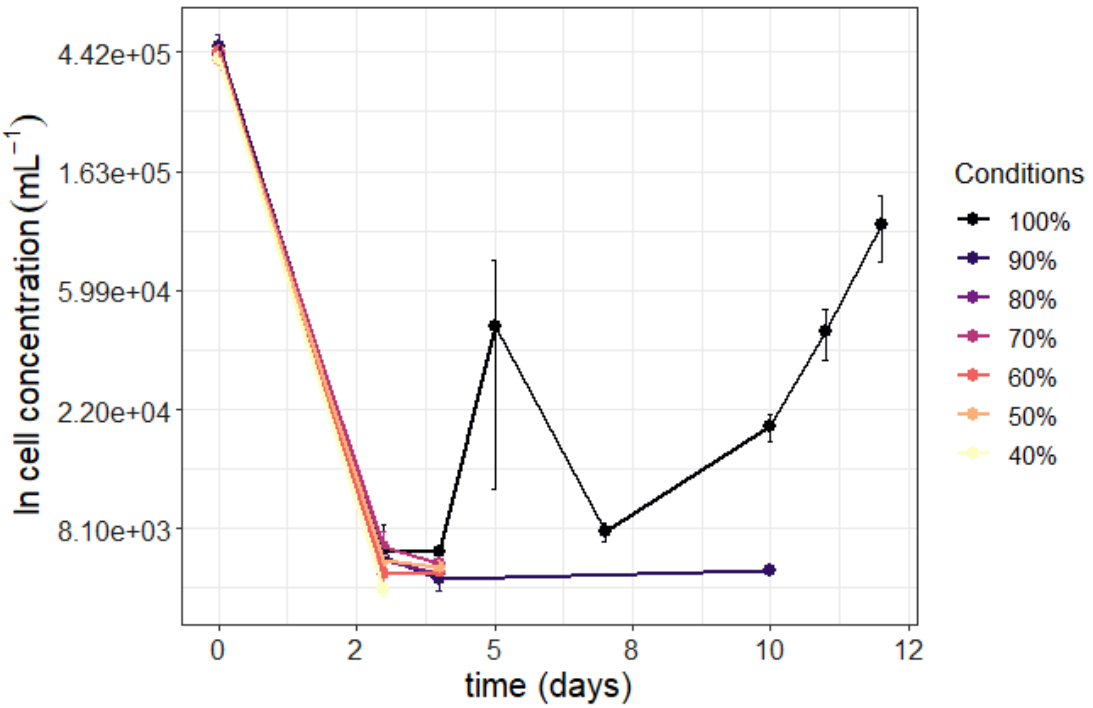

Figure 30 Cell concentrations of the second quick adaptation test with *Synechococcus* RCC2384 over twelve days. The average cell concentrations (per mL, n = 3) with standard deviation for conditions from 100% to 40% osmolarity (indicated by colour) are shown over time (days) in natural logarithm projection of the y-axis. After the 4th day, only the replicates of the control condition (100%) were followed further, apart from the 90% samples on day 10.

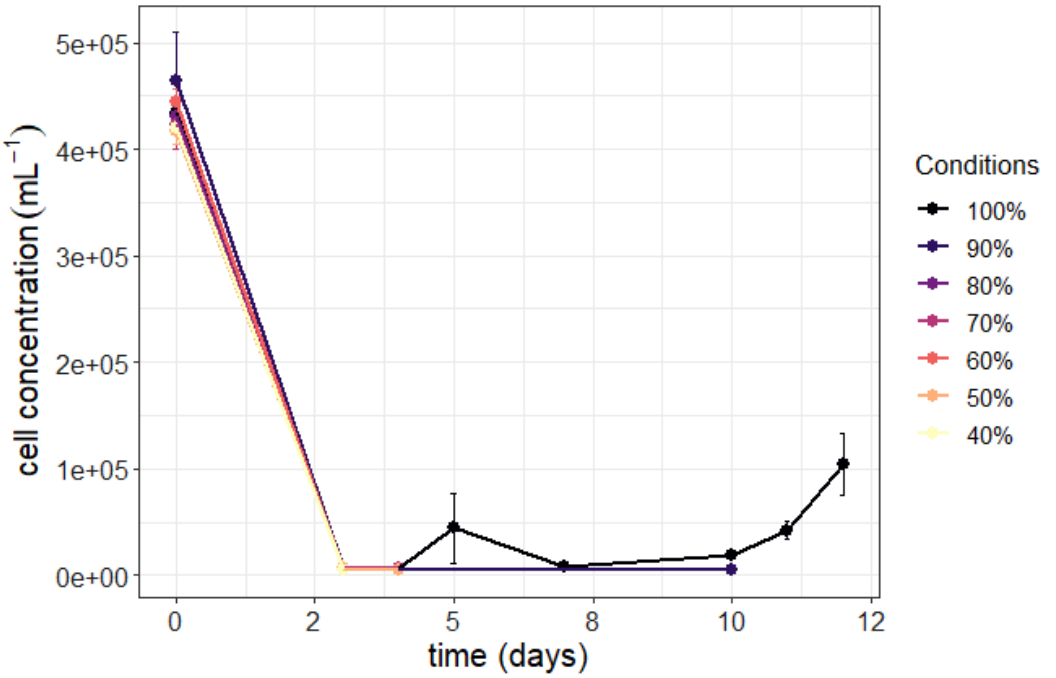

Figure 31 Cell concentrations of the second quick adaptation test with Synechococcus RCC2384 over twelve days. The average cell concentrations (per mL, *n = 3*) with standard deviation for conditions from 100% to 40% osmolarity (indicated by colour) are shown over time (days). After the 4th day, only the replicates of the control condition (100%) were followed further, apart from the 90% samples on day 10.

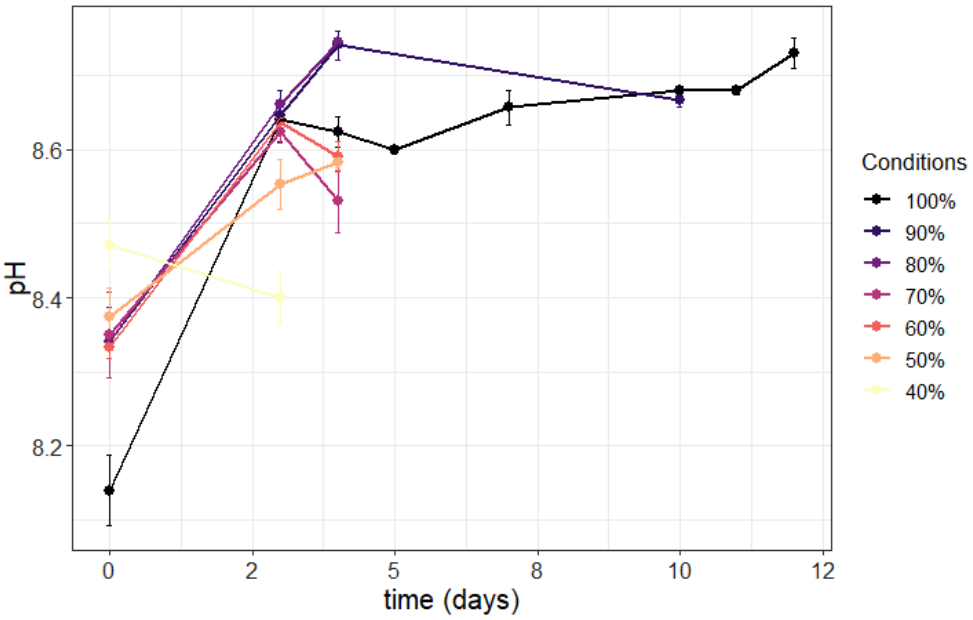

Figure 32 pH values of the second quick adaptation test with *Synechococcus* RCC2384 over twelve days. The average pH values (n = 3) measured in every condition with standard deviation for conditions from 100% to 40% osmolarity (indicated by colour) are shown over time (days). After the 4th day, only the replicates of the control condition (100%) were followed further, apart from the 90% samples on day 10.

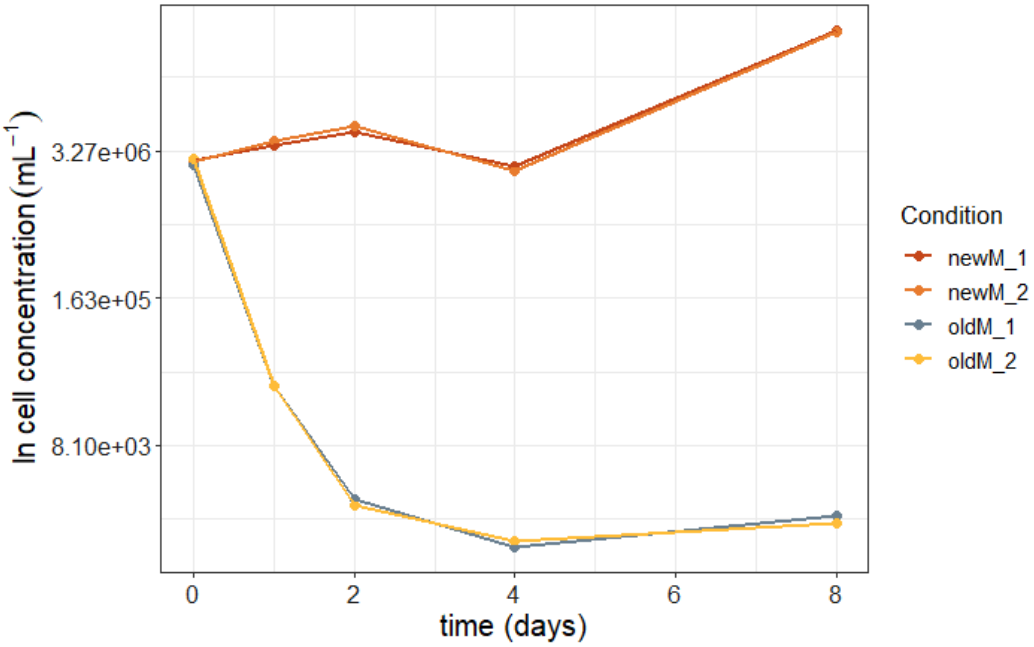

Figure 33 Cell concentrations of the medium test with *Synechococcus* RCC2384 over eight days, in conditions 'oldM' for ESAW medium prepared with salts from supplier I and 'newM' for medium prepared with salts from supplier II (see section 8.3.1). The cell concentrations (per mL) of the duplicates are given separately over time (days) in natural logarithm projection on the y-axis. The number and condition of each replicate is indicated by colour.

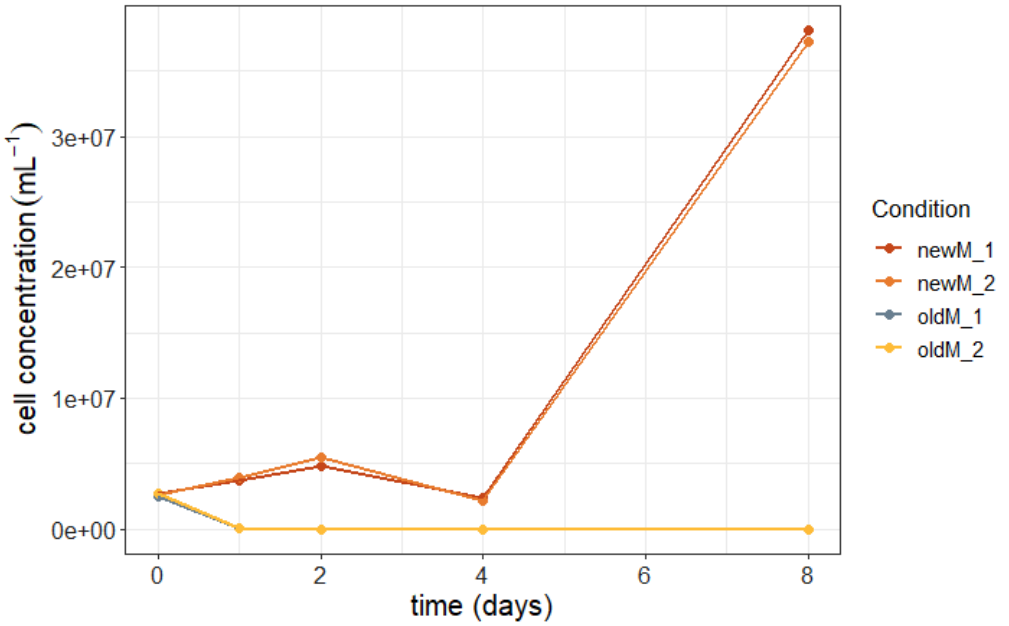

Figure 34 Cell concentrations of the medium test with *Synechococcus* RCC2384 over eight days, in conditions 'oldM' for ESAW medium prepared with salts from supplier I and 'newM' for medium prepared with salts from supplier II (see section 8.3.1). The cell concentrations (per mL) of the duplicates are given separately over time (days). The number and condition of each replicate is indicated by colour.

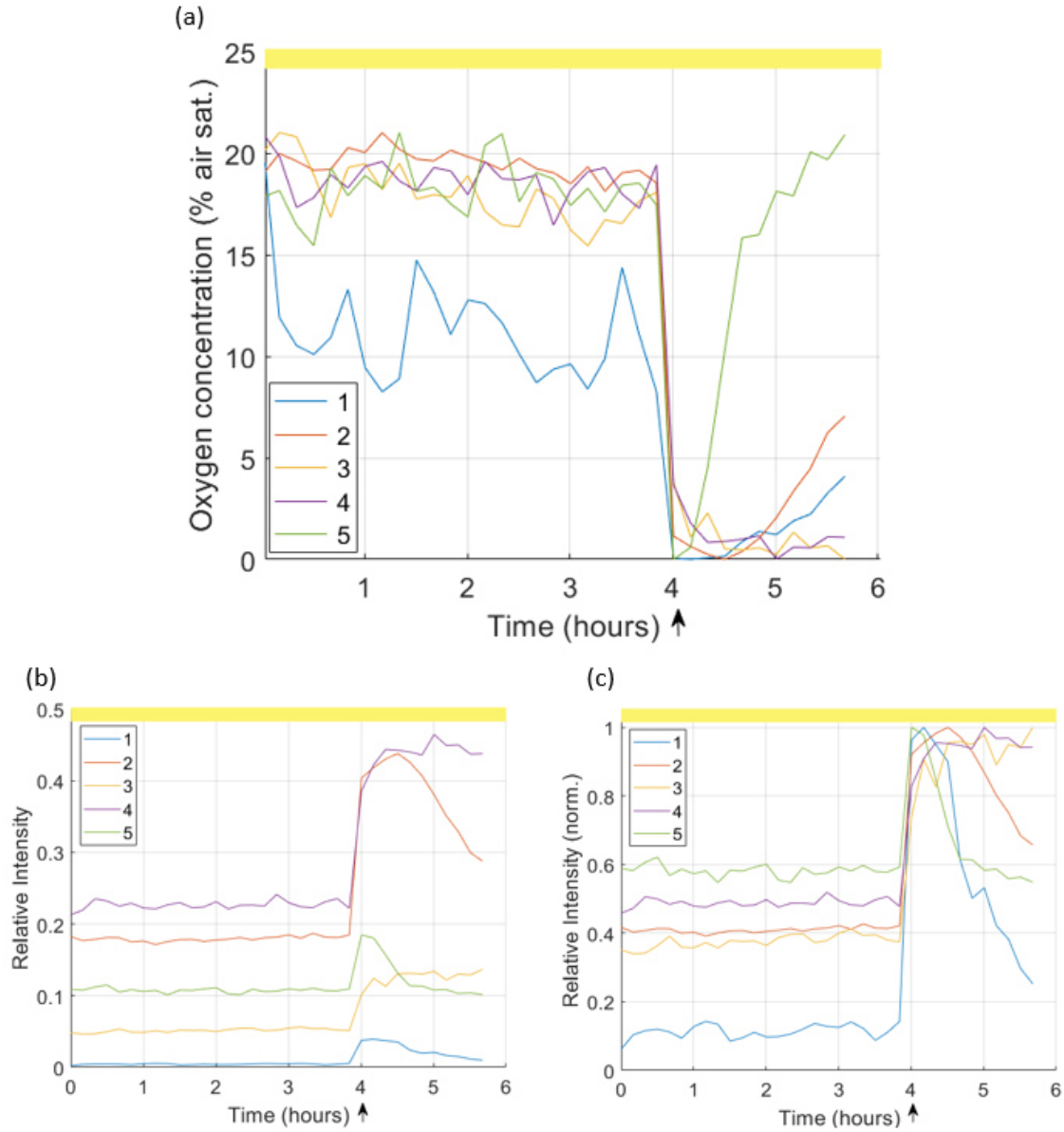

Figure 35 Oxygen measurement of 100% ESAW medium over 6 hours in the µRespirometer. The oxygen concentration (% air sat., a), relative intensity (b) and normalised relative intensity (c) recorded by the camera are plotted against time (hours). Shown here are the values from the five oxygen sensing spots (indicated in the legend) of the microfluidic chip. Pictures were taken every 10 min and the temperature was set to 30 °C. The measurement chamber was illuminated continuously over the course of the measurement (as indicated by the bar at the top) and the light was provided by a red-coloured LED at a current of 50 mA. Four hours after the start of measurement the system was flushed with water with an oxygen concentration of about 5% air sat.

8.1.2. *Synechococcus* PCC7002

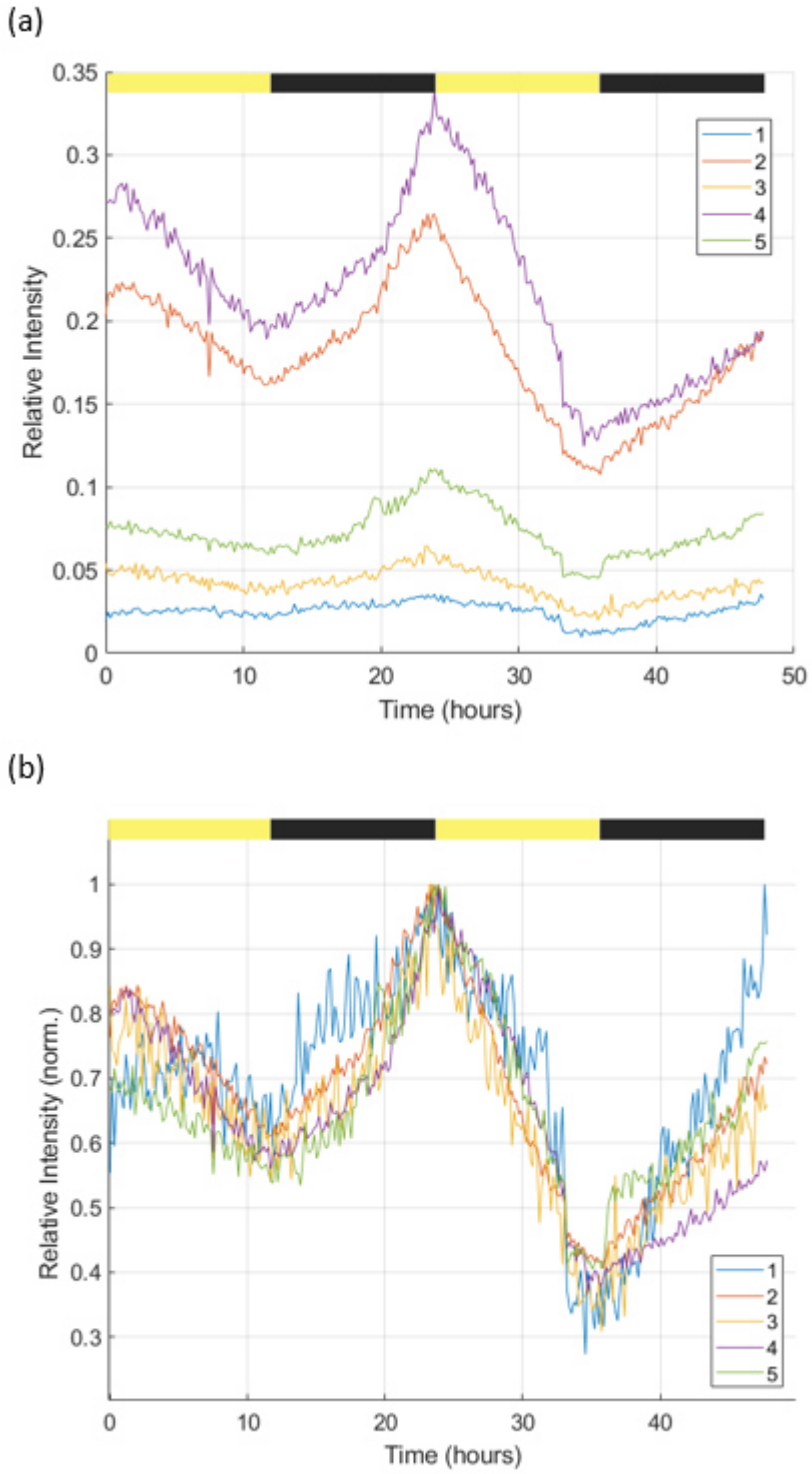

Figure 36 Oxygen measurement of *Synechococcus* PCC7002 over 48 hours in the µRespirometer. The relative (a) and normalised relative intensity (b) recorded by the camera are plotted against time (hours). Shown here are the values from the five oxygen sensing spots (indicated in the legend) of the microfluidic chip. Pictures were taken every 10 min and the temperature was set to 30 °C. The measurement chamber was illuminated in a 12:12 hour diurnal cycle from the start of the measurement (as indicated by the bar at the top) and the light was provided by a red-coloured LED at a current of 50 mA.

8.1.3. *Synechococcus* PCC7942

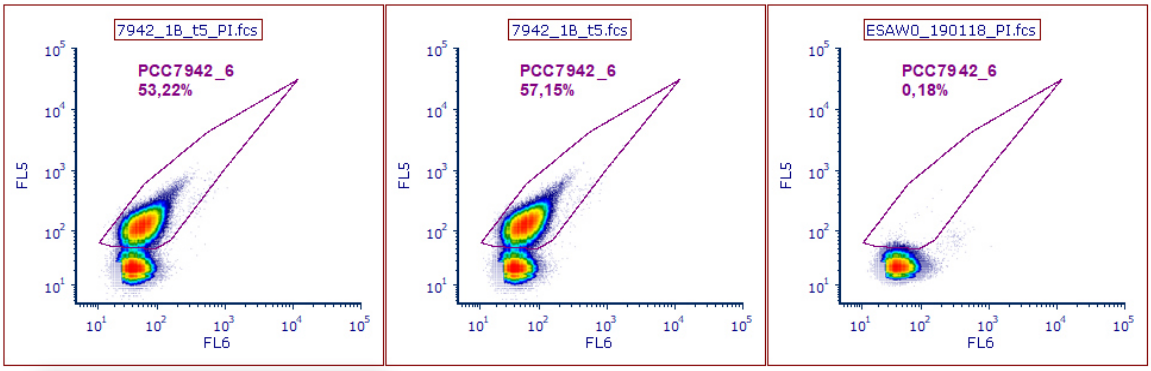

Figure 37 Exemplary presentation of the gates used to quantify the number of *Synechococcus* PCC7942 cells. Shown here is sample 1B at t_5 of the growth curve (30% ESAW pH 8.2) both stained with PI (left), unstained (middle) and sterile medium as a control (right).

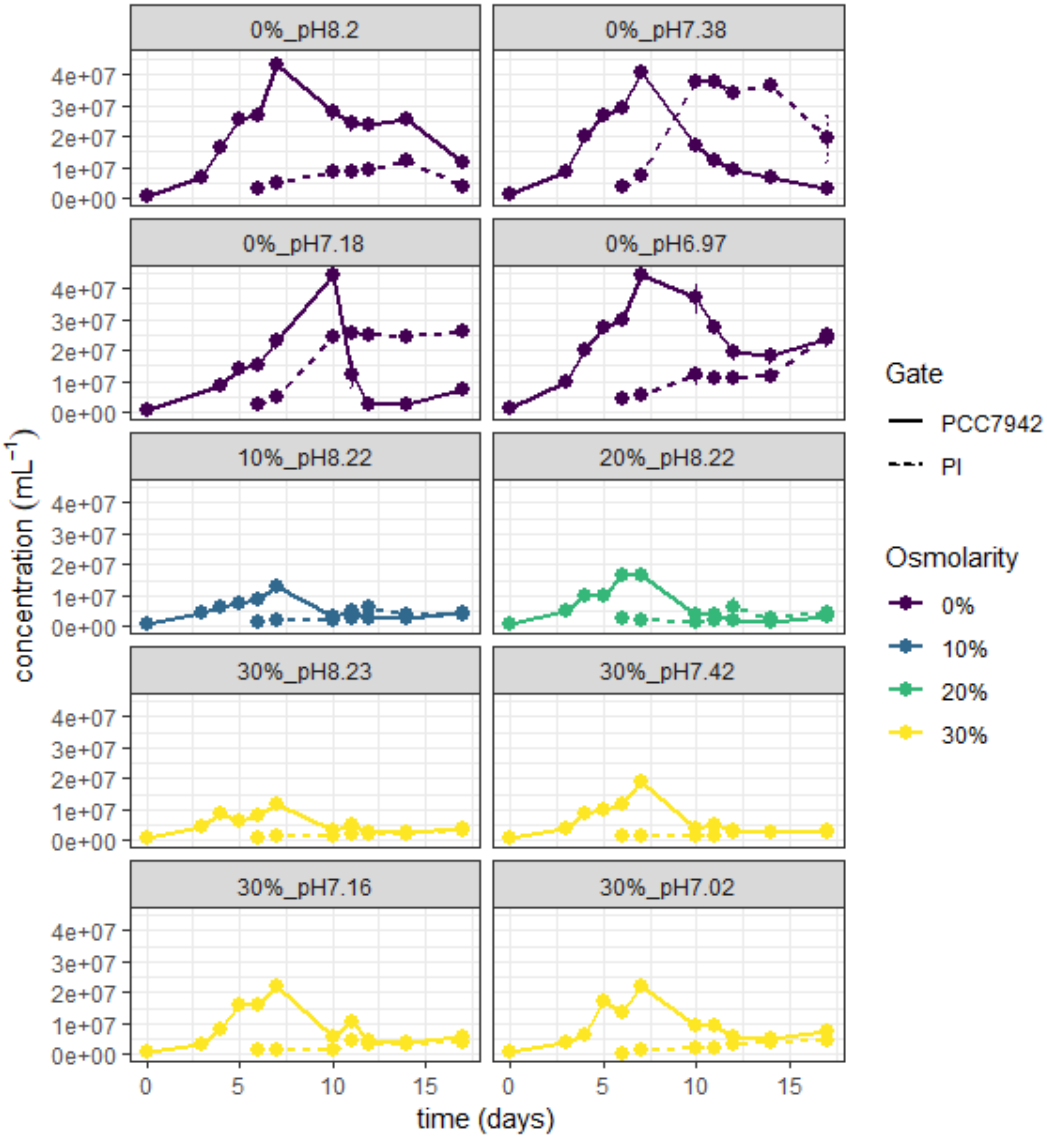

Figure 38 Growth curve of *Synechococcus* PCC7942 over 17 days. Shown here are the average concentrations (per mL, n = 4) with standard deviations for PCC7942 cells (solid line) and propidium stained particles (dashed line) over time (days) separated by condition. The osmolarity of the medium is indicated by colour.

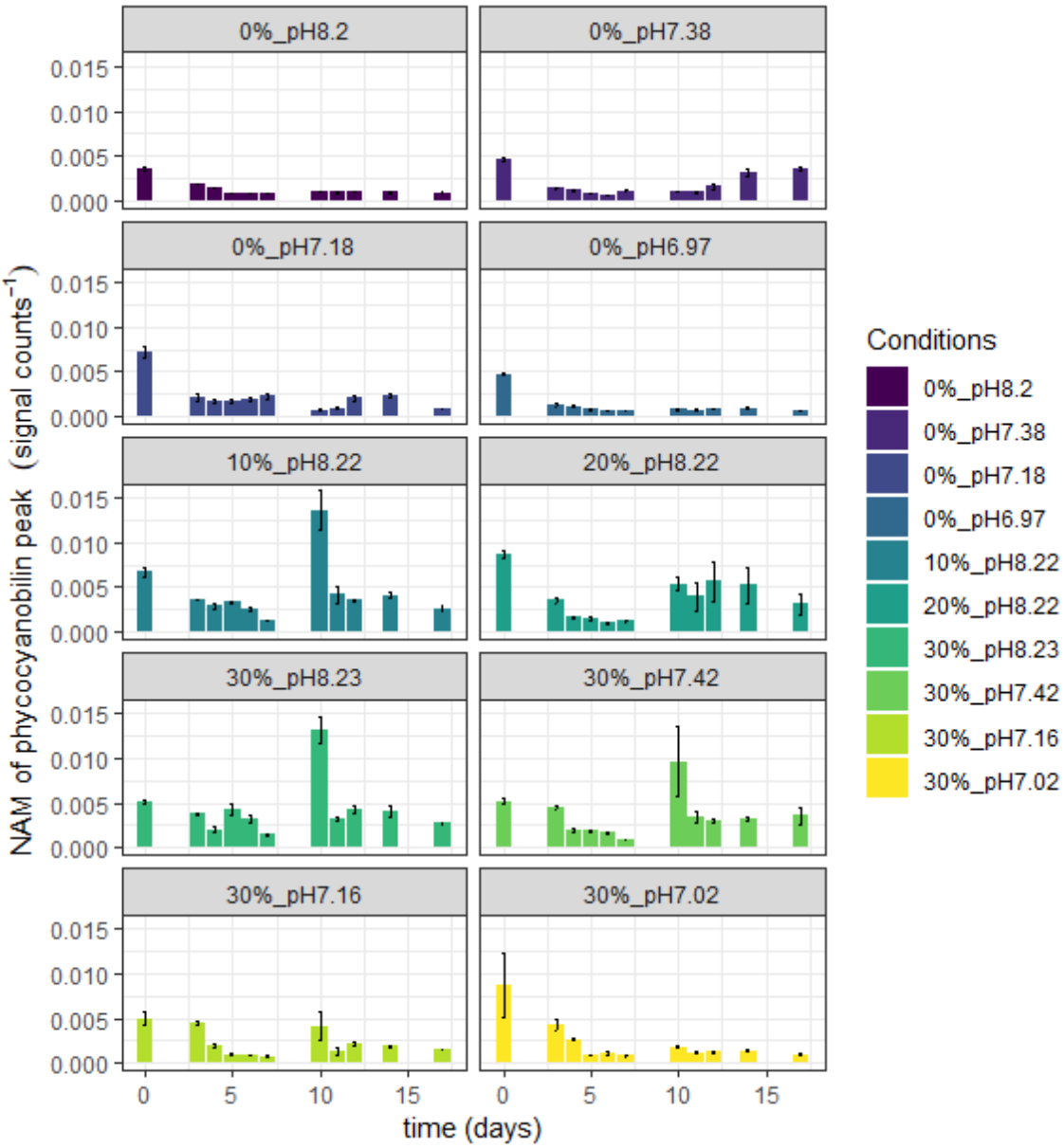

Figure 39 Normalised arithmetic means (NAM, signal counts^{-1}) of the phycocyanobilin peaks of *Synechococcus* PCC7942 plotted against time (days) and ordered by condition (indicated by colour). Shown here are the average values (n = 4) with standard deviations.

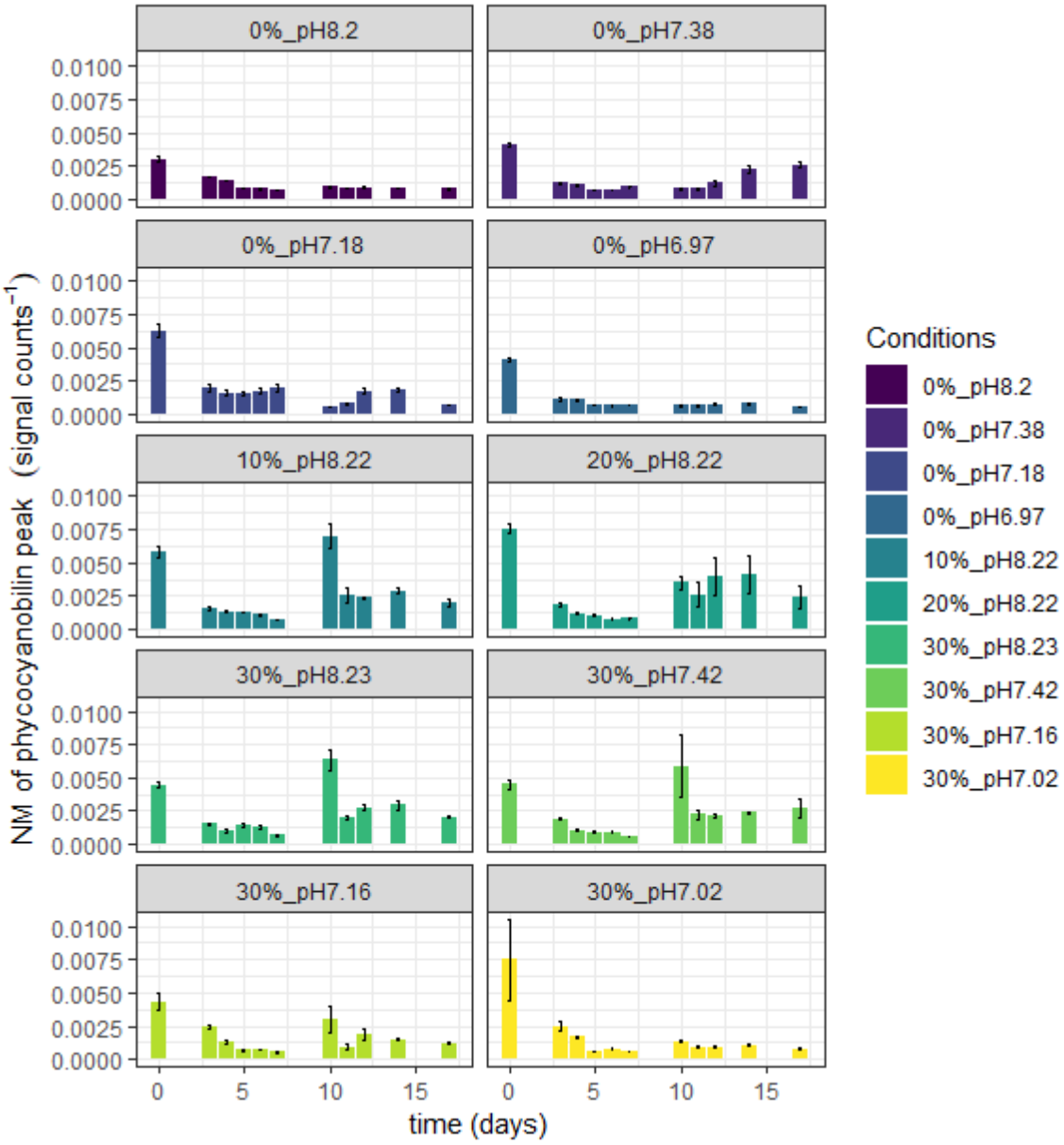

Figure 40 Normalised medians (NM, signal counts^{-1}) of the phycocyanobilin peaks of *Synechococcus* PCC7942 plotted against time (days) and ordered by condition (indicated by colour). Shown here are the average values (n = 4) with standard deviations.

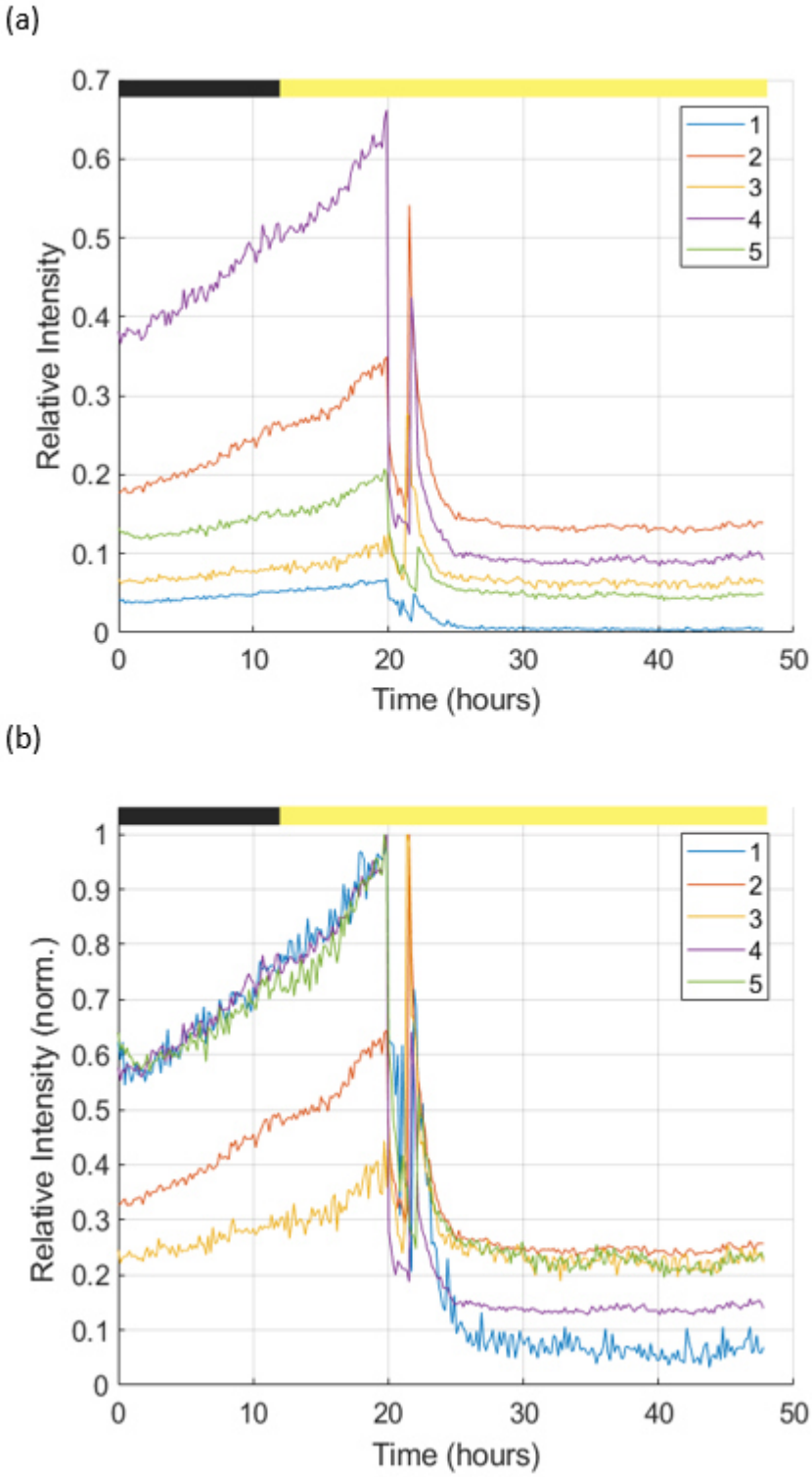

Figure 41 Oxygen measurement of Synechococcus PCC7942 over 48 hours in the µRespirometer. The relative (a) and normalised relative intensity (b) recorded by the camera are plotted against time (hours). Shown here are the values from the five oxygen sensing spots (indicated in the legend) of the microfluidic chip. Pictures were taken every 10 min and the temperature was set to 30 °C. The timespans of darkness and illumination are indicated by the bar at the top. The light was provided by a red-coloured LED at a current of 50 mA.

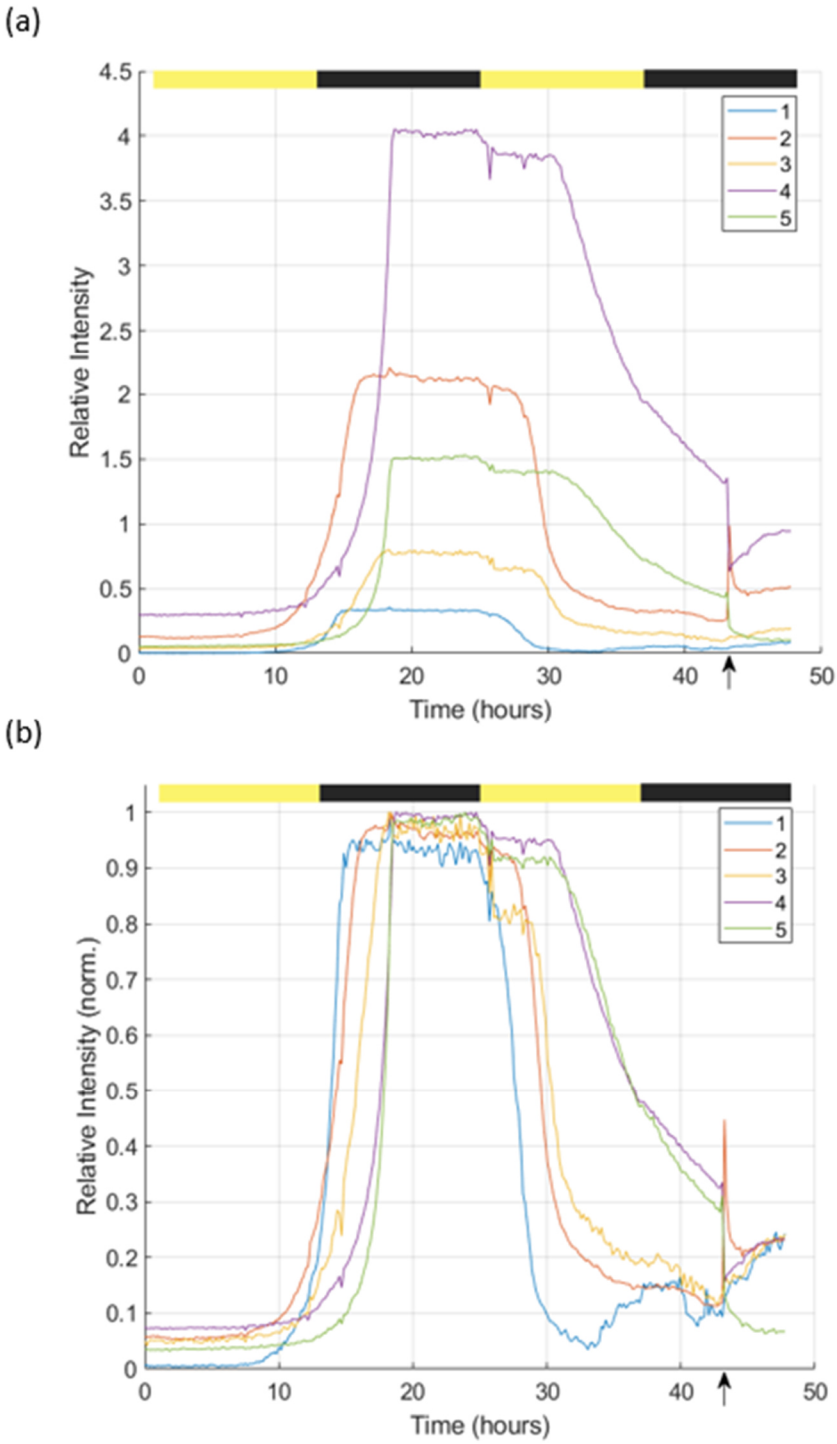

Figure 42 Oxygen measurement of *Synechococcus* PCC7942 over 48 hours in the µRespirometer as part of the growth curve (0% ESAW pH 8.2) 4 days after inoculation. The relative (a) and normalised relative intensity (b) recorded by the camera are plotted against time (hours). Shown here are the values from the five oxygen sensing spots (indicated in the legend) of the microfluidic chip. Pictures were taken every 10 min and the temperature was set to 30 °C. The measurement chamber was illuminated in a 12:12 hour diurnal cycle shifted one hour from the start of the measurement (as indicated by the bar at the top) and the light was provided by a red-coloured LED at a current of 50 mA. At 43 h and 20 min the system was flushed with water with an oxygen concentration of 3% air sat. (indicated by the arrow on the x-axis).

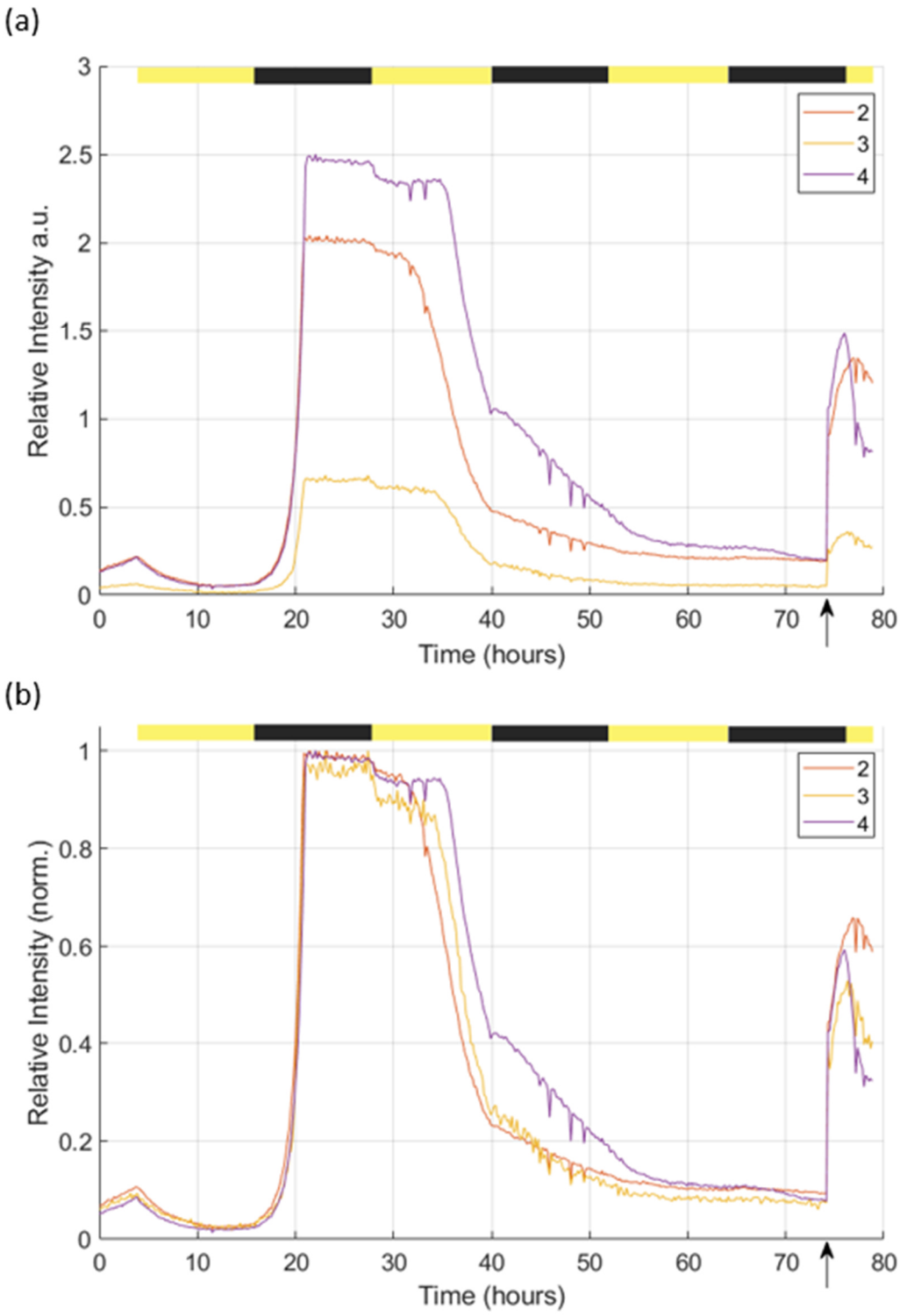

Figure 43 Oxygen measurement of *Synechococcus* PCC7942 over 79 hours in the µRespirometer as part of the growth curve (30% ESAW pH 7.0). The relative (a) and normalised relative intensity (b) recorded by the camera are plotted against time (hours). Shown here are the values from the five oxygen sensing spots (indicated in the legend) of the microfluidic chip. Pictures were taken every 10 min and the temperature was set to 30 °C. The measurement chamber was illuminated in a 12:12 hour diurnal cycle shifted four hours from the start of the measurement (as indicated by the bar at the top) and the light was provided by a red-coloured LED at a current of 50 mA. At 74 h and 10 min the system was flushed with water with an oxygen concentration of 3% air sat. (indicated by the arrow on the x-axis). The data from spots 1 and 5 were removed from the graph for clarity. At 74 h and 10 min the system was flushed with water with an oxygen concentration of 3% air sat. (indicated by the arrow on the x-axis).

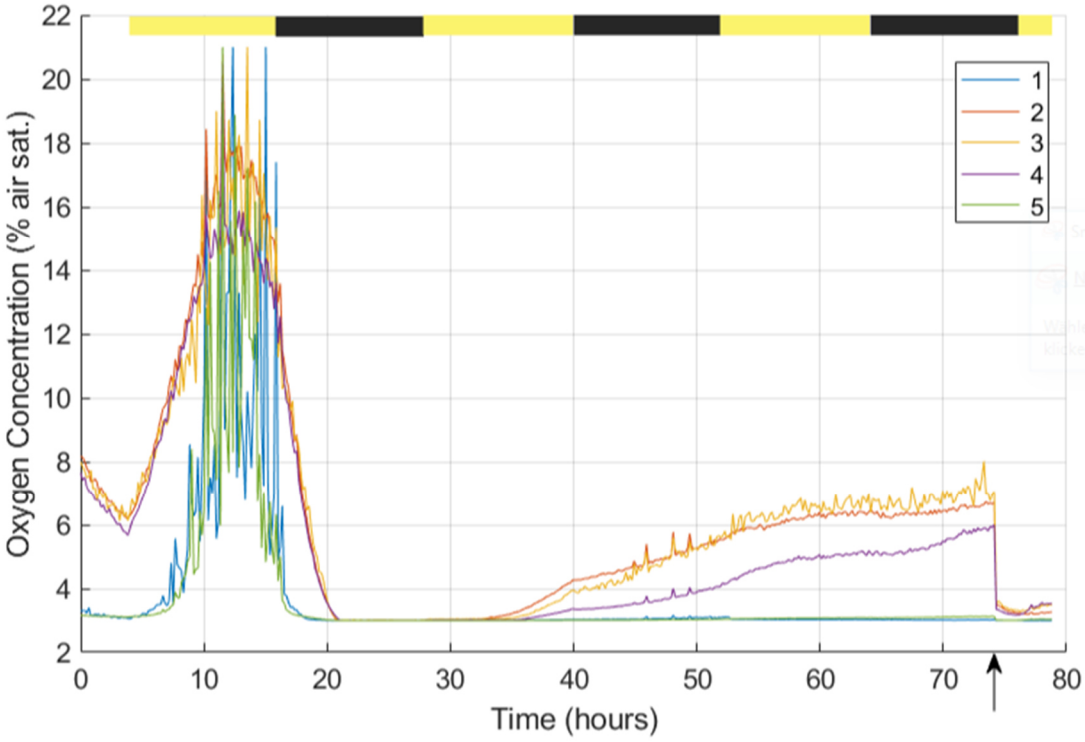

Figure 44 Oxygen measurement of *Synechococcus* PCC7942 over 79 hours in the µRespirometer as part of the growth curve (30% ESAW pH 7.0). The oxygen concentration (% air saturation) calculated from the intensity of the phosphorescent signal is plotted against time (hours). Shown here are the values from the five oxygen sensing spots (indicated in the legend) of the microfluidic chip. Pictures were taken every 10 min and the temperature was set to 30 °C. The measurement chamber was illuminated in a 12:12 hour diurnal cycle shifted four hours from the start of the measurement (as indicated by the bar at the top) and the light was provided by a red-coloured LED at a current of 50 mA. At 74 h and 10 min the system was flushed with water with an oxygen concentration of 3% air sat. (indicated by the arrow on the x-axis).

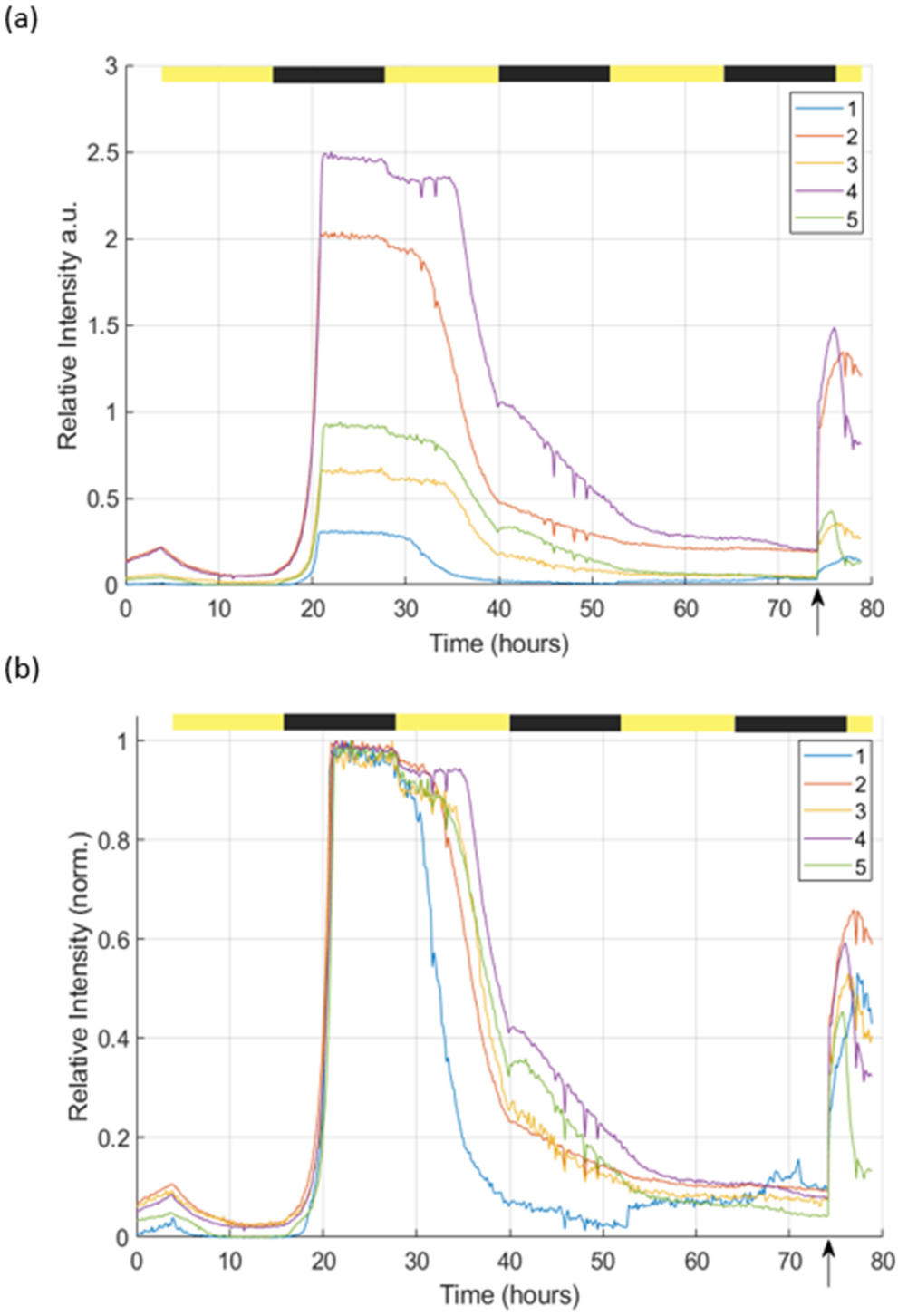

Figure 45 Oxygen measurement of *Synechococcus* PCC7942 over 79 hours in the µRespirometer as part of the growth curve (30% ESAW pH 7.0). The relative (a) and normalised relative intensity (b) recorded by the camera are plotted against time (hours). Shown here are the values from the five oxygen sensing spots (indicated in the legend) of the microfluidic chip. Pictures were taken every 10 min and the temperature was set to 30 °C. The measurement chamber was illuminated in a 12:12 hour diurnal cycle shifted four hours from the start of the measurement (as indicated by the bar at the top) and the light was provided by a red-coloured LED at a current of 50 mA. At 74 h and 10 min the system was flushed with water with an oxygen concentration of 3% air sat. (indicated by the arrow on the x-axis).

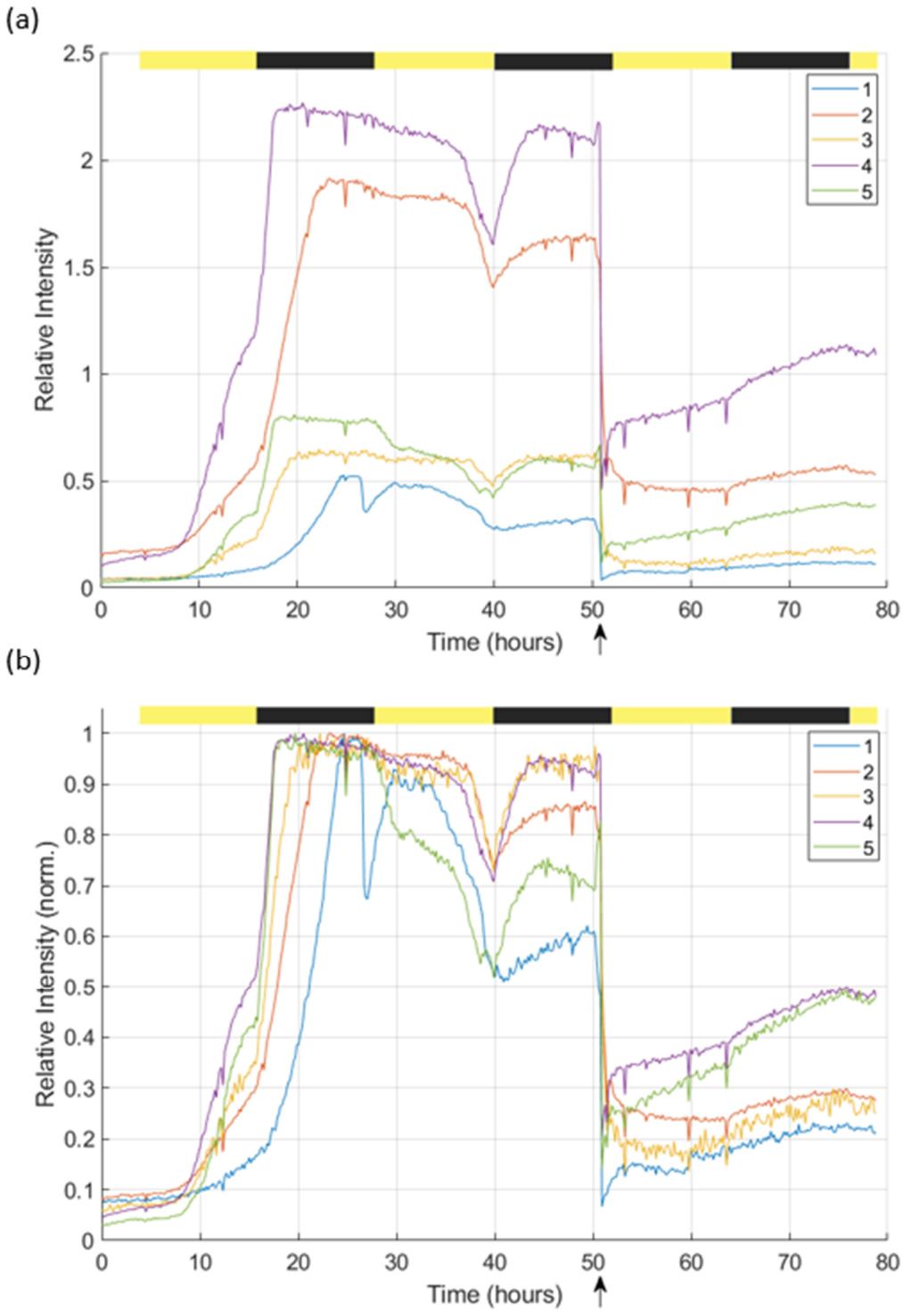

Figure 46 Oxygen measurement of *Synechococcus* PCC7942 over 79 hours in the µRespirometer as part of the growth curve (0% ESAW pH 8.2). The relative (a) and normalised relative intensity (b) recorded by the camera are plotted against time (hours). Shown here are the values from the five oxygen sensing spots (indicated in the legend) of the microfluidic chip. Pictures were taken every 10 min and the temperature was set to 30 °C. The measurement chamber was illuminated in a 12:12 hour diurnal cycle shifted four hours from the start of the measurement (as indicated by the bar at the top) and the light was provided by a red-coloured LED at a current of 50 mA. At 50 h and 50 min the system was flushed with water with an oxygen concentration of 2.7% air sat. (indicated by the arrow on the x-axis).

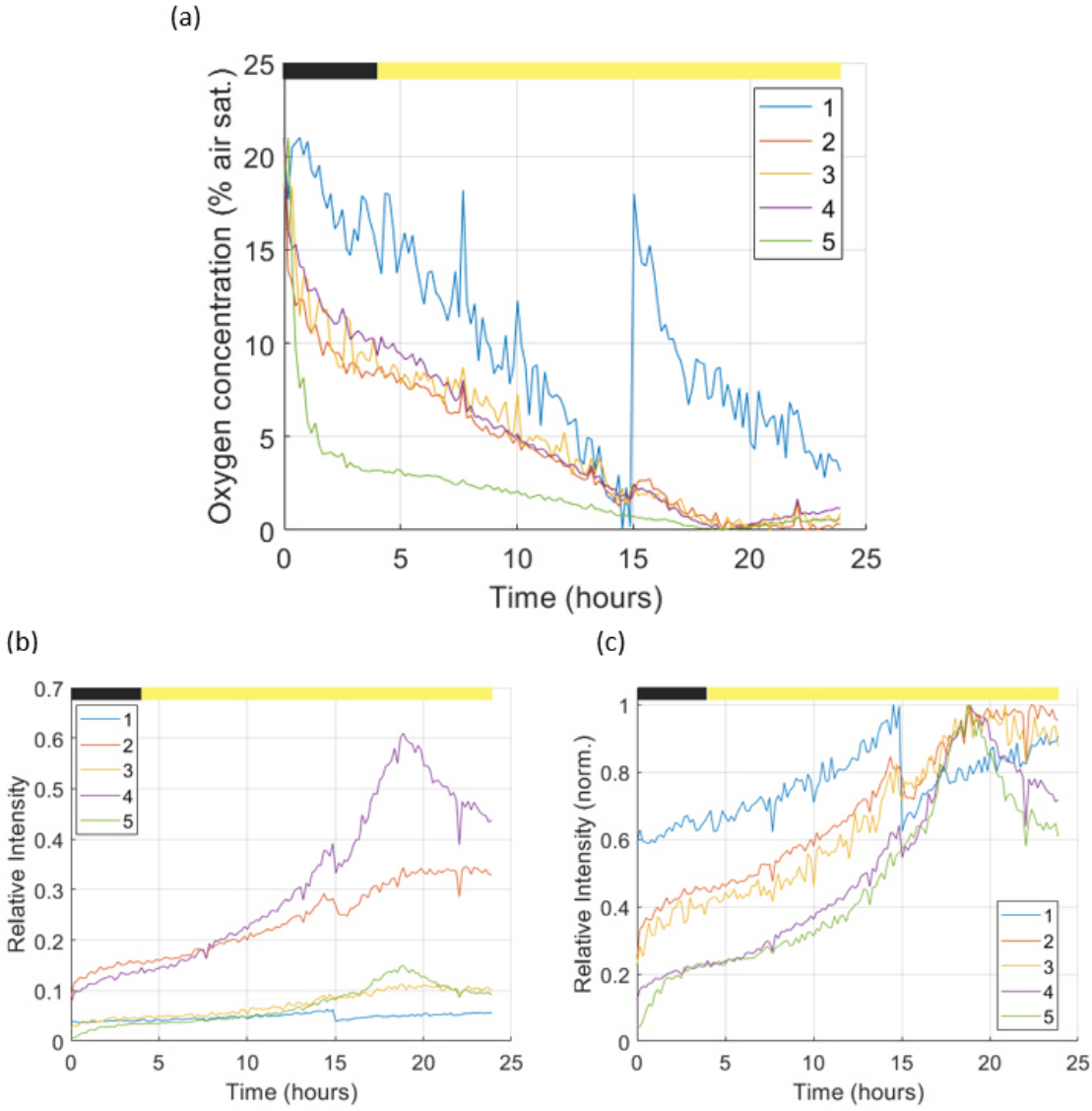

Figure 47 Oxygen measurement of 0% ESAW medium over 24 hours in the µRespirometer. The oxygen concentration (% air sat., a), relative intensity (b) and normalised relative intensity (c) recorded by the camera are plotted against time (hours). Shown here are the values from the five oxygen sensing spots (indicated in the legend) of the microfluidic chip. Pictures were taken every 10 min and the temperature was set to 30 °C. The measurement chamber was illuminated for 20 hours, shifted 4 hours after the start of measurement (as indicated by the bar at the top) and the light was provided by a red-coloured LED at a current of 50 mA.

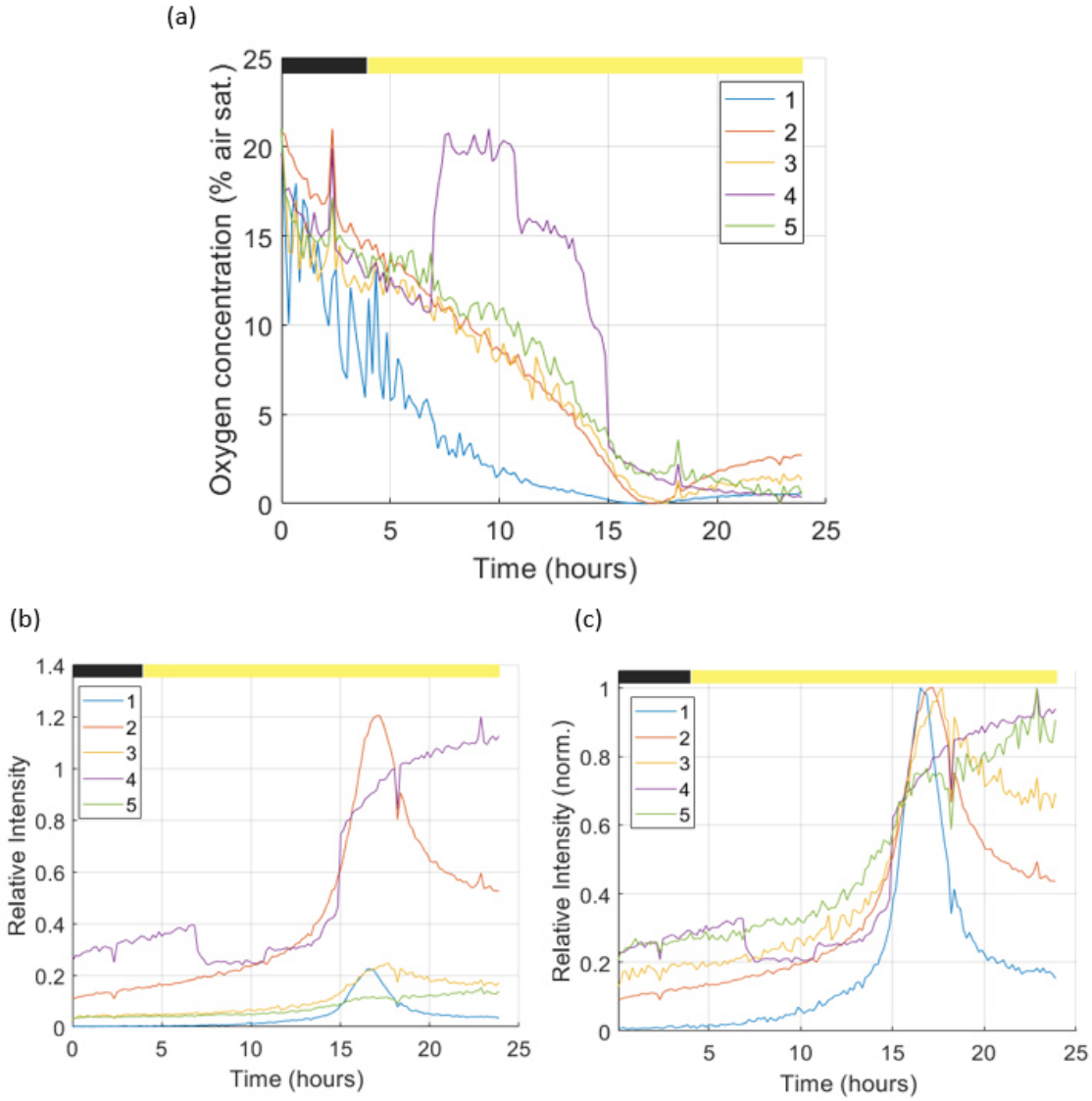

Figure 48 Oxygen measurement of 30% ESAW medium over 24 hours in the µRespirometer. The oxygen concentration (% air sat., a), relative intensity (b) and normalised relative intensity (c) recorded by the camera are plotted against time (hours). Shown here are the values from the five oxygen sensing spots (indicated in the legend) of the microfluidic chip. Pictures were taken every 10 min and the temperature was set to 30 °C. The measurement chamber was illuminated for 20 hours, shifted 4 hours after the start of measurement (as indicated by the bar at the top) and the light was provided by a red-coloured LED at a current of 50 mA.

8.2. Statistical Analysis

8.2.1. Effect of Propidium Iodide Staining

```
> bartlett.test(synperml ~ staining_f, data=growth_PI)

        Bartlett test of homogeneity of variances

data:  synperml by staining_f
Bartlett's K-squared = 2.1423e-05, df = 1, p-value = 0.9963

> bartlett.test(synperml ~ condition_f, data=growth_PI)

        Bartlett test of homogeneity of variances

data:  synperml by condition_f
Bartlett's K-squared = 28.78, df = 9, p-value = 0.0007057

> #Levene test
> leveneTest(synperml ~ staining_f, data=growth_PI)
Levene's Test for Homogeneity of Variance (center = median)
      Df F value Pr(>F)
group  1  0.0016 0.9677
      88
> leveneTest(synperml ~ condition_f, data=growth_PI)
Levene's Test for Homogeneity of Variance (center = median)
      Df F value  Pr(>F)
group  9  2.1816 0.03354 *
       70
---
Signif. codes:  0 ‘***’ 0.001 ‘**’ 0.01 ‘*’ 0.05 ‘.’ 0.1 ‘ ’ 1
> #Fligner test
> fligner.test(synperml ~ interaction(staining_f, condition_f),
data=growth_PI)

        Fligner-Killeen test of homogeneity of variances

data:  synperml by interaction(staining_f, condition_f)
Fligner-Killeen:med chi-squared = 27.398, df = 19, p-value = 0.09572

> fligner.test(synperml ~ staining_f, data=growth_PI)

        Fligner-Killeen test of homogeneity of variances

data:  synperml by staining_f
Fligner-Killeen:med chi-squared = 0.045406, df = 1, p-value = 0.8313

> fligner.test(synperml ~ condition_f, data=growth_PI)
```

```
        Fligner-Killeen test of homogeneity of variances

data:  synperml by condition_f
Fligner-Killeen:med chi-squared = 15.384, df = 9, p-value = 0.08092
```

```
> res.man <- aov(synperml ~ staining_f*condition_f, data =
growth_PI)
> summary(res.man,test = "Wilks")
                       Df    Sum Sq   Mean Sq F value Pr(>F)
staining_f              1 1.854e+12 1.854e+12   0.323  0.572
condition_f             9 1.105e+16 1.227e+15 214.120 <2e-16
***
staining_f:condition_f  9 1.671e+13 1.857e+12   0.324  0.964
Residuals              60 3.439e+14 5.732e+12
---
Signif. codes:  0 ‘***’ 0.001 ‘**’ 0.01 ‘*’ 0.05 ‘.’ 0.1 ‘ ’ 1
10 observations deleted due to missingness
```

8.2.2. Growthrates ($t_0 - t_1$) over pH t_0

```
bartlett.test(growthrate ~ osmolarity, data=growthrate_syn)

        Bartlett test of homogeneity of variances

data:  growthrate by osmolarity
Bartlett's K-squared = 18.349, df = 3, p-value = 0.0003727

bartlett.test(growthrate ~ pH_adjusted_f, data=growthrate_syn)

        Bartlett test of homogeneity of variances

data:  growthrate by pH_adjusted_f
Bartlett's K-squared = 15.199, df = 3, p-value = 0.001655

> leveneTest(growthrate ~ osmolarity, data=growthrate_syn)
Levene's Test for Homogeneity of Variance (center = median)
      Df F value Pr(>F)
group  3   0.352 0.7879
      36
> #Levene test
> leveneTest(growthrate ~ pH_adjusted_f, data=growthrate_syn)
Levene's Test for Homogeneity of Variance (center = median)
      Df F value Pr(>F)
group  3  1.4724 0.2384
      36
> fligner.test(growthrate ~ pH_actual, data=growthrate_syn)
```

```
        Fligner-Killeen test of homogeneity of variances

data:  growthrate by pH_actual
Fligner-Killeen:med chi-squared = 34.467, df = 31, p-value = 0.3054

> #Fligner test
> fligner.test(growthrate ~ interaction(pH_actual, osmolarity, pH_ad-
justed_f), data=growthrate_syn)

        Fligner-Killeen test of homogeneity of variances

data:  growthrate by interaction(pH_actual, osmolarity, pH_adjusted_f)
Fligner-Killeen:med chi-squared = 30.954, df = 35, p-value = 0.6638

> fligner.test(growthrate ~ osmolarity, data=growthrate_syn)

        Fligner-Killeen test of homogeneity of variances

data:  growthrate by osmolarity
Fligner-Killeen:med chi-squared = 4.0466, df = 3, p-value = 0.2565

> fligner.test(growthrate ~ pH_adjusted_f, data=growthrate_syn)

        Fligner-Killeen test of homogeneity of variances

data:  growthrate by pH_adjusted_f
Fligner-Killeen:med chi-squared = 3.9002, df = 3, p-value = 0.2724

> fligner.test(synperml ~ interaction(staining_f, condition_f),
data=growth_PI)

        Fligner-Killeen test of homogeneity of variances

data:  synperml by interaction(staining_f, condition_f)
Fligner-Killeen:med chi-squared = 27.398, df = 19, p-value = 0.09572

> fligner.test(synperml ~ staining_f, data=growth_PI)

        Fligner-Killeen test of homogeneity of variances

data:  synperml by staining_f
Fligner-Killeen:med chi-squared = 0.045406, df = 1, p-value = 0.8313

> fligner.test(synperml ~ condition_f, data=growth_PI)

        Fligner-Killeen test of homogeneity of variances
```

```
data:  synperml by condition_f
Fligner-Killeen:med chi-squared = 15.384, df = 9, p-value = 0.08092
```

```
> res.man <- aov(growthrate ~ pH_actual*osmolarity*pH_adjusted_f,
data = growthrate_syn)
> summary(res.man,test = "Wilks")
                                   Df Sum Sq Mean Sq F value Pr(>F)
pH_actual                           1   7.88   7.877   4.429 0.0482
*
osmolarity                          3   6.84   2.279   1.282 0.3078
pH_adjusted_f                       3   3.89   1.296   0.729 0.5468
pH_actual:osmolarity                3   0.01   0.004   0.002 0.9998
pH_actual:pH_adjusted_f             3   1.99   0.663   0.373 0.7733
osmolarity:pH_adjusted_f            3   1.05   0.351   0.198 0.8968
pH_actual:osmolarity:pH_adjusted_f  3   0.54   0.180   0.101 0.9582
Residuals                          20  35.57   1.778
---
Signif. codes:  0 ‘***’ 0.001 ‘**’ 0.01 ‘*’ 0.05 ‘.’ 0.1 ‘ ’ 1
```

8.2.3. Geometric Mean of Pigment ($t_0 - t_1$) over pH t_0

```
> #Bartlett's test of homogeneity of variances
> bartlett.test(normgmean ~ osmolarity, data=pigment_pH)

        Bartlett test of homogeneity of variances

data:  normgmean by osmolarity
Bartlett's K-squared = 4.368, df = 3, p-value = 0.2244

> #Levene test
> leveneTest(normgmean ~ osmolarity, data=pigment_pH)
Levene's Test for Homogeneity of Variance (center = median)
      Df F value Pr(>F)
group  3  1.4961 0.2321
      36
> #Fligner test
> fligner.test(normgmean ~ interaction(pH_actual, osmolarity), data=pig-
ment_pH)

        Fligner-Killeen test of homogeneity of variances

data:  normgmean by interaction(pH_actual, osmolarity)
Fligner-Killeen:med chi-squared = 32.573, df = 33, p-value = 0.4883

> fligner.test(normgmean ~ pH_actual, data=pigment_pH)

        Fligner-Killeen test of homogeneity of variances
```

```
data:  normgmean by pH_actual
Fligner-Killeen:med chi-squared = 31.736, df = 31, p-value = 0.4296

> fligner.test(normgmean ~ osmolarity, data=pigment_pH)

        Fligner-Killeen test of homogeneity of variances

data:  normgmean by osmolarity
Fligner-Killeen:med chi-squared = 4.4273, df = 3, p-value = 0.2189

> #MANOVA test Wilkes Counts
> res.man <- aov(normgmean ~ pH_actual*osmolarity, data = pigment_pH)
> summary(res.man,test = "Wilks")
                     Df    Sum Sq   Mean Sq F value   Pr(>F)
pH_actual             1 4.411e-06 4.411e-06  28.344 7.74e-06 ***
osmolarity            3 7.404e-06 2.468e-06  15.858 1.70e-06 ***
pH_actual:osmolarity  3 2.870e-07 9.600e-08   0.614    0.611
Residuals            32 4.980e-06 1.560e-07
---
Signif. codes:  0 ‘***’ 0.001 ‘**’ 0.01 ‘*’ 0.05 ‘.’ 0.1 ‘ ’ 1
```

8.3. Tables

8.3.1. Materials & Methods

Table 5 Recipe for the salt solution 1 (anhydrous salts) for ESAW medium (Berges *et al.*, 2001; Harrison *et al.*, 1980). The salts were dissolved in ddH_2O. The supplier is given for both the Alfred Wegener Institute (I) and for the University of Bremen (II).

Component	Quantity ($g\ L^{-1}$)	Final concentration (M)	Supplier I	Supplier II
NaCl	21.194	$3.63 \cdot 10^{-1}$	PanReac AppliChem, ITW Reagents (Darmstadt, Germany)	VWR International (Radnor, PE, USA)
Na_2SO_4	3.550	$2.50 \cdot 10^{-2}$	PanReac AppliChem	Sigma-Aldrich (St. Louis, MO, USA)
KCl	0.599	$8.03 \cdot 10^{-3}$	PanReac AppliChem	Janssen-Cilag (Neuss, Germany)
$NaHCO_3$	0.174	$2.07 \cdot 10^{-3}$	PanReac AppliChem	Sigma-Aldrich

KBr	0.0863	$7.25 \cdot 10^{-4}$	Acros Organics, Thermo Fisher Scientific (Waltham, MA, USA)	Acros Organics, Thermo Fisher Scientific
NaF	0.0028	$6.67 \cdot 10^{-5}$	Acros Organics	Sigma-Aldrich

Table 6 Recipe for the salt solution 2 (hydrated salts) for ESAW medium (Berges *et al.*, 2001; Harrison *et al.*, 1980). The salts were dissolved in ddH_2O. The supplier is given for both the Alfred Wegener Institute (I) and for the University of Bremen (II).

Component	Quantity ($g\ L^{-1}$)	Final concentration (M)	Supplier I	Supplier II
$MgCl_2 \cdot 6\ H_2O$	9.592	$4.71 \cdot 10^{-2}$	PanReac AppliChem, ITW Reagents (Darmstadt, Germany)	Honeywell Fluka™, Thermo Fisher Scientific (Waltham, MA, USA)
$CaCl_2 \cdot 2\ H_2O$	1.344	$9.14 \cdot 10^{-3}$	PanReac AppliChem	Merck (Darmstadt, Germany)
$SrCl_2 \cdot 6\ H_2O$	0.0218	$8.18 \cdot 10^{-5}$	Acros Organics, Thermo Fisher Scientific (Waltham, MA, USA)	Acros Organics

Table 7 Stock solutions for major nutrients for ESAW medium (Berges *et al.*, 2001; Harrison *et al.*, 1980). The dry ingredients were dissolved in ddH_2O and sterile filtered (polycarbonate filters with 0.22 µm diameter), prior to storage at 4 °C. 1 or 2 mL of each of the major nutrients was added per litre of ESAW Medium. The supplier is given for both the Alfred Wegener Institute (I) and for the University of Bremen (II).

Component	Stock concentration ($g\ L^{-1}$)	Quantity ($ml\ L^{-1}$)	Final concentration (M)	Supplier I	Supplier II
$NaNO_3$	46.67	1	$5.49 \cdot 10^{-4}$	neoFroxx (Einhausen, Germany)	Merck (Darmstadt, Germany)
$NaH_2PO_4 \cdot H_2O$	3.094	1	$2.24 \cdot 10^{-5}$	Merck	Honeywell Fluka™, Thermo Fisher Scientific (Waltham, MA, USA)

$Na_2SiO_3 \cdot 9\ H_2O$	15	2	$1.06 \cdot 10^{-4}$	Acros Organics, Thermo Fisher Scientific (Waltham, USA)	Acros Organics

Table 8 Composition of the stock solutions for the Iron-EDTA stock solution for ESAW medium (Berges *et al.*, 2001; Harrison *et al.*, 1980). The dry ingredients were dissolved individually in ddH_2O and sterile filtered (polycarbonate filters with 0.22 µm diameter), prior to storage at 4 °C. 1 mL of Iron EDTA stock solution was added per litre of ESAW medium. The supplier is given for both the Alfred Wegener Institute (I) and for the University of Bremen (II).

Component	Stock concentration	Quantity ($g\ L^{-1}$)	Final concentration (M)	Supplier I	Supplier II
$Na_2EDTA \cdot 2\ H_2O$	-	2.44	$6.56 \cdot 10^{-6}$	PanReac AppliChem, ITW Reagents (Darmstadt, Germany)	Carl Roth (Karlsruhe, Germany)
$FeCl_3 \cdot 6\ H_2O$	-	1.77	$6.55 \cdot 10^{-6}$	Honeywell Fluka™, Thermo Fisher Scientific (Waltham, MA, USA)	Merck (Darmstadt, Germany)

Table 9 Composition of the trace metal stock solution for ESAW medium (Berges *et al.*, 2001; Harrison *et al.*, 1980). The dry ingredients were dissolved individually in ddH_2O and sterile filtered (polycarbonate filters with 0.22 µm diameter), prior to storage at 4 °C. 1 mL of trace metal stock solution was added per litre of ESAW medium. The supplier is given for both the Alfred Wegener Institute (I) and for the University of Bremen (II).

Component	Stock concentration	Quantity	Final concentration (M)	Supplier I	Supplier II
$Na_2EDTA \cdot 2\ H_2O$	-	$3.09\ g\ L^{-1}$	$8.30 \cdot 10^{-6}$	PanReac AppliChem, ITW Reagents (Darmstadt, Germany)	PanReac AppliChem
$ZnSO_4 \cdot 7\ H_2O$	-	$0.073\ g\ L^{-1}$	$2.54 \cdot 10^{-7}$	Bernd Kraft (Duisburg, Germany)	Merck (Darmstadt, Germany)

$CoSO_4 \cdot 7\ H_2O$	-	0.016 g L^{-1}	$5.69 \cdot 10^{-8}$	Carl Roth (Karlsruhe, Germany)	Merck
$MnSO_4 \cdot 4\ H_2O$	-	0.54 g L^{-1}	$2.42 \cdot 10^{-6}$	Thermo Fisher Scientific (Waltham, MA, USA)	Merck
$Na_2MoO_4 \cdot 2\ H_2O$[g]	1.48 g L^{-1}	1 mL L^{-1}	$6.12 \cdot 10^{-9}$	Carl Roth	Merck
Na_2SeO_3[g]	0.17 g L^{-1}	1 mL L^{-1}	$1.00 \cdot 10^{-9}$	Sigma-Aldrich (St. Louis, MO, USA)	Sigma-Aldrich
$NiCl_2 \cdot 6\ H_2O$[g]	1.49 g L^{-1}	1 mL L^{-1}	$6.27 \cdot 10^{-9}$	Sigma-Aldrich	Sigma-Aldrich

Table 10 Composition of the vitamin stock solution for ESAW medium (Berges et al., 2001; Harrison et al., 1980). The dry ingredients were dissolved individually in ddH_2O and sterile filtered (polycarbonate filters with 0.22 µm diameter), prior to storage at 4 °C. 1 mL of the vitamin solution was added per litre of ESAW medium.

Component	Stock concentration	Quantity	Final concentration (M)	Supplier
Thiamine · HCl (vit. B_1)	-	0.1 g L^{-1}	$2.96 \cdot 10^{-7}$	Sigma-Aldrich (St. Louis, MO, USA)
Biotine (vit. H)	1.0 g L^{-1}	1 mL L^{-1}	$4.09 \cdot 10^{-9}$	Sigma-Aldrich
Cyanocobalamin (vit. B_{12})	2.0 g L^{-1}	1 mL L^{-1}	$1.48 \cdot 10^{-9}$	Merck (Darmstadt, Germany)

8.3.2. Results

Table 11 Centrifugation test of *Synechococcus* RCC2383. Average cell concentrations (per mL, n = 3) and pH (n = 3) are given per condition and time-point.

Osmolarity	Centrifugation	Time-point	Time (days)	pH	Cell Concentration (mL^{-1})
100%	no	t_0	0	8.40	4.68E+05
100%	yes	t_0	0	8.51	7.16E+05
60%	no	t_0	0	8.71	4.93E+05
60%	yes	t_0	0	8.62	7.77E+05
100%	no	t_1	1		3.70E+05
100%	yes	t_1	1		6.08E+05
60%	no	t_1	1		3.64E+05
60%	yes	t_1	1		6.05E+05
100%	no	t_2	2	8.44	9.94E+04
100%	yes	t_2	2	8.47	1.34E+05
60%	no	t_2	2	8.43	3.42E+04
60%	yes	t_2	2	8.44	9.10E+04
100%	no	t_3	5	8.67	1.40E+04
100%	yes	t_3	5	8.62	3.04E+04
60%	no	t_3	5	8.53	4.05E+03
60%	yes	t_3	5	8.57	1.82E+04
100%	no	t_4	6	8.66	2.85E+04
100%	yes	t_4	6	8.60	4.35E+04
60%	no	t_4	6	8.49	4.28E+03

60%	yes	t_4	6	8.56	2.87E+04
100%	no	t_5	7	8.72	4.63E+04
100%	yes	t_5	7	8.69	5.28E+04
60%	no	t_5	7	8.63	4.13E+03
60%	yes	t_5	7	8.62	4.21E+04

Table 12 First quick adaptation test of *Synechococcus* RCC2384. The average cell concentrations (mL^{-1}, n = 5) are given per condition and time-point.

Osmolarity	Time-point	Time (days)	Cell Concentration (mL^{-1})
100%	t_0	0	2.48E+04
29%	t_0	0	2.14E+04
100%	t_1	1	2.16E+04
29%	t_1	1	1.45E+04
100%	t_2	2	2.27E+04
29%	t_2	2	1.17E+04
100%	t_3	3	3.07E+04
29%	t_3	3	2.62E+03
100%	t_4	4	4.65E+04
29%	t_4	4	3.07E+02
100%	t_5	5	1.36E+05
29%	t_5	5	1.19E+02
100%	t_6	6	2.65E+05
29%	t_6	6	1.00E+02

100%	t_7	7	4.63E+05
29%	t_7	7	8.67E+01
100%	t_8	8	8.57E+05
29%	t_8	8	1.31E+02
100%	t_9	9	1.60E+06
29%	t_9	9	9.42E+01
100%	t_{10}	10	2.42E+06
29%	t_{10}	10	9.93E+01
100%	t_{11}	11	4.46E+06
29%	t_{11}	11	1.02E+02

Table 13 Second quick adaptation test of *Synechococcus* RCC2384. Average pH values (n = 3) and average cell concentrations (per mL, n = 3) are given per osmolarity condition and time-point.

Osmolarity	Time-point	Time (days)	pH	Cell Concentration (mL^{-1})
100%	t_0	0	8.14	4.55E+05
90%	t_0	0	8.34	4.85E+05
80%	t_0	0	8.34	4.49E+05
70%	t_0	0	8.35	4.35E+05
60%	t_0	0	8.33	4.55E+05
50%	t_0	0	8.37	4.18E+05
40%	t_0	0	8.47	4.24E+05
100%	t_1	3	8.64	8.92E+03
90%	t_1	3	8.65	7.03E+03

80%	t_1	3	8.66	1.00E+04
70%	t_1	3	8.62	8.82E+03
60%	t_1	3	8.64	5.53E+03
50%	t_1	3	8.55	5.59E+03
40%	t_1	3	8.40	5.15E+03
100%	t_2	4	8.62	7.32E+03
90%	t_2	4	8.74	5.85E+03
80%	t_2	4	8.74	6.49E+03
70%	t_2	4	8.53	5.71E+03
60%	t_2	4	8.59	5.94E+03
50%	t_2	4	8.58	5.45E+03
40%	t_2	4	8.42	5.48E+03
100%	t_3	5	8.60	4.58E+04
100%	t_4	7	8.66	1.19E+04
100%	t_5	10	8.68	4.81E+04
90%	t_5	10	8.67	6.60E+03
100%	t_6	11	8.68	7.49E+04
100%	t_7	12	8.73	1.38E+05
100%	t_8	31	8.40	4.04E+07

Table 14 Medium test of *Synechococcus* RCC2384. Cell concentrations (mL^{-1}) per condition and time-point are given in duplicates per conditions.

Sample	Time-point	Time (days)	Cell Concentration (mL^{-1})
2384_new1_t0	t_0	0	2.75E+06
2384_new2_t0	t_0	0	2.64E+06
2384_old1_t0	t_0	0	2.49E+06
2384_old2_t0	t_0	0	2.78E+06
2384_new1_t1	t_1	1	3.78E+06
2384_new2_t1	t_1	1	4.09E+06
2384_old1_t1	t_1	1	3.09E+03
2384_old2_t1	t_1	1	2.88E+03
2384_new1_t2	t_2	2	5.53E+06
2384_new2_t2	t_2	2	6.13E+06
2384_old1_t2	t_2	2	8.82E+03
2384_old2_t2	t_2	2	8.09E+03
2384_new1_t3	t_3	4	2.56E+06
2384_new2_t3	t_3	4	2.37E+06
2384_old1_t3	t_3	4	2.00E+03
2384_old2_t3	t_3	4	2.09E+03
2384_new1_t4	t_4	8	3.90E+07
2384_new2_t4	t_4	8	3.76E+07
2384_old1_t4	t_4	8	8.22E+03
2384_old2_t4	t_4	8	8.25E+03

Table 15 Average concentrations (per mL, n = 4) of both cyanobacterial cells (PCC7942) and PI stained particles, as well as average pH values (n = 4) recorded during the growth curve of *Synechococcus* PCC7942 are given per condition and time-point.

Condition	Time-point	Time (days)	pH	PCC7942 (mL^{-1})	PI (mL^{-1})
0%_pH8.2	t_0	0	6.87	8.76E+05	
0%_pH7.38	t_0	0	6.89	1.10E+06	
0%_pH7.18	t_0	0	6.67	6.23E+05	
0%_pH6.97	t_0	0	7.05	1.23E+06	
10%_pH8.22	t_0	0	7.76	7.64E+05	
20%_pH8.22	t_0	0	7.70	5.74E+05	
30%_pH8.23	t_0	0	7.79	1.06E+06	
30%_pH7.42	t_0	0	7.69	1.06E+06	
30%_pH7.16	t_0	0	7.56	1.16E+06	
30%_pH7.02	t_0	0	7.60	8.54E+05	
0%_pH8.2	t_1	3	8.73	6.70E+06	
0%_pH7.38	t_1	3	9.09	8.77E+06	
0%_pH7.18	t_1	3	7.90	5.42E+06	
0%_pH6.97	t_1	3	8.84	9.78E+06	
10%_pH8.22	t_1	3	8.90	4.58E+06	
20%_pH8.22	t_1	3	8.71	5.00E+06	
30%_pH8.23	t_1	3	9.05	4.29E+06	
30%_pH7.42	t_1	3	8.99	3.90E+06	
30%_pH7.16	t_1	3	8.88	3.31E+06	
30%_pH7.02	t_1	3	8.81	3.73E+06	

0%_pH8.2	t_2	4	9.35	1.64E+07	
0%_pH7.38	t_2	4	9.45	2.00E+07	
0%_pH7.18	t_2	4	8.49	8.88E+06	
0%_pH6.97	t_2	4	9.29	1.99E+07	
10%_pH8.22	t_2	4	9.22	6.50E+06	
20%_pH8.22	t_2	4	8.89	9.59E+06	
30%_pH8.23	t_2	4	9.23	8.79E+06	
30%_pH7.42	t_2	4	9.16	8.50E+06	
30%_pH7.16	t_2	4	8.73	8.31E+06	
30%_pH7.02	t_2	4	8.64	6.50E+06	
0%_pH8.2	t_3	5	9.35	2.54E+07	
0%_pH7.38	t_3	5	9.45	2.67E+07	
0%_pH7.18	t_3	5	8.49	1.43E+07	
0%_pH6.97	t_3	5	9.29	2.73E+07	
10%_pH8.22	t_3	5	9.22	7.31E+06	
20%_pH8.22	t_3	5	8.89	9.73E+06	
30%_pH8.23	t_3	5	9.23	6.03E+06	
30%_pH7.42	t_3	5	9.16	9.96E+06	
30%_pH7.16	t_3	5	8.73	1.58E+07	
30%_pH7.02	t_3	5	8.64	1.72E+07	
0%_pH8.2	t_4	6	10.07	2.65E+07	3.18E+06
0%_pH7.38	t_4	6	9.56	2.90E+07	3.43E+06

0%_pH7.18	t_4	6	9.63	1.53E+07	2.28E+06
0%_pH6.97	t_4	6	9.94	2.95E+07	4.30E+06
10%_pH8.22	t_4	6	9.26	8.84E+06	1.28E+06
20%_pH8.22	t_4	6	9.14	1.63E+07	2.75E+06
30%_pH8.23	t_4	6	9.28	7.81E+06	7.54E+05
30%_pH7.42	t_4	6	9.28	1.18E+07	1.19E+06
30%_pH7.16	t_4	6	9.30	1.61E+07	1.46E+06
30%_pH7.02	t_4	6	9.26	1.34E+07	1.38E+05
0%_pH8.2	t_5	7	9.05	4.48E+07	1.55E+06
0%_pH8.2_PI	t_5	7	9.05	4.32E+07	4.95E+06
0%_pH7.38	t_5	7	8.67	4.06E+07	3.78E+05
0%_pH7.38_PI	t_5	7	8.92	4.05E+07	7.62E+06
0%_pH7.18	t_5	7	8.99	2.33E+07	1.73E+05
0%_pH7.18_PI	t_5	7	8.99	2.31E+07	4.78E+06
0%_pH6.97	t_5	7	9.50	4.38E+07	9.06E+04
0%_pH6.97_PI	t_5	7	9.50	4.46E+07	5.37E+06
10%_pH8.22	t_5	7	9.19	1.36E+07	7.65E+05
10%_pH8.22_PI	t_5	7	9.19	1.32E+07	1.77E+06
20%_pH8.22	t_5	7	9.18	1.74E+07	5.19E+05
20%_pH8.22_PI	t_5	7	9.18	1.65E+07	1.68E+06
30%_pH8.23	t_5	7	8.81	1.28E+07	8.75E+05
30%_pH8.23_PI	t_5	7	8.81	1.18E+07	1.48E+06

30%_pH7.42	t_5	7	8.92	1.97E+07	8.46E+05
30%_pH7.42_PI	t_5	7	8.92	1.92E+07	1.32E+06
30%_pH7.16	t_5	7	8.96	2.32E+07	3.99E+05
30%_pH7.16_PI	t_5	7	8.96	2.24E+07	1.46E+06
30%_pH7.02	t_5	7	8.88	2.03E+07	3.72E+05
30%_pH7.02_PI	t_5	7	8.88	2.21E+07	1.63E+06
0%_pH8.2	t_6	10		2.81E+07	8.55E+06
0%_pH7.38	t_6	10		1.68E+07	3.75E+07
0%_pH7.18	t_6	10		4.46E+07	2.44E+07
0%_pH6.97	t_6	10		3.68E+07	1.20E+07
10%_pH8.22	t_6	10		3.17E+06	2.13E+06
20%_pH8.22	t_6	10		3.84E+06	1.45E+06
30%_pH8.23	t_6	10		3.24E+06	1.59E+06
30%_pH7.42	t_6	10		3.73E+06	1.55E+06
30%_pH7.16	t_6	10		6.01E+06	1.24E+06
30%_pH7.02	t_6	10		9.55E+06	2.05E+06
0%_pH8.2	t_7	11	7.29	2.40E+07	8.75E+06
0%_pH7.38	t_7	11	7.36	1.20E+07	3.77E+07
0%_pH7.18	t_7	11	9.33	1.21E+07	2.54E+07
0%_pH6.97	t_7	11	7.59	2.77E+07	1.11E+07
10%_pH8.22	t_7	11	7.75	4.71E+06	2.80E+06
20%_pH8.22	t_7	11	7.80	3.84E+06	2.04E+06

30%_pH8.23	t_7	11	7.79	5.15E+06	1.79E+06
30%_pH7.42	t_7	11	7.76	5.22E+06	1.62E+06
30%_pH7.16	t_7	11	7.67	1.06E+07	4.75E+06
30%_pH7.02	t_7	11	7.85	9.29E+06	1.80E+06
0%_pH8.2	t_8	12	7.53	2.35E+07	9.16E+06
0%_pH7.38	t_8	12	7.55	9.06E+06	3.40E+07
0%_pH7.18	t_8	12	8.19	2.47E+06	2.49E+07
0%_pH6.97	t_8	12	7.75	1.94E+07	1.08E+07
10%_pH8.22	t_8	12	7.78	2.80E+06	6.06E+06
20%_pH8.22	t_8	12	7.85	1.92E+06	6.04E+06
30%_pH8.23	t_8	12	7.84	2.69E+06	2.21E+06
30%_pH7.42	t_8	12	7.80	2.99E+06	2.71E+06
30%_pH7.16	t_8	12	7.81	4.37E+06	3.18E+06
30%_pH7.02	t_8	12	7.81	5.88E+06	3.55E+06
0%_pH8.2	t_9	14	8.56	2.53E+07	1.22E+07
0%_pH7.38	t_9	14	8.10	6.67E+06	3.63E+07
0%_pH7.18	t_9	14	8.10	2.53E+06	2.43E+07
0%_pH6.97	t_9	14	7.88	1.82E+07	1.18E+07
10%_pH8.22	t_9	14	7.83	2.39E+06	3.80E+06
20%_pH8.22	t_9	14	8.06	1.53E+06	2.74E+06
30%_pH8.23	t_9	14	8.05	2.44E+06	1.97E+06
30%_pH7.42	t_9	14	7.91	2.51E+06	2.54E+06

30%_pH7.16	t_9	14	7.90	3.67E+06	3.38E+06
30%_pH7.02	t_9	14	7.87	5.10E+06	4.04E+06
0%_pH8.2	t_{10}	17	7.65	1.13E+07	3.92E+06
0%_pH7.38	t_{10}	17	7.49	3.37E+06	1.92E+07
0%_pH7.18	t_{10}	17	7.27	7.34E+06	2.64E+07
0%_pH6.97	t_{10}	17	7.49	2.38E+07	2.50E+07
10%_pH8.22	t_{10}	17	7.66	4.27E+06	3.72E+06
20%_pH8.22	t_{10}	17	7.76	3.38E+06	4.36E+06
30%_pH8.23	t_{10}	17	7.84	3.97E+06	3.04E+06
30%_pH7.42	t_{10}	17	7.83	3.50E+06	2.57E+06
30%_pH7.16	t_{10}	17	7.80	5.48E+06	3.98E+06
30%_pH7.02	t_{10}	17	7.80	7.41E+06	4.26E+06

Table 16 Cell concentrations (per mL) of cultures that were measured in the µRespirometer as additional data to the growth curve of *Synechococcus* PCC7942, are given with the respective time-points of sampling.

Condition	Time (days)	Cell Concentration (mL^{-1})
0% ESAW pH 8.2	4 (t_2)	1.32E+07
30% ESAW pH 7.0	7 (t_5)	1.85E+07
0% ESAW pH 8.2	12 (t_8)	2.12E+07

Table 17 Pigment signal strength statistics recorded during flow cytometric counts as part of the growth curve of *Synechococcus* PCC7942 over 17 days. Average geometric means, arithmetic means and medians (signal counts^{-1}, n = 4) of the phycocyanobilin peak are given per condition and time-point both as raw values and normalised (norm.) for the number of events.

Condition	Time-point	Time (days)	Number of Events	Average					
				Geometric Mean	Norm. Geometric Mean	Arithmetic Mean	Norm. Arithmetic Mean	Median	Norm. Median
0%_pH8.2	t0	0	39433.56	98.01	0.0025	142.52	0.0036	120.97	0.0031
0%_pH7.38	t0	0	38470.44	148.26	0.0039	181.25	0.0047	160.50	0.0042
0%_pH7.18	t0	0	28530.05	130.09	0.0046	166.50	0.0058	145.74	0.0051
0%_pH6.97	t0	0	38458.13	165.48	0.0043	194.60	0.0051	171.49	0.0045
10%_pH8.22	t0	0	21338.09	147.51	0.0069	174.64	0.0082	151.44	0.0071
20%_pH8.22	t0	0	19239.29	146.61	0.0076	171.58	0.0089	149.66	0.0078
30%_pH8.23	t0	0	31025.2	153.84	0.0050	180.16	0.0058	155.99	0.0050
30%_pH7.42	t0	0	41660.14	153.04	0.0037	178.91	0.0043	154.99	0.0037
30%_pH7.16	t0	0	24338.07	154.74	0.0064	181.26	0.0074	157.39	0.0065
30%_pH7.02	t0	0	8795.85	150.95	0.0172	176.36	0.0200	153.74	0.0175
0%_pH8.2	t1	3	108400.07	173.35	0.0016	198.43	0.0018	177.35	0.0016
0%_pH7.38	t1	3	122829.12	165.59	0.0013	184.74	0.0015	168.74	0.0014
0%_pH7.18	t1	3	100114.56	156.77	0.0016	173.53	0.0017	157.22	0.0016
0%_pH6.97	t1	3	95189.14	158.21	0.0017	175.54	0.0018	161.52	0.0017
10%_pH8.22	t1	3	67369.96	147.85	0.0022	264.50	0.0039	116.13	0.0017
20%_pH8.22	t1	3	83701.91	169.17	0.0020	275.37	0.0033	143.66	0.0017
30%_pH8.23	t1	3	68793.24	140.61	0.0020	266.78	0.0039	106.71	0.0016
30%_pH7.42	t1	3	65788.94	151.12	0.0023	281.15	0.0043	117.87	0.0018
30%_pH7.16	t1	3	61848.48	153.65	0.0025	239.77	0.0039	129.81	0.0021

30%_pH7.02	t1	3	88254.51	158.04	0.0018	237.01	0.0027	138.92	0.0016
0%_pH8.2	t2	4	108489.65	139.72	0.0013	151.75	0.0014	141.75	0.0013
0%_pH7.38	t2	4	113469.19	130.83	0.0012	141.14	0.0012	132.17	0.0012
0%_pH7.18	t2	4	79866	138.15	0.0017	148.75	0.0019	139.23	0.0017
0%_pH6.97	t2	4	111124.57	129.41	0.0012	139.39	0.0013	130.72	0.0012
10%_pH8.22	t2	4	44242	91.60	0.0021	159.80	0.0036	74.45	0.0017
20%_pH8.22	t2	4	66157.79	100.70	0.0015	129.10	0.0020	90.57	0.0014
30%_pH8.23	t2	4	55845.85	88.33	0.0016	145.20	0.0026	73.85	0.0013
30%_pH7.42	t2	4	58963.02	90.36	0.0015	142.22	0.0024	76.42	0.0013
30%_pH7.16	t2	4	85264.28	97.62	0.0011	129.24	0.0015	86.84	0.0010
30%_pH7.02	t2	4	65692.53	102.32	0.0016	139.39	0.0021	89.92	0.0014
0%_pH8.2	t3	5	160979.99	127.57	0.0008	136.41	0.0008	128.24	0.0008
0%_pH7.38	t3	5	152912.85	121.22	0.0008	128.98	0.0008	121.01	0.0008
0%_pH7.18	t3	5	129073	166.49	0.0013	178.30	0.0014	167.99	0.0013
0%_pH6.97	t3	5	153333.11	120.60	0.0008	128.87	0.0008	120.87	0.0008
10%_pH8.22	t3	5	48974.65	82.15	0.0017	173.98	0.0036	68.34	0.0014
20%_pH8.22	t3	5	104749	89.08	0.0009	117.69	0.0011	81.24	0.0008
30%_pH8.23	t3	5	54849.88	88.56	0.0016	198.92	0.0036	71.32	0.0013
30%_pH7.42	t3	5	77723.3	86.20	0.0011	147.55	0.0019	73.38	0.0009
30%_pH7.16	t3	5	96707.72	90.66	0.0009	117.54	0.0012	84.17	0.0009
30%_pH7.02	t3	5	132255.69	93.78	0.0007	118.97	0.0009	87.60	0.0007
0%_pH8.2	t4	6	175219.96	126.94	0.0007	136.17	0.0008	127.47	0.0007
0%_pH7.38	t4	6	176901.58	115.67	0.0007	123.69	0.0007	114.73	0.0006

0%_pH7.18	t4	6	115051	159.11	0.0014	170.62	0.0015	160.99	0.0014
0%_pH6.97	t4	6	182047.34	120.17	0.0007	128.38	0.0007	120.71	0.0007
10%_pH8.22	t4	6	70392.14	77.42	0.0011	154.06	0.0022	66.37	0.0009
20%_pH8.22	t4	6	136024.66	458.59	0.0034	568.16	0.0042	405.54	0.0030
30%_pH8.23	t4	6	63463.61	79.74	0.0013	160.63	0.0025	67.03	0.0011
30%_pH7.42	t4	6	1450.12	512.43	0.3534	693.38	0.4782	450.45	0.3106
30%_pH7.16	t4	6	1130.42	513.62	0.4544	657.31	0.5815	450.87	0.3988
30%_pH7.02	t4	6	68544.48	77.76	0.0011	103.12	0.0015	71.20	0.0010
0%_pH8.2	t5	7	176230.08	120.43	0.0007	129.40	0.0007	119.98	0.0007
0%_pH7.38	t5	7	164636.61	152.90	0.0009	178.36	0.0011	142.69	0.0009
0%_pH7.18	t5	7	107187	173.09	0.0016	191.57	0.0018	171.59	0.0016
0%_pH6.97	t5	7	176533.33	113.53	0.0006	121.82	0.0007	112.47	0.0006
10%_pH8.22	t5	7	86661.84	70.74	0.0008	119.69	0.0014	60.74	0.0007
20%_pH8.22	t5	7	138589.74	91.86	0.0007	123.61	0.0009	85.76	0.0006
30%_pH8.23	t5	7	90376.1	68.30	0.0008	123.04	0.0014	57.69	0.0006
30%_pH7.42	t5	7	131662.6	78.63	0.0006	112.73	0.0009	72.38	0.0005
30%_pH7.16	t5	7	131924.55	81.42	0.0006	101.96	0.0008	77.42	0.0006
30%_pH7.02	t5	7	131260.17	82.93	0.0006	109.45	0.0008	77.36	0.0006
0%_pH8.2	t6	10	90091.99	90.02	0.0010	99.42	0.0011	88.28	0.0010
0%_pH7.38	t6	10	68200.39	64.41	0.0009	73.56	0.0011	58.67	0.0009
0%_pH7.18	t6	10	123759.69	78.87	0.0006	93.00	0.0008	72.63	0.0006
0%_pH6.97	t6	10	97487.52	72.67	0.0007	80.41	0.0008	69.39	0.0007
10%_pH8.22	t6	10	6601.37	81.47	0.0123	126.10	0.0191	65.14	0.0099

20%_pH8.22	t6	10	17855.59	59.10	0.0033	80.47	0.0045	52.43	0.0029
30%_pH8.23	t6	10	10793.21	82.12	0.0076	133.20	0.0123	64.43	0.0060
30%_pH7.42	t6	10	4843.5	68.96	0.0142	94.71	0.0196	59.16	0.0122
30%_pH7.16	t6	10	10532.87	63.97	0.0061	78.74	0.0075	58.50	0.0056
30%_pH7.02	t6	10	36202.75	60.44	0.0017	75.43	0.0021	55.44	0.0015
0%_pH8.2	t7	11	84275.9	88.34	0.0010	97.83	0.0012	87.97	0.0010
0%_pH7.38	t7	11	57949.7	62.30	0.0011	71.46	0.0012	56.87	0.0010
0%_pH7.18	t7	11	46896.08	48.88	0.0010	54.24	0.0012	45.50	0.0010
0%_pH6.97	t7	11	137958.9	71.93	0.0005	78.08	0.0006	69.74	0.0005
10%_pH8.22	t7	11	13448.07	69.14	0.0051	95.43	0.0071	59.63	0.0044
20%_pH8.22	t7	11	29665.48	54.62	0.0018	72.91	0.0025	48.76	0.0016
30%_pH8.23	t7	11	27477.91	67.25	0.0024	95.68	0.0035	58.17	0.0021
30%_pH7.42	t7	11	30996.36	66.04	0.0021	87.10	0.0028	58.84	0.0019
30%_pH7.16	t7	11	33780.28	61.02	0.0018	76.97	0.0023	56.39	0.0017
30%_pH7.02	t7	11	57148.08	58.64	0.0010	73.33	0.0013	54.40	0.0010
0%_pH8.2	t8	12	95177.02	90.01	0.0009	99.44	0.0010	89.51	0.0009
0%_pH7.38	t8	12	33723.98	67.01	0.0020	78.48	0.0023	59.56	0.0018
0%_pH7.18	t8	12	24382.05	47.30	0.0019	51.84	0.0021	43.49	0.0018
0%_pH6.97	t8	12	90823.98	71.23	0.0008	76.93	0.0008	69.24	0.0008
10%_pH8.22	t8	12	22749.04	67.24	0.0030	89.09	0.0039	59.17	0.0026
20%_pH8.22	t8	12	48601.85	58.50	0.0012	73.40	0.0015	53.17	0.0011
30%_pH8.23	t8	12	23547.88	69.99	0.0030	95.02	0.0040	61.21	0.0026
30%_pH7.42	t8	12	30816.19	63.67	0.0021	80.39	0.0026	57.65	0.0019

30%_pH7.16	t8	12	43856.01	57.60	0.0013	67.35	0.0015	54.46	0.0012
30%_pH7.02	t8	12	60055.53	60.28	0.0010	74.45	0.0012	55.96	0.0009
0%_pH8.2	t9	14	97922.51	92.05	0.0009	101.31	0.0010	91.32	0.0009
0%_pH7.38	t9	14	24151.48	81.78	0.0034	100.14	0.0041	70.71	0.0029
0%_pH7.18	t9	14	31393.4	55.89	0.0018	61.92	0.0020	51.78	0.0016
0%_pH6.97	t9	14	84651.76	72.75	0.0009	78.35	0.0009	70.24	0.0008
10%_pH8.22	t9	14	16834.04	65.63	0.0039	82.57	0.0049	58.00	0.0034
20%_pH8.22	t9	14	28902.79	52.14	0.0018	60.97	0.0021	49.15	0.0017
30%_pH8.23	t9	14	1247	117.81	0.0945	152.80	0.1225	99.45	0.0797
30%_pH7.42	t9	14	24342.26	60.25	0.0025	72.32	0.0030	54.96	0.0023
30%_pH7.16	t9	14	1237	127.91	0.1034	176.66	0.1428	108.41	0.0876
30%_pH7.02	t9	14	62534.58	57.38	0.0009	69.07	0.0011	53.69	0.0009
0%_pH8.2	t10	17	71812.34	61.84	0.0009	66.08	0.0009	59.25	0.0008
0%_pH7.38	t10	17	31865.58	106.37	0.0033	133.27	0.0042	98.23	0.0031
0%_pH7.18	t10	17	68886.44	55.32	0.0008	59.98	0.0009	52.63	0.0008
0%_pH6.97	t10	17	142930.58	79.74	0.0006	86.78	0.0006	77.99	0.0005
10%_pH8.22	t10	17	39177.63	63.83	0.0016	76.83	0.0020	58.13	0.0015
20%_pH8.22	t10	17	43059.57	52.58	0.0012	62.71	0.0015	48.72	0.0011
30%_pH8.23	t10	17	27246.6	63.82	0.0023	76.72	0.0028	57.96	0.0021
30%_pH7.42	t10	17	13639	61.85	0.0045	74.55	0.0055	55.98	0.0041
30%_pH7.16	t10	17	41932.94	56.99	0.0014	67.12	0.0016	53.45	0.0013
30%_pH7.02	t10	17	66049.1	55.65	0.0008	65.05	0.0010	52.21	0.0008